Interferometric investigation of optical beams with phase singularities

A THESIS

submitted for the Award of Ph.D degree of

Mohan Lal Sukhadia University

in the

Faculty of Science

BY

Sanjoy Roychowdhury

Under the Supervision of

Dr. R. P. Singh
Physical Research Laboratory

QUANTUM OPTICS AND QUANTUM INFORMATION DIVISION
PHYSICAL RESEARCH LABORATORY, AHMEDABAD.

MOHANLAL SUKHADIA UNIVERSITY, UDAIPUR

Year of submission: 2006

CERTIFICATE

This is to certify that the thesis entitled "Interferometric investigation of optical beams with phase singularities" submitted for the award of the degree of Doctor of Philosophy of Mohanlal Sukhadia University in the faculty of Science is a record of bonafide investigations carried out by Shri. Sanjoy Roychowdhury under my supervision and guidance.

This is an original piece of work on which no one has been awarded a degree in this University or in any other University.

The literary presentation of the thesis is satisfactory and it is in a form suitable for publication. The work presented in the thesis has been done after registration in this University.

Further, the candidate has put in attendance of more than 200 days in my institution as required under rule 7(b) and thus completed the residential requirement.

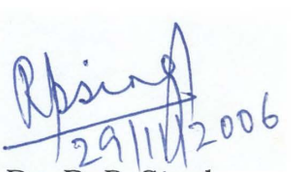

Dr. R. P. Singh
(SUPERVISOR)

to

To all physics loving people

Contents

Acknowledgement

I express my sincere gratitude to Dr. Ravindra Pratap Singh for his excellent guidance. I have benefited much from his clarity of physical ideas, working on fundamental problems and overall his doubtful approach in solving the problems. His good behavior and his exceptional capacity to work on many different areas of the subject, always inspires me to take application of my research to become a truth. His initiation to give colour vortex in experiment and theory is happen to be a more time taking problem to solve. His introduction to creating vortex in lab and introducing iris and finding focal length of lens and plotting elliptical phase started my research carrier. His constant inspiration to find out Wigner distribution function of optical vortex, helped me to complete my work. Again I would like to thank my guide for proof reading of my thesis. I would like to thank Mr. V.K. Jaiswal for association with some of my problems. I am grateful to him on the spiral fringe that he recorded on CCD and other experimental assistance. I would like to thank Mr. Ranpura for his help in developing holographic film and recording fringe. I thank Prof. J. Banerji who helped me to find out topological charge inversion from mirror and also thank him to show how to give colour to a fringe by simulation. I would like to thank Prof. P. K. Panigrahi for giving chance to tell my interesting result in front of him and finding out theory of diffraction in front of him. I would like to thank Prof. V. K. B. Kota & Prof. P. K. Panigrahi for pointing out the problem of dimensionality of Wigner distribution function. In that way I clarified my doubt. I would like to thank our previous Dean Prof. V. B. Sheorey to pointing out the problem of Husimi function. I would like to thank Prof. V. K. B. Kota to pointing out the problem of discreteness of experimental Wigner function. I would like to thank Prof. G. S. Agarwal for encouraging me to read books and introduction to Mach-Zehnder interferometer in course work. I

would like to thank Workshop people for their kind attention to make a particular arrangement associated with set up. I would like to thank all concerned scientist in all my review board to keep my research going. I would like to thank concerned library and computer center and administrative staff for their kind attention and continuous help to make a dream possible. Above all the enthusiasm of research came from useful discussion with Tarak, Asoka, Rajnish, Srecharan, Subranshu, Subimal, Suranjana, Utpal, Manimaran, Anirban, Santosh, Prasanta, Jayendra, Lokesh, Sarika, Hemchandra, Ramkrishna, Jitendra and my batch mates Dilip, Murtikai, Nagar, Murrari, Bhabesh, Murli, Jayesh and all other students. I would like to thank our recent Dean Prof. S. K. Bhattacharya for my foreign visit for learning on the same topic of my research. Prof. P. Sharma helped me a lot during the course of my study. Above all enthusiasm of research came from environment by locality and nature. Finally, I would like to thank my parents, wife Sagarika, brother Sayan and my daughter Megha for their support and encouragement and love. Above all God move me as if I am water in a river.

Sanjoy Roychowdhury

Sanjoy Roychowdhury

Abstract

Vortices, manifestation of phase singularities, are characterized by topological charges and recognized as important features common to all waves. The vortex of a wave field is defined by the point where the imaginary as well as the real part of the wave field vanishes simultaneously and the phase becomes singular. These structures can be seen at macro level in water whirlpool, tornadoes, gravitational wave field, as well as at micro level in Bose Einstein Condensate and superfluid. Therefore, knowledge gained through the study of optical vortices can be very helpful in understanding many of these systems. An optical vortex has zero intensity at its center and a wave front that is helical. In this thesis, an understanding of phase singularities has been developed using interferometric techniques.

In Chapter 1, phase singular beams are introduced with their generation, properties and use, and an outline of the thesis is presented. For the generation of beams with phase singularities various diffractive optical elements have been used. Diffraction is one of the scattering phenomena that can produce various kinds of light structures depending on the scattering potential provided by diffractive optical elements. We produce mainly Gaussian vortex beams, Bessel beams, and Bessel vortex beams. At the outset we mention that all experiments and simulations are done in the optical domain with red light of He-Ne Laser and white light of Quartz Tungsten Halogen (QTH) lamp. The experimental images of red light are taken through black and white (monochrome) CCD camera for convenience and accordingly the theoretical images are given as black and white. However, experimental colour images re-

lated to polychromatic Gaussian vortex beams are taken from colour CCD camera. The theoretical simulations related to white light Gaussian vortex beams are shown in colour to have a better comparison with the experimental results.

In chapter 2, the theoretical background of the generation of optical vortices and other singular beams have been given. It also describes the Wigner distribution function (WDF), a phase space (quasi)probability distribution that can provide coherence information in terms of joint position and momentum variables. Solutions of wave equation from scattering potential, like phase singularity, give vortices from diffraction. Modulation with Gaussian or Bessel function produces Gaussian vortex beams or Bessel vortex beams. Experimentally, this modulation in diffracted order is given by the hologram that is made out of these functional modulated beams and plane wave interference. Theory of interference of these beams is given. Principle of heterodyne interferometry is introduced. Theoretical model of lens effect on topological charge inversion is given.

Chapter 3 gives methods for generating various phase singular beams in the laboratory. The interference patterns of Gaussian vortex beam, Bessel beam, Bessel vortex beam with plane wave give rise to the respective holograms for producing that beam. Material and size of the hologram is discussed. The resulting beams and their hologram preparation are discussed. At first, a transparent sheet is used to optimize the size of the hologram for a particular beam width. Then this size (typical 0.19 cm) is printed by a laser printer to a holographic sheet. Holograms are produced by developing the holographic film. Then these holograms are developed and bleached. Gaussian vortex beam is produced by forked computer generated hologram with high efficiency at first order diffraction. Various interference patterns as holograms to generate beams with phase singularities are done by holographic film as well as LCD display of spatial light modulator (SLM).

Chapter 4 illustrates various interferometric techniques to study their properties. Number of intertwined fringe lines, when a vortex beam interferes with a plane wave, is the measure of topological charge of vortex, the first thing we verify with our interferometric experiments. After that, interaction of various phase singular beams with one another is studied. Interactions of Gaussian vortex beams with same and different topological charges, showing the effect of shear and charge in their interaction, are described with theory and experiment. At zero shear, annihilation occurs for vortices with same charge. With increasing shear or separation between beams, fringe width in the interferogram decreases. Lens and mirror effect on topological charge inversion along with vortex-vortex interaction are discussed. Inversion of radial singularity of a Gaussian beam is discussed through a Twyman-Green Interferometer. Singular beams related to Bessel function are also discussed. Next, we present the theory and experiment related to white light interferometry. Integer topological charge related to singularity and fractional topological charges related to singularity are differentiated. Splitting of topological charge is described, both experimentally and theoretically. Using interferometric techniques, it has been shown that mirror and lens (spherical and cylindrical) invert topological charges. The theoretical simulations give the same results. It is seen that this is true for both, monochromatic and polychromatic singular beams. Mach-Zehnder and shearing-Sagnac interferometer were used as interferometric tools for these studies.

In chapter 5, experimental determination of the WDF of an optical vortex has been given. The chapter starts with introduction to the Wigner function. It is shown that using basic principles, intensity in position and momentum space can be retrieved from the Wigner function. Vortex-vortex interaction in a shearing Sagnac interferometer is used to calculate mutual correlation function. The Fourier transform of this experimentally obtained complex mutual correlation function provides us with the Wigner distribution function. The Wigner function of opti-

cal vortices of different topological charge is obtained theoretically and experimentally. The results for Gaussian vortex beams have been compared with Gaussian beams without vortices to get a better insight into the coherence properties of the beams carrying vortices. Spatial coherence properties of the beams are described through the Wigner distribution function at two different propagation distances for same topological charge.

Chapter 6 deals with applications of optical vortices realized in the laboratory. Implementation of logic gates using charge inversion properties of optical vortices is described through NOT gate and CNOT gate. The logic of CNOT gate that uses two inputs, is built by controlling the output of one beam by another beam. Another application is a new optical imaging method that is described with theory and experiment. This is actually tomography of fork grating. The study is related to the understanding of scattering depth, biological tissue imaging and pattern recognition like finger print diagnosis. Lastly, it is pointed out that various phenomena related to optical vortices, their interference and diffraction can be extended to matter waves. The thesis ends with concluding remarks and future outlook.

Chapter 1

Introduction

Till ancient time physicist tried to find out the laws of nature by explaining it in the language of mathematics, logical concept and experimental verification in the domain of matter and wave. Singular optics is a new branch of modern physical optics that deals with a class of effects associated with phase singularities in wave fields, as well as with the topology of wave fronts [1]. In brief, phase of a wave can experience a π-jump, corresponding to half of a wavelength in a wave train, producing a phase defect of a wavefront along a continuous line in space. For instance, some physical reasons can be responsible for local changes of the phase velocity across a wavefront. Resulting wave-front rapture can lead to a tear of the wavefront, and phase becomes indeterminate, or singular along the tear. The necessary condition for a phase singularity to appear is the vanishing of the field amplitude. Whewell in 1833 discovered the phase singularities in the tidal waves. Hamilton in 1832 discovered another type of singularities, namely polarization light singularities. The general types of polarization singularities were analyzed later by Nye. More recently the results of optical singularities investigations are treated in Singular Optics, a branch of modern optics studying new important features of light, which are absent in the traditional optics of waves with smooth wave fronts. In general, vortices are inherent to any wave phenomena, including even complex probability wave function in quantum mechanics. In the case of phase singularities in light, much of the revived interest has come from the ability of lasers to generate and easily manipulate a great variety of optical fields. In the paper written by Allen et al. topological charge and the presence of orbital angular

momentum, one of the most specific feature of optical vortices are introduced in the context of Laguerre-Gaussian beam [2]. This is the new feature absent in light fields with a smooth wavefront. The important feature of the light vortex is that the field amplitude vanishes on the axis of the vortex. The lines of zero amplitude were the axes of vortices.

The essential role of phase singularity has been recognized by the study of wave singularities in optics only after publication of the seminal paper by Nye and Berry 1974 [3] and in analogy with defects in crystal, wavefront dislocations were introduced. A wave dislocation can be defined in terms of an integral around a circuit that contains within an isolated dislocation line $\oint d\phi = 2l\pi$ where the integer l, which may be positive or negative, is the winding number, or a charge of a dislocation.

In 1932 Wigner proposed a function called Wigner distribution function in quantum mechanics [4]. I have in our laboratory find out Wigner distribution function of phase singular beam interferometrically and tried to retrieve phase and intensity [5]. Wigner distribution function (WDF) of the general helical Laguerre-Gaussian modes are calculated in an analytical form [6]. In fact optical patterns of Laguerre-Gaussian modes, optical vortex, and Gaussian vortex beam are same. Spatial coherence (numerical value) and information entropy in optical vortex field in 1D is discussed [7]. A closed-form Wigner representation of Laguerre-Gaussian beam and connection between Hermite-Gaussian beam is given [8]. Mansuripur et al. introduce expression for linear optical vortices [9]. In this thesis understanding of all phenomena is based upon interferometric techniques. Diffraction is one of the scattering phenomena. In this process depending upon the scattering potential or hologram Gaussian beam, Gaussian vortex beam, Bessel beam, Bessel Vortex beam can be produced and the effect of spherical and cylindrical lens on these beams. Formation of these beams can be used to explain many natural phenomena. Iaconis et al. introduced shearing Sagnac interferometer to measure two-point field correlation function for Gaussian beam [10]. Chung-Chieh Cheng and M. G. Raymer in their article introduced the concept of Wigner distribution function in the context of shearing Sagnac interferometer [11]. In shearing Sagnac interferometer two beams are having similarity but

they are distinguishable and denoted by $E_1(\eta, \xi)$ and $E_2(\eta, \xi)$ with same orthogonal coordinates. Their Wigner distribution function calculation give insight of dimension reduction due to constrained. They are sheared in two opposite directions. A. Wax and J. E. Thomas measured smoothed Wigner phase-space distribution for small angle scattering in a turbid medium [12]. I have utilized the concept of geometric phase to determine complex mutual correlation function. The similar concept was used in the paper complex self-coherence function determination using geometric phase technique by Jose A. Ferrari et al [13]. The heterodyne interferometry is introduced in the thesis of Adam P. Wax [14]. There are lots of distribution function for phase space determination [15]. Similar generation of non-diffracting beams by spiral fields is studied [16]. Similar effect in circling optical vortices are shown [17]. I have done interference with higher order phase due to nonlinear lens effect [18]. These beams in the diffraction regime interfere all together give new optical imaging technique. Their monochromatic and polychromatic study with propagation and coherence has meaning of explaining with same experimental and theoretical footing. Polychromatic simulation is done by me [19]. These study can predict the other functional beams. I V Basisty et al. has studied fractional charges are earlier [20]. The solution of scattering potential like $\eta^2 + \xi^2$ is the product of two hermite polynomials in two dimension is derived [21]. This is used in calculating diffraction of vortex potential. The conversion of vortices from hermite polynomial is discussed [22,23]. Optical vortices and their propagation is studied [24] with respect to vortices in same beam. I have studied with respect to vortices in same and as well as for two different beams. Non-canonical optical vortices is studied [25]. I have studied cylindrical lens effect with respect to that. Annihilation and superposed state was constructed looking at the reference [26]. Topological charge is associated with scattering depth in terms of diffraction orders. Topological charges in diffracted orders are shown in [27]. This coherence analysis of diffused femtosecond laser pulses is introduced [28]. The problem of Wigner function of an vortex or two vortex beam is the problem of twin paradox. Actually it is two oppositely separated interfering beams. Intensity equalization of two arms of heterodyne interferometer is introduced [29]. The heterodyne principle is given [30]. This concept is used in my calculation.

The concept of diffraction efficiency and hologram construction is introduced in [31]. C. F. R. Caron, R. M. Potvliage introduce Bessel-modulated Gaussian beams with quadratic radial dependence [32]. Again the fractional Bessel vortex beam is studied by me following [33,34]. Few typical interferometric pattern is studied by me following [35]. Scaling for soliton or Laguerre Gaussian or Gaussian vortex beam are came into calculation in looking through the following papers [36-38]. People are already studied interference of singular beams [39]. But our model gives the true value. In BEC similar phenomenon of vortices interaction happens [40,41]. Coherence properties in vortices are discussed [42]. Similar lens like properties are seen in cold atoms [43]. Lens effect is discussed in a different way [44]. Tomography of speckles is same as beams is follows from [45]. Speckles are regular vortex is shown in [46]. Ambiguity function and Wigner distribution function are distinguished [47]. Introduction to Wigner distribution function is given by consulting [48]. Experimental observation of elliptical phase in Bessel beam is introduced [49]. Appendix is written following [50]. Discrete fourier transform is done and shown that it is equivalent to continuous fourier transform and it is done following the reference [51]. A matlab program to determine Wigner distribution function is given in the appendix. Vortex is defined by the point where imaginary as well as real part of the wave field vanishes simultaneously and the phase becomes singular and wavefront is torn. Phase singularities are generic to all scattered or diffracted wave fields. As natural phenomena, these structures have a similarity at macro level in water whirl pool, tornadoes, gravitational wave field, as well as at micro level in Bose-Einstein Condensate (BEC) and super fluid. Therefore knowledge gained through the study of optical vortices can be very helpful in understanding many of these systems. The objective is to generate optical beams with phase singularities using computer generated hologram in the laboratory and to study their properties through interferometry.

Chapter 2

Theoretical background

Wave equation for transverse electric field in a scattering potential give solution like vortex beam and bessel beam. This is equivalent to Schrödinger equation for a scattering potential. Gaussian beam is also called Hermite Gaussian beam and is a complex function. Similarly Laguerre-Gaussian and Bessel beams are also complex functions. They are solutions of wave equation with a scattering potential. The Maxwell's equation with a singular kind of scatterer is given by

$$\frac{\partial^2}{\partial\eta^2}E(C\eta, C\xi, z) + \frac{\partial^2}{\partial\xi^2}E(C\eta, C\xi, z) + (\eta^2 + \xi^2)E(C\eta, C\xi, z) = 0 \tag{2.1}$$

$$E(C\eta, C\xi, z) = \sum_{u=0}^{m+n}(i)^{2u}H(m+n-u, C\eta)H(u, C\xi)e^{-(\eta^2+\xi^2)}e^{-ikz} \tag{2.2}$$

The various possible solutions of $E(C\eta, C\xi, z)$ as Gaussian vortex beams of various topological charges after diffraction are given below. Without scattering potential the solution is Gaussian. With scattering potential central order of diffracted pattern is Gaussian. If the scattering potential is such that the solution of the differential wave equation or Maxwell's wave equation for electric field give bessel function, the laser light passing through that potential gives a Bessel beam. This vortex beam when passed through a hole having circular cross section give a solution like Bessel beam of zeroth order. Some scientists have used axicon to have Bessel beam from Laguerre or vortex beam. But the reverse transformation is not possible. It is observed that a vortex beam can also generate vortex beam.

Electromagnetic wave equation after passing through a scattering vortex potential, which is for example $\eta^2 + \xi^2$, give solutions of product of two Hermite

polynomial in two dimensions of order m+n-u and u and where u runs from 0 to m+n. In case of diffraction m runs from 0 to an integer and n runs from any integer to 0. With suitable combination of phase in front of Hermite polynomials, the wave equation gives a solution of positive ($m < n$) and negative ($m > n$) orders of vortices with central Gaussian at m=n.

$$x = \sum_{u=0}^{m+n}((-1)^u/((2)^u u!)((2*i)^u/2^u$$
$$H(m+n-u, C\eta)H(u, C\xi)e^{-(\eta^2+\xi^2)} \tag{2.3}$$

$$b = 2^{m+n}(-1)^n n! C(\eta + i\xi)^{m-n} e^{-(\eta^2+\xi^2)} \tag{2.4}$$

$$x \approx b \tag{2.5}$$

where "x" is the solution of the above mentioned wave equation. "b" is the equivalent solution for vortex. In the expression of b, $(\eta - i\xi)^{m-n}$ are also possible solutions for various m and n. This structure "b" is a vortex. This can be modulated by Gaussian or Bessel function. Then it is gaussian or Bessel vortex beam. Hence up to 4th diffracted orders of beams at 45^0 oriented from fork grating is written as

$$D = |\sum_{l=-4}^{4}(a)^{|l|}((\eta - l*S) + iSign(l)(\xi - l*S))^{|l|}e^{(((\eta-l*S)^2+(\xi-l*S)^2)/\sigma_0^2)}e^{-ik_l z}|^2,$$

where "S" is a scaling factor, k_l is $2*\pi/\lambda_l$ and λ_l is the wavelength of l-th order. Hence Gaussian vortex beams with increasing topological charge with opposite sign are produced on both sides. The $(a)^{|l|}$ is contributing intensity to higher orders. The horizontal diffraction from fork grating is written as

$$D = |\sum_{l=-4}^{4}(a)^{|l|}((\eta - l*S) + iSign(l)(\xi))^{|l|}e^{(((\eta-l*S)^2+(\xi)^2)/\sigma_0^2)}e^{-ik_l z}|^2. \tag{2.6}$$

The vertical diffraction from fork grating is written as

$$D = |\sum_{l=-4}^{4}(a)^{|l|}((\eta) + iSign(l)(\xi - l*S))^{|l|}e^{(((\eta)^2+(\xi-l*S)^2)/\sigma_0^2)}e^{-ik_l z}|^2.$$

To get back the fork grating with the same orientation, all diffracted orders are combined with the orientation angle or scanning angle α and given by

$$D = |\sum_{l=-4}^{4} (a)^{|l|}((\eta) + iSign(l)(\xi))^{|l|} e^{(((\eta)^2+(\xi)^2)/\sigma_0^2)} e^{-ik_l(z-Sign(l)(x\cos(\alpha)-y\sin(\alpha)))}|^2.$$

It is supposed that two beams are having perpendicular orthogonal co-ordinate axes. The orientation angle of axes of one beam with respect to the other beam is the scanning angle α. It is supposed that in shearing Sagnac interferometer two beams are having the same frequency. Interference is the scanning of two beams with an angle α. Scanning of two beam with an angle α is shown in Fig. 2.1. The

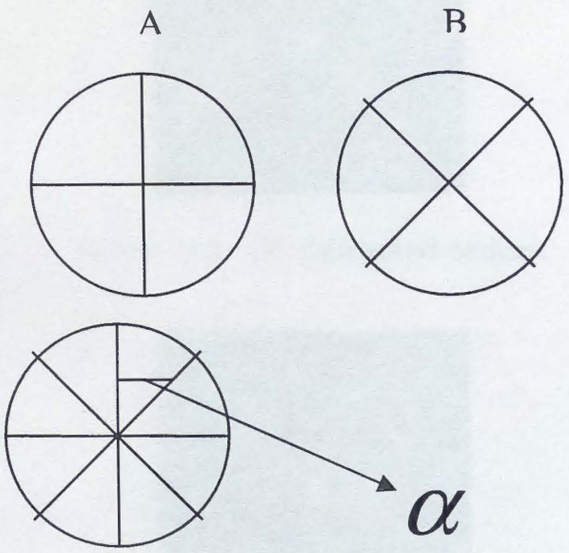

Scanning with an angle α of beams A and B

Figure 2.1: Scanning of two beams with an angle α.

proportion in the η, ξ shear is the angle of orientation of the diffracted orders and it is the same angle as that of the orientation of the fork grating with respect to laser. Diffraction is written by the term D, when a coherent light falls on a fork grating. The order l can be any number depending upon the intensity of the laser beam. The expression with $l = 0$ is the central Gaussian. On one side, topological charge(l) is negative and on the other side it is positive. l may be fraction as well. S is scaling factor of displacement of orders of Gaussian vortex beams. a is a positive number, varies according to the diffraction efficiency of the diffracted

orders. The theoretical simulation of diffracted orders in 45^0 orientation in space are given by Fig. 2.2. Horizontal diffracted orders for monochromatic light is shown in Fig. 2.3. Horizontal Gaussian vortex diffracted orders for white coherent light fall on fork grating are shown in Fig. 2.4. Experimental diffraction pattern for white coherent light is shown in Fig. 2.5. Gaussian horizontal diffracted orders are shown in Fig. 2.6. Gaussian horizontal diffracted orders for coherent white light diffracted from plane grating is shown in Fig. 2.7. For a Gaussian

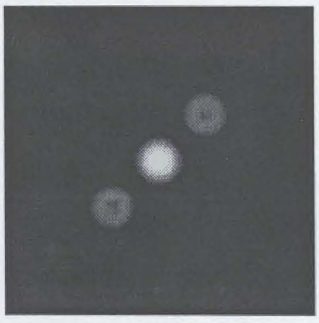

Figure 2.2: 45^0 diffracted orders.

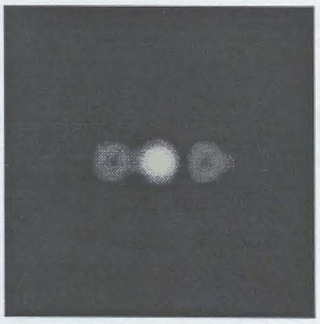

Figure 2.3: Horizontal diffracted orders.

beam passed through a line grating the diffracted orders(3rd) are given by the expression

$$D = |\sum_{l=-3}^{3} (a)^{|l|} e^{(((\eta - l*S)^2 + (\xi)^2)/\sigma_0^2)} e^{-i*k*(((\eta - l*S)^2 + (\xi)^2)/2*R)} e^{-ik_l z}|^2,$$

where "R" is equivalent focal length and is inversely proportional to divergence and "a" is fraction for Gaussian diffraction with appropriate diffraction efficiency. That is why when Gaussian beam, which is a solution of Maxwell's equation in TEM_{00} mode, is passed in scattering potential like fork embedded in a transparency or

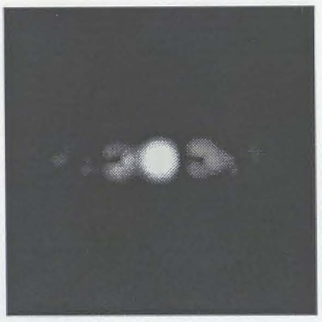

Figure 2.4: Horizontal Gaussian vortex diffracted orders for white coherent light fall on fork grating.

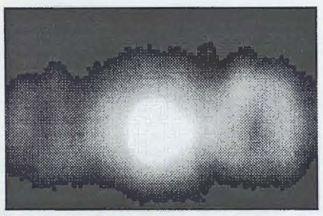

Figure 2.5: Experimental diffraction pattern for white coherent light from a fork grating.

holographic sheet having a potential like vortex and a phase $e^{ik\eta\cos\alpha+ik\xi\sin\alpha}$ depending on the orientation of the fork, generates vortices in the diffraction pattern having a phase that of potential. Our beam divergence is 0.844^o. Hence we have taken a diverging term in the solution $e^{ik((\eta^2+\xi^2)/2R)}$ where k is $2\pi/\lambda$, λ is the wavelength and σ_0 is the minimum beam waist and z is the propagation distance and it is the diverging term depending upon the equivalent focal length R. But it is to be noted that except propagation it is proper to neglect this diverging term in simulation quite some time for a CCD plane. All simulations are scale

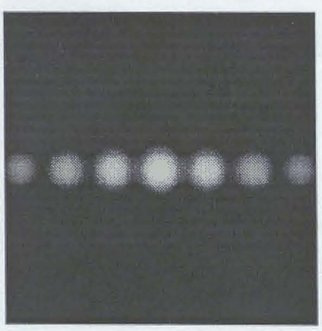

Figure 2.6: Gaussian horizontal diffracted orders.

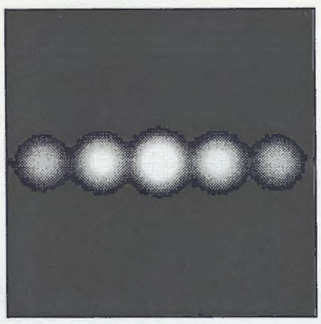

Figure 2.7: Gaussian horizontal diffracted orders for coherent white light diffracted from plane grating.

invariant. This term is associated with LG or vortex beam or soliton. For example vortex beam of charge +1 passed through a small aperture is transformed into Bessel beam of charge +1 and similarly Gaussian beam is passed through a small aperture is transformed into Bessel beam of charge 0. The diverging term only contribute to scale and at large distance intensity reduction. In diffraction phenomena diffracted orders or patterns rotate according to the rotation of the grating. Interference of horizontal diffracted orders are shown in Fig. 2.8. Experimental Diffraction pattern with Bessel beam are shown in Fig. 2.9. Beam with fractional topological charge are shown in Fig. 2.10. To generate fractional

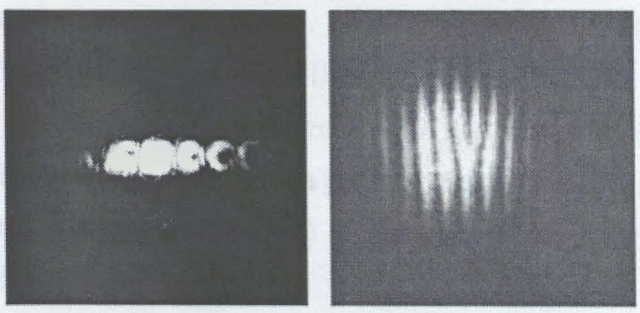

Figure 2.8: Horizontal diffracted orders interference

Gaussian vortex beam diffraction is given by

$$D = |\sum_{l=-(1/2)}^{(1/2)} (a)^{|l|}((\eta) + iSign(l)(\xi - l*S))^{|l|} e^{(((\eta)^2+(\xi-l*S)^2)/\sigma_0^2)} e^{-ik_l z} + e^{-ikz} + e^{(((\eta)^2+(\xi)^2)/\sigma_0^2)} e^{-ikz}|^2, \quad (2.7)$$

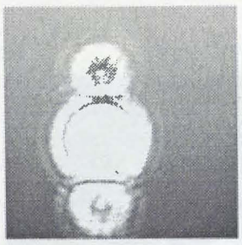

Figure 2.9: Experimental Diffraction pattern with Bessel beam

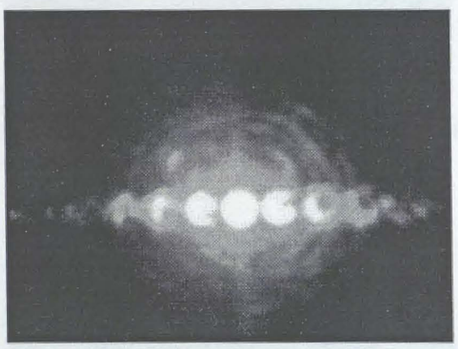

Figure 2.10: Beam with fractional topological charge.

where $a = 50$ to generate fractional Gaussian vortex beam. Bessel vortex beam of fractional topological charge is shown in Fig. 2.11. Bessel beam produced in the diffraction pattern is shown in Fig. 2.12. Bessel vortex beam produced in the diffraction pattern is shown in Fig. 2.13. Bessel beam of zeroth order produced in the 1st order diffraction pattern The theoretical diffraction pattern is shown in Fig. 2.14. Bessel vortex beam produced in the 1st order diffraction pattern is shown in Fig. 2.15. Theoretical diffraction pattern to generate fractional Gaussian vortex beam of topological charge (+1/2) produced in the 1st order diffraction pattern is shown in Fig. 2.16.

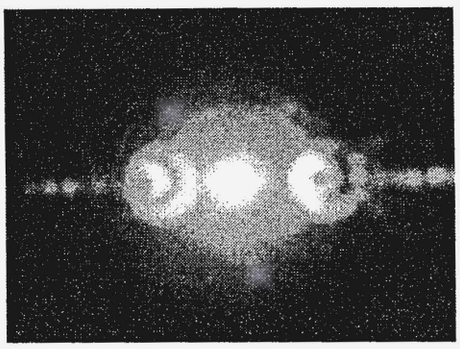

Figure 2.11: Bessel vortex beam of fractional topological charge.

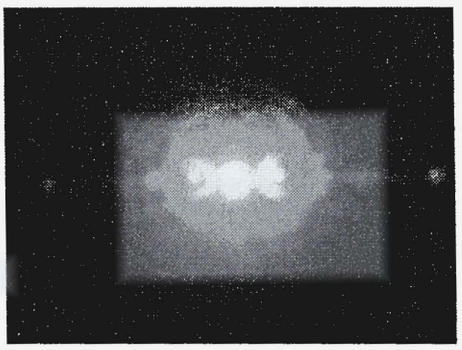

Figure 2.12: Bessel beam produced in the diffraction pattern.

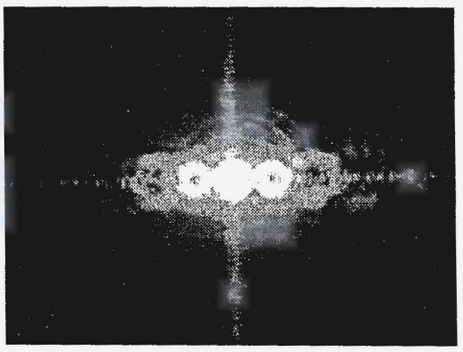

Figure 2.13: Bessel vortex beam produced in the diffraction pattern.

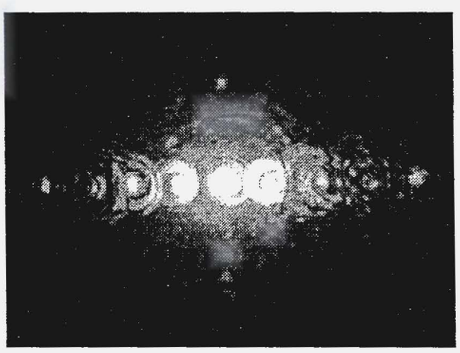

Figure 2.14: Bessel beam of zeroth order produced in the 1st order diffraction pattern.

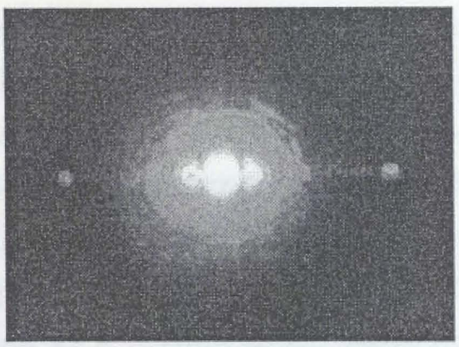

Figure 2.15: Bessel vortex beam produced in the 1st order diffraction pattern.

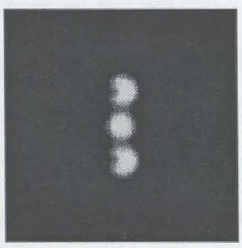

Figure 2.16: Theoretical diffraction pattern to generate fractional Gaussian vortex beam of topological charge (+1/2) produced in the 1st order diffraction pattern.

To generate Bessel vortex beam, we use,

$$D = |\sum_{l=-(1)}^{(1)} (a)^{|l|}((\eta) + iSign(l)(\xi - l * S))^{|l|}(Ef/(1 + iz/zR))J(|m|, u2)$$
$$e^{(((\eta)^2+(\xi-l*S)^2)/\sigma_0^2)/(1+iz/zR))}$$
$$e^{(ikz(1-((\sin(\alpha))^2/(2(1+iz/zR)))))}$$
$$e^{-ik_l z}|^2 \quad , \tag{2.8}$$

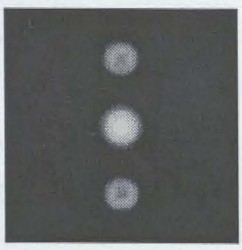

Figure 2.17: Theoretical diffraction pattern to generate Bessel vortex beam of order 1 of topological charge (+1) produced in the 1st order diffraction pattern.

with a ≈ 0.007 nearly. The theoretical diffraction pattern to generate Bessel vortex beam of order1 is shown in Fig. 2.17. For Bessel beam diffraction coefficient "a" is a integer. For Bessel vortex beam which is the modulation of vortex with a bessel beam the hologram grating will be the interference pattern of Bessel vortex beam with a plane wave. For example if the fork grating is vertical then diffracted orders are horizontal and when grating hologram is horizontal the diffracted orders are vertical. If the grating is rotated at a certain angle patterns are also rotated at that angle. If we combine these diffracted orders we will get the image of hologram back. When a plane wave is diffracted from holographic grating, phase and amplitude of the electromagnetic wave are modulated and in the diffraction pattern vortices are generated with central Gaussian. These are characterized by topological charge associated with them. Topological charge can be defined by number of intertwined fringe lines when a vortex interfere with a plane wave. For example topological charge three vortex will have three intertwined fringe line when it interfere with a plane wave.

To observe vortex-vortex interaction Gaussian vortex beam of particular order is selected through iris and interferes with itself in Mach-Zehnder interferometer and shearing Sagnac interferometer. It is observed that more close the distance between mirrors and beam-splitter,the more the separation between two beams in the CCD. When propagation directions are same there is no beating but only the two beam intensities are added. At zero shear when one beam scans the other beam, two beams topological charge will annihilate. With increasing shear given by the glass block, firstly two opposite forks will appear. With more shear intermediate fringe lines will appear between two opposite forks. Any of the two vortex beams in Mach-Zehnder interferometer is interfered . It is observed that to get better fringe stability Sagnac interferometer is suitable compared to Mach-Zehnder interferometer but to study interaction of vortices of different orders, Mac-Zehnder interferometer is the only choice compared to Sagnac interferometer. Expression of a Gaussian vortex beam is

$$E = ((\eta - \eta_0) + i(\xi - \xi_0))e^{-(\eta^2+\xi^2)/\sigma_z^2}e^{ik((\eta^2+\xi^2)/2R)}e^{-ik_1 z - iw_1 t}, \tag{2.9}$$

where η_0 and ξ_0 are the bosonic shift or core shift of the Gaussian vortex beam.

The core size increases with increase of topological charge but this size is less than the sum total of two separate charge. This is not true for fermions. Artificially these bosons can be given fractional charges. This is still to be seen in nature. Two vortex beam are interfered with same frequency. Hence frequencies of two beams i.e. w_1 and $w_2$are same. Hence k_1 and k_2 are same and is equal to k. Where

$$k = 2 * pi/\lambda. \tag{2.10}$$

As space and time are related through an a.c. frequency or wavelength and therefore it is proper to omit w*t term from phase term because space and time are related. Hence the interference pattern in shearing Sagnac is stable with time or space. Considering same frequency (Homodyne) vortex interference, it is better to omit the frequency part in the expression. Hence the expression for Gaussian vortex beam can be written as

$$E(\eta, \xi, z) = C((\eta - \eta_0) + i(\xi - \xi_0))e^{-(\eta^2+\xi^2)/\sigma_z^2} e^{ik((\eta^2+\xi^2)/2R)} e^{-ikz} \tag{2.11}$$

where C is a scaling factor of intensity and σ_0 is the beam width at the initial propagation plane. σ_z is the beam width at propagation plane z. Where σ_z is σ_0 tan(γ)and divergence angle is given by $\gamma\sigma_0$ is the width at a initial propagation plane. Where R is the equivalent focal length. For simplicity we have taken C to be 1. Considering there is no effective divergence it is suitable to not consider the term $e^{ik((\eta^2+\xi^2)/2R)}$ in the expression. Equation of beam with shifted vortex is

$$E = ((\eta - \eta_0) + i(\xi - \xi_0))e^{-(\eta^2+\xi^2)/\sigma_z^2} e^{-ikz} \tag{2.12}$$

Expression of left shifted vortex with shifted beam is

$$E_1 = ((\eta - d_\eta) + i(\xi - d_\xi))e^{-((\eta-d_\eta)^2+(\xi-d_\xi)^2)/\sigma_z^2} e^{-ikz} \tag{2.13}$$

Expression of right shifted vortex with shifted beam is

$$E_2 = ((\eta + d_\eta) + i(\xi + d_\xi))e^{-((\eta+d_\eta)^2+(\xi+d_\xi)^2)/\sigma_z^2} e^{-ik(z-\cos(\alpha)\eta-\sin(\alpha)\xi)} \tag{2.14}$$

Expression of beam with sheared vortex of charge +2 is

$$E = ((\eta - \eta_0) + i(\xi - \xi_0))((\eta - 2\eta_0) + i(\xi - 2\xi_0)) \\ e^{-(x^2+\xi^2)/\sigma_z^2} e^{-ikz} \tag{2.15}$$

where (η_0, ξ_0),$(2\eta_0, 2\xi_0)$is the co-ordinate of the two vortex. Expression of left shifted vortex with shifted beam propagation in z direction is

$$A = ((\eta - d_\eta) + i(\xi - d_\xi)) e^{-((\eta-d_\eta)^2+(\xi-d_\xi)^2)/\sigma_0^2} \\ e^{-ikz} \tag{2.16}$$

Expression of right shifted vortex with shifted beam propagation in z direction is

$$B = ((\eta + d_\eta) + i(\xi + d_\xi)) \\ e^{-((\eta+d_\eta)^2+(\xi+d_\xi)^2)/\sigma_0^2} e^{ik((\eta^2+\xi^2)/2R)} e^{-ikz} \tag{2.17}$$

Interference between two beams when they scan each other having electric fields A and B is given by

$$I = |A + Be^{ik\eta\cos(\alpha)+ik\xi\sin(\alpha)}|^2 \tag{2.18}$$

where α is the angle in which one beam scans the other beam. z is the propagation direction. The fringe width depends on the interference plane from the beam-splitter and shear between the beam. Interference between two beams having amplitude E_1 and E_2 is given by

$$I = ((E_1(\eta, \xi, d_\eta, d_\xi, z) + E_2(\eta, \xi, d_\eta, d_\xi, z - \eta\cos(\alpha) - \xi\sin(\alpha)))^*) \\ (E_1(\eta, \xi, d_\eta, d_\xi, z) + E_2(\eta, \xi, d_\eta, d_\xi, z - \eta\cos(\alpha) - \xi\sin(\alpha))) \tag{2.19}$$

or,

$$I = |E_1(\eta, \xi, d_\eta, d_\xi, z) + E_2(\eta, \xi, d_\eta, d_\xi, z - \eta\cos(\alpha) - \xi\sin(\alpha)))|^2 \tag{2.20}$$

The horizontal shear due to glass block is calculated by the formula given below, the shift in sine of angle of individual beams due to unit screw movement x is sin(((0.55/200)/5.25)*(180/π)*v),where v is the number of units of rotation and refractive index of the glass block is $\mu is\sqrt{2.295346202}$ as supplied for Bk7 glass, the horizontal shear of the individual beam of the two beams is given by the

formula $d_\eta isx(1-(\sqrt{(1-x^2)}/(\sqrt{\mu^2-x^2})))$. The vertical shear due to glass block is calculated by the formula given below where shift of sine of angle of individual beam due to one unit screw movement y is sin(((0.6/200)/6)*(180/π)*v), refractive index of the glass block is $\mu = \sqrt{2.295346202}$, shear in the individual beam is given by the formula $d_\xi = y(1-(\sqrt{(1-y^2)}/(\sqrt{\mu^2-y^2})))$. As both horizontal and vertical screws are rotated by 5 units simultaneously for a single shear interferogram. Hence d_η and d_ξ are the two dimensional shear for a single beam, as used in our expression. For two beams, net shear is $2d_\eta$ and $2d_\xi$. It is seen that horizontal shear make the horizontal separation between the two beams but vertical shear make a oscillation of vortex core and beams around a mean position. Though horizontal and vertical shear steps are not equal this does not make any problem in the calculation. Gaussian vortex beam diameter is 0.28 c.m. CCD gain is nearly 3 times that at the computer screen on MaxImDL software compared to CCD shutter plane. One pixel of CCD is 13 μm. There are 1024 pixels in one dimension. If the equivalent movement is in a particular orientation then fringes are made horizontal through rotation by same amount in opposite direction. Interference fringe with zero shear is made with zero reading of the rotating screws to calibrate the system. At zero shear fringe is annihilated. Below, we calculate the fringe width in the interferometer. The fringe used is given below.

$$AM^2 - AC^2 = D^2 + (\eta + d_\eta)^2 - D^2 - \eta^2 = 2d_\eta\eta \tag{2.21}$$

Neglecting d_η^2 compared to $\eta\ d_\eta$

$$(AM + AC)(AM - AC) = 2d_\eta\eta \tag{2.22}$$

$$2D\Delta\eta = 2d_\eta\eta \tag{2.23}$$

$$2D\Delta\eta = 2(m+1)\lambda/2 - 2m\lambda/2 \tag{2.24}$$

when

$$\eta_{m+1} - \eta_m = \beta \tag{2.25}$$

where β is the fringe width. Fringe width is calculated from experiment as well as with theory. Both are matching. Fringe width is proportional to wavelength and the distance from the beam-splitter to CCD but is inversely proportional to

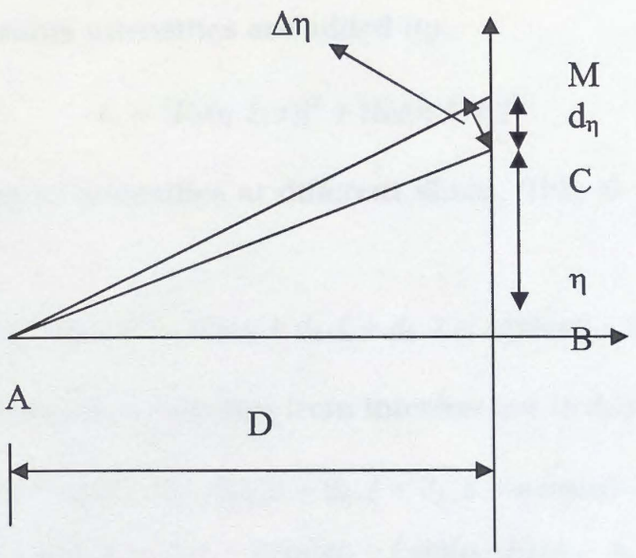

Figure 2.18: Fringe width calculation in a interferometer

shear as shown in Fig. 2.18. The expression is checked from experimental fringe patterns and CCD pixel size. Relative fringes at particular shears remain the same for theory as well as experiments. The relative values for fringe width for shear 1 to 2 are given from theoretical fringe as well as from the expression for the experimental fringe width,

$$\beta = \lambda D/d_\eta. \tag{2.26}$$

The fringe width depends on the interference plane from the beam-splitter and shear between the beams. In other way, interference expression, if one beam scans the other beam at an angle α can be written as

$$\begin{aligned} I = |E_1(\eta - d_\eta, \xi - d_\xi, z)|^2 + |E_2(\eta + d_\eta, \xi + d_\xi, z - (\cos(\alpha)\eta + \sin(\alpha)\xi))|^2 + \\ E_1^*((\eta, d_\eta, \xi, d_\xi, z))E_2((\eta, d_\eta, \xi, d_\xi, z - \eta\cos(\alpha) - \xi\sin(\alpha))) + \\ E_2^*((\eta, d_\eta, \xi, d_\xi, z - \eta\cos(\alpha) - \xi\sin(\alpha)))E_1((\eta, d_\eta, \xi, d_\xi, z)) \end{aligned} \tag{2.27}$$

$$\begin{aligned} I = |E_1(\eta - d_\eta, \xi - d_\xi, z)|^2 + |E_2(\eta + d_\xi, \xi + d_\xi, z - \eta\cos(\alpha) - \xi\sin(\alpha))|^2 \\ +E_1^*(\eta - d_\eta, \xi - d_\xi, z)E_2(\eta + d_\eta, \xi + d_\xi, z - \eta\cos(\alpha) - \xi\sin(\alpha)) \\ +E_2^*(\eta + d_\eta, \xi + d_\xi, z - \eta\cos(\alpha) - \xi\sin(\alpha))E_1(\eta - d_\eta, \xi - d_\xi, z) \end{aligned} \tag{2.28}$$

At zero shear two beams intensities are added up,

$$I_0 = |E_1(\eta, \xi, z)|^2 + |E_2(\eta, \xi, z)|^2. \tag{2.29}$$

This is equal to sum of intensities at different shear. This is due to energy conservation.

$$I_0 = |E_1(\eta - d_\eta, \xi - d_\xi, z)|^2 + |E_2(\eta + d_\eta, \xi + d_\xi, z - \eta\cos(\alpha) - \xi\sin(\alpha))|^2 \tag{2.30}$$

Hence the mutual coherence function from interference is described by

$$\begin{aligned}(I - I_0) = E_1^*(\eta - d_\eta, \xi - d_\xi, z)E_2(\eta + d_\eta, \xi + d_\xi, z - \eta\cos(\alpha) - \xi\sin(\alpha)) \\ +E_2^*(\eta + d_\eta, \xi + d_\xi, z - \eta\cos(\alpha) - \xi\sin(\alpha))E_1(\eta - d_\eta, \xi - d_\xi, z)\end{aligned} \tag{2.31}$$

In our experiment d_η and d_ξ are given together for a single image frame and by applying both the shear, η and ξ move in same amount due to symmetry. Individual shear is the average of the total shear. Let us find out mutual coherence function Γ_1 from the the interference pattern discussed above. We assume a function M whose real part is M_1 and imaginary part is M_2 i.e. $M = M_1 + iM_2$.

$$M_1 = (I - I_0)/2 \tag{2.32}$$

when phase is changed by 90^0 $\cos(k\eta\cos(\alpha) + k\xi\sin(\alpha))$ becomes $\sin(k\eta\cos(\alpha) + k\xi\sin(\alpha))$ and $\sin(k\eta\cos(\alpha) + k\xi\sin(\alpha))$ becomes $\cos(k\eta\cos(\alpha) + k\xi\sin(\alpha))$. Substituting this we get imaginary part M_2. $M_1 + iM_2$ is equal to Γ provided $(\xi d_\eta - \eta d_\xi)$ is zero. As net shear in individual beam is shift in η or ξ.

$$\eta = \sum d_\eta \tag{2.33}$$

$$\xi = \sum d_\xi \tag{2.34}$$

and as we are giving both shear together for a single image frame, the combined shear becomes d_η or d_ξ,

$$d_\eta = d_\xi \tag{2.35}$$

Hence $(\xi d_\eta - \eta d_\xi)$ is zero. Alternatively, experimentally and theoretically, E_1 and E_2 interference pattern is same in changing sides of two equal beams, means positive shear becomes negative shear and then negative scanning becomes positive

scanning. Doing that we get,

$$E_2^*(\eta - d_\eta, \xi - d_\xi)E_1(\eta + d_\eta, \xi + d_\xi)e^{i(k\eta\cos(\alpha)+k\xi\sin(\alpha)} = E_2^*(\eta + d_\eta, \xi + d_\xi)E_1(\eta - d_\eta, \xi - d_\xi)e^{-i(k\eta\cos(\alpha)+k\xi\sin(\alpha)} \quad (2.36)$$

$$E_2^*(\eta - d_\eta, \xi - d_\xi)E_1(\eta + d_\eta, \xi + d_\xi)e^{i(k\eta\cos(\alpha)+k\xi\sin(\alpha)} = E_1^*(\eta - d_\eta, \xi - d_\xi)E_2(\eta + d_\eta, \xi + d_\xi)e^{i(k\eta\cos(\alpha)+k\xi\sin(\alpha)} \quad (2.37)$$

Then we can take substitution of this equal term. Initially we used polarizer and retardation plates in our experiment at the same axes, we get real part of it,

$$\Gamma_1 = Re|E_1^*(\eta - d_\eta, \xi - d_\xi)E_2(\eta + d_\eta, \xi + d_\xi)e^{i(k\eta\cos(\alpha)+k\xi\sin(\alpha))}|. \quad (2.38)$$

Later,half-wave plate is rotated by 45^0. Then the phase of the two beams compared to the earlier two beams is changed 90^0. Then separable phase is also changed by 90^0. Then imaginary part of mutual correlation function is obtained. It is seen the intensity change from rotating plates and rotating by 90^0. This is due to polarization explained in 2D.

$$\Gamma_2 = Im|E_1^*(\eta - d_\eta, \xi - d_\xi)E_2(\eta + d_\eta, \xi + d_\xi)e^{i(k\eta\cos(\alpha)+k\xi\sin(\alpha))}| \quad (2.39)$$

$$\Gamma = M_1 + iM_2 \quad (2.40)$$

then

$$M_1 = \Gamma_1 \quad (2.41)$$

$$M_2 = \Gamma_2 \quad (2.42)$$

$$\Gamma_1(\eta, \xi, d_\eta, d_\xi) = Re|E_1^*(\eta - d_\eta, \xi - d_\xi)E_2(\eta + d_\eta, \xi + d_\xi)e^{(ik\eta\cos(\alpha)+ik\xi\sin(\alpha))}| \quad (2.43)$$

Hence imaginary part of complex mutual coherence function Γ_2.

$$\Gamma_2(\eta, \xi, d_\eta, d_\xi) = Im|E_1^*(\eta - d_\eta, \xi - d_\xi)E_2(\eta + d_\eta, \xi + d_\xi)e^{(ik\eta\cos(\alpha)+ik\xi\sin(\alpha))}| \quad (2.44)$$

Complex mutual coherence function is defined by

$$\Gamma = \Gamma_1 + i\Gamma_2 \quad (2.45)$$

Hence as E_1 and E_2 are same and otherwise, due to symmetry of the problem the contribution from the term $(\xi d_\eta - \eta d_\xi)$ is zero. Hence total mutual coherence function is written as

$$\Gamma = E_1^*(\eta - d_\eta, \xi - d_\xi)E_2(\eta + d_\eta, \xi + d_\xi)e^{(ik\eta\cos(\alpha)+ik\xi\sin(\alpha))} \tag{2.46}$$

Wigner function is given by

$$W(\eta, \xi, p_\eta, p_\xi) = \int \Gamma e^{-i(p_\eta d_\eta + p_\xi d_\xi)} dd_\eta dd_\xi \tag{2.47}$$

Let us consider interference of two Bessel beams, The fields corresponding to two beams can be written,

$$(Ef/(1+iz/zR))J(|m|, u2)e^{(-(((\eta+d_\eta)^2+(\xi+d_\xi)^2)/\sigma_0^2)/(1+iz/zR))}e^{(ikz(1-((\sin(\alpha))^2/(2(1+iz/zR)))))}e^{(-ik(z))}$$

and

$$(Ef/(1-iz/zR))J(|m|, u1)e^{(-(((\eta-d_\eta)^2+(\xi-d_\xi)^2)/\sigma_0^2)/(1+iz/zR))}e^{(-ik(z)(1-((\sin(\alpha))^2/(2(1+iz/zR)))))}e^{-ik(z-\eta)}.$$

Therefore, interference is given by,

$$\begin{aligned} I = |&(Ef/(1+iz/zR))J(|m|, u2) \\ &e^{(-(((\eta+d_\eta)^2+(\xi+d_\xi)^2)/\sigma_0^2)/(1+iz/zR))} \\ &e^{(ikz(1-((\sin(\alpha))^2/(2(1+iz/zR)))))} \\ &e^{(-ik(z))} + (Ef/(1-iz/zR))J(|m|, u1) \\ &e^{(-(((\eta-d_\eta)^2+(\xi-d_\xi)^2)/\sigma_0^2)/(1+iz/zR))} \\ &e^{(-ik(z)(1-((\sin(\alpha))^2/(2(1+iz/zR)))))} \\ &e^{-ik(z-\eta)}|^2 \end{aligned} \tag{2.48}$$

where typical values of different parameter are given to draw the plot,λ is 632.8*$10^{(-7)}$ c.m., k is 2 π /λ,σ_0 = 1000 λ, m = 1 , Ef is 1 ,z is $10^{(6)}$ λ,α = 0.001 ,ϕ is $\pi/2$, K is k σ_0 sin(α), zR = k σ_0^2 /2 ,$d_\eta = d_\xi$ = 800 λ,ϕ = $\pi/2$,$zR = k\sigma_0^2/2$and K is k ξ_0 sin(α)

$$u1 = (K(((\eta - d_\eta)^2 + (\xi - d_\xi)^2))^{1/2}/\sigma_0)/(1 + iz/zR) \tag{2.49}$$

$$u2 = (K(((\eta + d_\eta)^2 + (\xi + d_\xi)^2))^{1/2}/\sigma_0)/(1 + iz/zR) \tag{2.50}$$

ϱ is defined by,

$$\varrho = ((\eta)^2 + (\xi)^2)^{1/2} \tag{2.51}$$

Interference of Bessel vortex beam with each other is given below

$$\begin{aligned} I = |&(\eta + i\xi)^l (Ef/(1 + iz/zR))J(|m|, u2) \\ &e^{(-(((\eta+d_\eta)^2+(\xi+d_\xi)^2)/\sigma_0^2)/(1+iz/zR))} \\ &e^{(ikz(1-((\sin(\alpha))^2/(2(1+iz/zR)))))} \\ e^{(-ik(z))} + &(\eta + i\xi)^l (Ef/(1 - iz/zR))J(|m|, u1) \\ &e^{(-(((\eta-d_\eta)^2+(\xi-d_\xi)^2)/\sigma_0^2)/(1+iz/zR))} \\ &e^{(-ik(z)(1-((\sin(\alpha))^2/(2(1+iz/zR)))))} \\ &e^{-ik(z-\eta)}|^2, \end{aligned} \tag{2.52}$$

where another typical values for the parameters are given below l is the topological charge, λ is $632.8 * 10^{(-7)}$c.m., k is 2 π /λ, $\sigma_0 = 1000\ \lambda$, $m = 1$, $Ef = 1$,$z = 10^{(6)}$ λ,α is 0.001 ,ϕ is $\pi/2$, K is k σ_0 sin(α), $zR = k\ \sigma_0^2$ /2 ,$d_\eta = d_\xi = 800\ \lambda$,$\phi = \pi/2$,zR is k $\sigma_0^2/2$and$K = k\sigma_0 \sin(\alpha)$ and l is the topological charge embedded in the bessel beam.

$$u1 = (K(((\eta - d_\eta)^2 + (\xi - d_\xi)^2))^{1/2}/\sigma_0)/(1 + iz/zR) \tag{2.53}$$

$$u2 = (K(((\eta + d_\eta)^2 + (\xi + d_\xi)^2))^{1/2}/\sigma_0)/(1 + iz/zR) \tag{2.54}$$

$$\varrho = ((\eta)^2 + (\xi)^2)^{1/2} \tag{2.55}$$

Interference of sheared topological charge two vortex with a Bessel beam is given

below

$$I = |((\eta + d_\eta) + i(\xi + d_\xi))(\eta + \xi)(Ef/(1 + iz/zR))J(|m|, u2)$$
$$e^{(-(((\eta+d_\xi)^2+(\eta+d_\xi)^2)/\sigma_0^2)/(1+iz/zR))}$$
$$e^{(ikz(1-((\sin(\alpha))^2/(2(1+iz/zR)))))}$$
$$e^{(-ik(z))} + (Ef/(1 - iz/zR))J(|m|, u1)$$
$$e^{(-(((\eta-d_\eta)^2+(\xi-d_\xi)^2)/\sigma_0^2)/(1+iz/zR))}$$
$$e^{(-ik(z)(1-((\sin(\alpha))^2/(2(1+iz/zR)))))}$$
$$e^{-ik(z-\eta)}|^2 \tag{2.56}$$

where d_η and d_ξ are the shears in the vortices embedded in bessel beam. Interference of a Bessel vortex beam with a plane wave is given below

$$I = |((\eta + d_\eta) + i(\xi + d_\xi))(\eta + i\xi)(Ef/(1 + iz/zR))J(|m|, u2)$$
$$e^{(-(((\eta+d_\eta)^2+(\xi+d_\xi)^2)/\sigma_0^2)/(1+iz/zR))}$$
$$e^{(ikz(1-((Sin(\alpha))^2/(2(1+iz/zR)))))}$$
$$e^{(-ik(z))} + e^{-ik(z-\eta)}|^2 \tag{2.57}$$

Expression of a Gaussian beam propagating along z direction is

$$E(\eta, \xi) = Ce^{-(\eta^2+\xi^2)/\sigma_0^2}e^{-ikz} \tag{2.58}$$

Expression of a Gaussian beam propagating along z direction passing through a spherical lens having focal length f is

$$E(\eta, \xi) = Ce^{-(\eta^2+\xi^2)/\sigma_0^2}e^{-ikz}e^{ik((\eta^2+\xi^2)/2f)} \tag{2.59}$$

where C is a scaling factor of intensity and σ_0 is the beam width. For simplicity we have taken C to be 1. Expression of beam with shifted Gaussian is

$$E(\eta, \xi) = e^{-((\eta-\eta_0)^2+(\xi-\xi_0)^2)/\sigma_0^2}e^{-ikz} \tag{2.60}$$

Expression of left shifted Gaussian beam without the phase associated with propagation direction is

$$A(\eta, \xi) = e^{-((\eta-d_\eta)^2+(\xi-d_\xi)^2)/\sigma_0^2} \tag{2.61}$$

Expression of right shifted Gaussian with shifted beam without the phase associated with propagation direction is

$$B(\eta,\xi) = e^{-((\eta+d_\eta)^2+(\xi+d_\xi)^2)/\sigma_0^2} \tag{2.62}$$

Interference of beam B having passed through a spherical lens of focal length f with plane wave is given by

$$I = |e^{-ik(z-\eta)} + Be^{-ik(z-(\cos(\alpha)\eta^2+\sin(\alpha)\xi^2)/2f)}|^2 \tag{2.63}$$

Expression of a vortex propagating along z direction is

$$E = C(\eta + i\xi)e^{-(\eta^2+\xi^2)/\sigma_0^2}e^{-ikz} \tag{2.64}$$

Expression of a vortex propagating along z direction passing through a spherical lens having focal length f is

$$E = C(\eta + i\xi)e^{-(\eta^2+\xi^2)/\sigma_0^2}e^{-ikz}e^{ik((\eta^2+\xi^2)/2f)} \tag{2.65}$$

where C is a scaling factor of intensity and w0 is the beam width. For simplicity we have taken C to be 1. Expression of beam with shifted vortex is

$$E(\eta,\xi) = ((\eta-\eta_0) + i(\xi-\xi_0))e^{-(\eta^2+\xi^2)/\sigma_0^2}e^{-ikz} \tag{2.66}$$

Expression of left shifted vortex beam without the phase associated with propagation direction is

$$A(\eta,\xi) = ((\eta-d_\eta) + i(\xi-d_\xi))e^{-((\eta-d_\eta)^2+(\xi-d_\xi)^2)/\sigma_0^2} \tag{2.67}$$

Expression of right shifted vortex with shifted beam without the phase associated with propagation direction is

$$B(\eta,\xi) = ((\eta+d_\eta) + i(\xi+d_\xi))e^{-((\eta+d_\eta)^2+(\xi+d_\xi)^2)/\sigma_0^2} \tag{2.68}$$

Interference beam B having passed through a spherical lens of focal length f with plane wave is given by

$$I(\eta,\xi) = |e^{-ik(z-\eta)} + Be^{-ik(z-(\cos(\alpha)\eta^2+\sin(\alpha)\xi^2)/2f)}|^2 \tag{2.69}$$

Lens effect for topological charge inversion is given below. After charge inversion sign of topological charge changes. Interference vortex beam having passed

through a cylindrical lens of focal length f1 and f2 with plane wave on a plane before focus of the spherical lens of focal length f is given by

$$\begin{aligned} I(\eta,\xi,d_\eta,d_\xi) = |(\eta+i\xi)e^{ik((\eta^2+\xi^2)/2f)}e^{-ik(z-\eta)} \\ +((\eta-d_\eta)-i(\xi-d_\xi))e^{-((\eta^2/2f1+\xi^2/2f2))} \\ e^{-ik(z-(\cos(\alpha)\eta^2/2f_1)+(\sin(\alpha)\xi^2)/2f_2)}|^2 \end{aligned} \tag{2.70}$$

Gaussian vortex beam having passed through a cylindrical lens and at a plane after the imaging spherical lens is given by,

$$\begin{aligned} I = |(\eta+i\xi)e^{ik((\eta^2+\xi^2)/2f)}e^{-ik(z+\eta)} + e^{-((\eta^2/2f1+\xi^2/2f2))} \\ e^{-ik(z-(\cos(\alpha)\eta^2/2f_1)+(\sin(\alpha)\xi^2)/2f_2)}|^2 \end{aligned} \tag{2.71}$$

The term associated with elliptical beam is elliptical phase and intensity. The difference in before focus and after focus is due to phase change of π or side of linear scan is opposite. Where α is the angle in which one beam scan the other beam. z is the propagation distance.

Chapter 3

Production of optical beams with phase singularities

Hologram is the interference of an object beam with a reference beam. Hologram for the Gaussian vortex beam, Bessel beam and Bessel vortex beam is made theoretically by writing the interference pattern of these beams with a reference beam. Then laser print of these theoretical hologram is taken on a holographic sheet. In the diffraction of a plane wave passing through these holograms, first order diffraction is the consequent beam. Also liquid crystal display of spatial light modulator is used to make array of Bessel beams and Bessel vortex beams. Transparency can be used to make holograms for effective cost reduction. Only thing to take care for transparency hologram is that the beam size and the pattern size must be comparable such that Gaussian vortex beams become separable. If the scatterer size is less diffracted beam separation will be more. In the printed transparency hologram if the pattern equation involves divergence term the output beam will not be spherical instead will be elliptical. LCD system is very fast method for production of phase singular beams.

3.1 Material and preparation of hologram

Experimental fringe is laser printed on holographic sheet. Again another process is that taking print of fringe from computer to holographic sheet by afga hologram writer. But my method is different. The method is written below. Computer

generated hologram is the interference of the object beam with a reference wave.

Hologram preparation

Composition of Developer (19B)

For Two litter

Part 1:

Metol(elone)- 5 gm

Hydroquinone- 16 gm

Sodium sulphite- 30 gm

Water- 500 ml

part-2

Sodium sulphate- 150 gm

Sodium Carbonate- 90 gm

Potassium Bromide-10 gm

Water- 1.5 litter

Remember one has to do part-1 then part-2 with it.

Fixing

AMI Fixer(Johnson and Johnson) 4 litter (Instruction given)

Bleaching:

Potassium Ferricyanide- 100 gm

Water- 400 ml

After developing and fixing the reddish colour of the hologram will be perfectly dark. Developing time is kept at 1 minutes and fixing time is taken as 4 minutes.

During process 3 drops of Fixer +little water should be given to have a better result. Then by using bleaching, hologram will be totally transparent.

It is seen that when the fractional charge $(+1/2)$ or $(-1/2)$ interfere with a plane wave, then give similar structure of holograms in computation. When this hologram printed on a transparency and a plane wave is passed it gives the Gaussian fractional vortex beam, vortex lines in the beam being in two opposite directions of the two first order diffracted beams. But when it is printed on a holographic sheet and developed, vortex lines are in the same direction as in the simulation. So nature permits both the solution. First solution (opposite vortex lines) is still not achieved computationally. It has been observed both theoretically and

experimentally that if the diffraction efficiency of the first order vortex is more the tomographic image of hologram in the 3D beam will be prominent than other configuration. The more the hologram material thickness the more will be the separation in the diffracted order. The more the intense laser more will be orders in diffraction pattern. Fringe orientation depend upon grating orientation also. When the grating is rotated at an angle vertical hologram is rotated at same angle and similarly the diffraction pattern will rotate at the same angle. For example if the hologram is rotated from vertical to horizontal the diffraction pattern rotate from horizontal to vertical. If another grating is used all orders interfere with itself and hence up and down fork will appear. Fringe width and size of the hologram are inversely proportional.

3.2 Testing of prepared holograms

Gaussian vortex beam is produced and used in Sagnac shearing interferometer and Mach-zehnder interferometer to study its interaction. This interaction depends on shear and order and sign of topological charge introduced between the two beams of the interferometer. When light is diffracted from a fork hologram a speckle, spatial dark soliton, which has another name called vortex is formed at a propagation plane. On both side of the diffracted pattern opposite sign vortices with the increasing order or topological charge are produced. Gaussian vortex beams having a particular order and sign are selected and their interaction among each other is studied. These beams are also called LG beams because it will diverge as it propagates. It is modelled as a Gaussian vortex beam to study interaction of vortices at a plane. However, all models in all scales will give the same result. Few patterns of Bessel beam interfering with plane wave were obtained for holograms of bessel beam and similarly Bessel vortex beam were also tested. Few patterns describing lens effect on Bessel beam and Bessel vortex beam. If the beam size is larger than image size then the reflected or transmitted beam will be the image bearing beam. This is only phase modulation. If the hologram fringe line is nearly 25, hologram width is 0.6 c.m. and fringe width for central fringe is 0.0461 cm., then the first order diffraction efficiency is more.

Other kind hologram is that diffracted orders are more. Again with the increase with laser intensity diffracted orders will be more.

3.3 Use of hologram to generate various beams by spatial light modulator

At first interfacing is done with dual VGA card in a PC. Gaussian singular wave diffracted from a computer generated hologram made and then transferred from computer with a properly placed in the SLM software window with proper size and computer monitor picture is replicated in to the Liquid Crystal Display (LCD). Laser beam is diffracted in reflected mode and diffraction pattern is recorded in CCD.

Chapter 4

Properties of singular beams through interferometry:

After producing various phase singular beams using CGH and SLM interfaced with computer, it becomes important to study their properties. As discussed earlier, we have produced mainly Gaussian vortex beams,Bessel beams and Bessel vortex beams. We will describe the interferometric techniques used to find out the topological charge associated with the beams, the charge inversion, and also their interaction with each other. Vortices with fractional topological charges have also been produced. We will see how do they differ from vortices with integer topological charge.

4.1 Determination of topological charge

There are many methods available to make a Gaussian vortex beam or Bessel vortex beam, however we have used a computer-generated hologram (CGH)as a grating imposed on a holographic sheet or a SLM to introduce a vortex of charge n (n=+1,-1,+2,-2 and so on) in the Gaussian beam of a He-Ne laser. These vortices are paraxial solutions of electromagnetic equations just like LG beams. The laser passing through the branch point of the CGH produces various diffraction orders. First order diffraction giving a vortex of charge one was selected by an iris. Similarly higher order charges are selected through iris. With the increasing order, the topological charge increases and on both sides of the diffraction pattern

charges are of opposite sign. The experimental set-up to find out the topological charge is given in Fig. 4.1, that is a standard Mach-Zehnder interferometer gives experimental fringe pattern for a topological charge +1 vortex. Now let us discuss

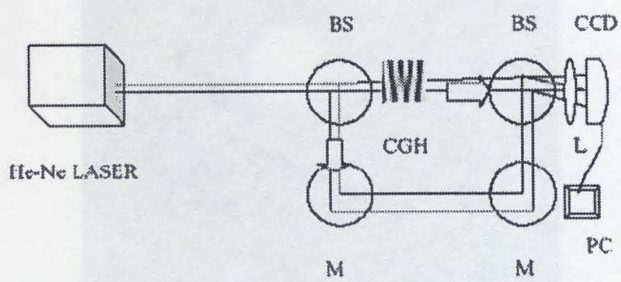

Figure 4.1: Mach-Zehnder Interferometer set up

the vortex beam with fractional charge looks like a integer charge vortex beam. The only difference is in the structure of interference pattern. Fractional topological charges can be of any fraction. Fractional topological charges can exist along with separately like integer charges as well as they can exist with integer charges. Difference between integer and fractional topological charge is that fork is not complete for fractional charges whereas forks are complete for integer topological charges[13]. This fractional charge beam when interferes with a Gaussian beam it produces interference pattern with fractional fork. A hologram, made of this fractional fork gives a vortex beam with a fractional topological charge. Two beams of opposite i.e. positive and negative fractional charge give an interference pattern, characteristic of an integer charge equal to sum of absolute value of fractional charge. For example, $+1/2$ and $-1/2$ give topological charge +1. $+2/3$ and $-1/3$ give topological charge $+1$ interference pattern. Gaussian vortex beam of topological charge $+1/2$ interfering with a plane wave give the interference pattern, which is the hologram for generation of a fractional charge beam as first order diffracted beam when a plane wave passes through this hologram. This beam is produced due to fractional topological charge $(+1/2)$ interferes with a plane wave with same propagation direction. This will look like line vortex on a plane from the beam center to the one end of the beam. This is due to the hologram in which the one portion will act like a generator of plane wave and other portion will act like a generator of Gaussian vortex beam of topological charge

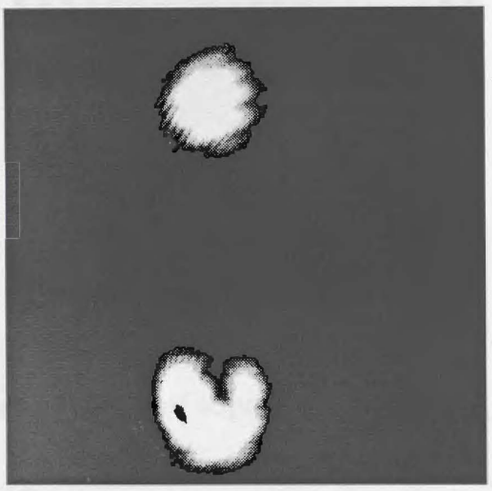

Figure 4.2: Experimental Diffraction pattern with beam of topological charge(1/2)

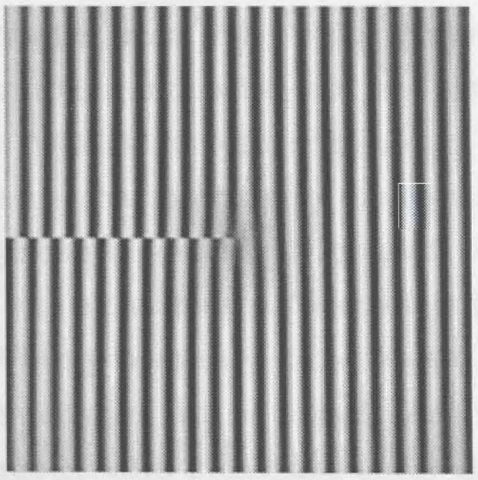

Figure 4.3: Gaussian vortex beam of topological charge $(-1/2)$ interfere with a plane wave.

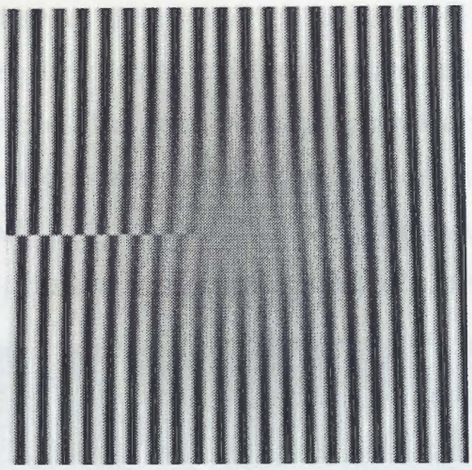

Figure 4.4: Gaussian vortex beam of topological charge $(-3/2)$ with a plane wave.

$(+1/2)$. They interfere with same propagation direction. The other side diffracted order is like a phase change of π of that line vortex. Experimental Diffraction pattern with beam of topological charge(1/2) is shown in Fig. 4.2. For example, it can be 1/2,1/3,1/8,or 3/8 . Interference patterns of topological charge $-1/2$ and $-3/2$ are shown in Fig. 4.3, 4.4 respectively.

4.1.1 Splitting of topological charge

When plane wave is diffracted from Holographic grating, phase and amplitude and frequency of the electromagnetic wave are modulated. Optical vortices are phase singularities in the field and recognized by a dark point where amplitude of the field vanishes. These are characterized by topological charge associated with them. Topological charge can be defined by number of intertwined fringe lines when a vortex interferes with a plane wave. Beams interfere with itself in shearing Sagnac interferometer. When propagation direction are same, there is no beating but only the two beam intensities will be added. At zero shear two beam topological charge will annihilate. With increasing shear given by glass block firstly two opposite fork will appear. Various order and sign of Gaussian vortex beam of topological charge i.e. +1,+2,+3 and -1,-2,-3 are produced in the diffraction patterns. We have selected a vortex of particular order through iris. Higher order topological charge are actually having as many number of single charge as the

order of the topological charge. They may be separated due to an unequal force on the vortices in opposite directions. In Mach-Zehnder interferometer that shear may be given by a lens placed at a particular propagation plane. With more shear between vortices more vortices are resolved into their individual vortices. From top to bottom, first two columns shows Fig. 4.5., topological charge two without splitting and with splitting in Mach-Zehnder interferometer.

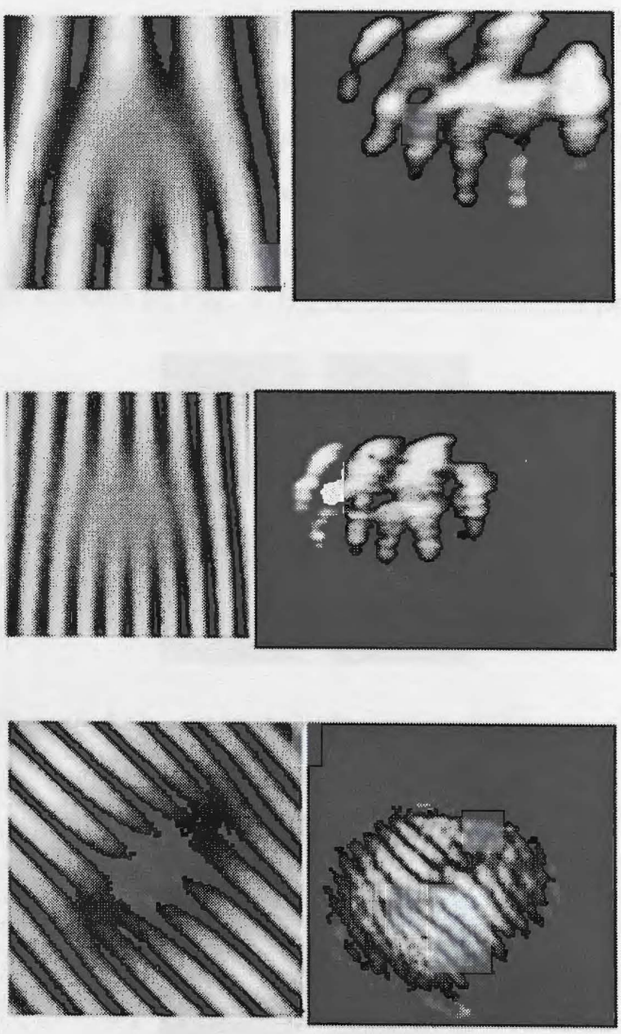

Figure 4.5: From top to bottom first two column figure shows topological charge two without splitting and with splitting in Mach-zehnder interferometer and third topological charge two splitting in shearing Sagnac Interferometer

4.1.2 Potential of optical vortices wave

The partial derivative with respect to coordinates η and ξ give potential of the vortex. A vortex amplitude is represented by its transverse electric field. How the potential of optical vortices are same as a diatomic molecule is explained in this chapter. How the potential differ from ordinary Gaussian and topological charge +1 and topological charge +2 vortices are described by figures. On both sides of the diffracted pattern opposite sign vortices with the increasing order or topological charge are produced. Partial derivative of this electric field in η and ξ for topological charge +1 and topological charge +2 vortex are taken to find respective potentials. It is observed that how the container of charge or so called potential change its position with shear and potential well is bigger for topological charge +2 than +1 as shown in Fig. 4.6 , 4.7. Equation of potential

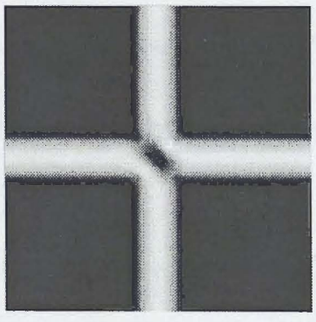

Figure 4.6: potential of vortex of charge +1

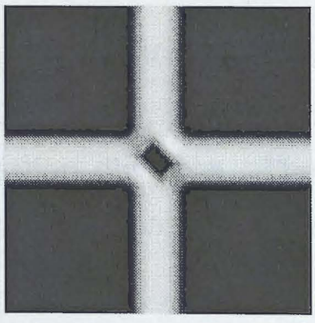

Figure 4.7: potential of vortex of charge +2

$$V = -\int E_\eta d\eta - \int E_\xi d\xi, \tag{4.1}$$

where η and ξ are two orthogonal coordinates of the light wave.

4.1.3 chirp of optical vortex

Lens effect produce chirp for a single beam in 2D. A line drawn on the surface for the same η and ξ coordinates is the chirp in 1D. Expression of a vortex or soliton at a plane that is propagating along z direction is

$$E(\eta,\xi) = C(\eta + i\xi)e^{-(\eta^2+\xi^2)/\sigma_0^2}e^{-ikz} \tag{4.2}$$

. where C is a scaling factor of intensity and σ_0 is the beam width. For simplicity we have taken C to be 1. Expression of beam with shifted vortex is

$$E(\eta,\xi) = ((\eta - \eta_0) + i(\xi - \xi_0))e^{-(\eta^2+\xi^2)/\sigma_0^2}e^{-ikz} \tag{4.3}$$

Expression of left shifted vortex or soliton with shifted beam without the phase associated with propagation direction is

$$A(\eta,\xi) = ((\eta - d_\eta) + i(\xi - d_\xi))e^{-((\eta-d_\eta)^2+(\xi-d_\xi)^2)/\sigma_0^2} \tag{4.4}$$

Expression of right shifted vortex with shifted beam without the phase associated with propagation direction is

$$B(\eta,\xi) = ((\eta + d_\eta) + i(\xi + d_\xi))e^{-((\eta+d_\eta)^2+(\xi+d_\xi)^2)/\sigma_0^2} \tag{4.5}$$

Interference between two beams having amplitude A and B is given by

$$I = |Ae^{-ikz} + Be^{-ik(z-\cos(\alpha)\eta-\sin(\alpha)\xi)}|^2 \tag{4.6}$$

In equation(4.6) chirp is given by $Be^{-ik(z-cos(\alpha)\eta-sin(\alpha)\xi)}$, where α is the angle in which one beam scans the other beam. This is 2D chirp. 1D chirp is given by when $\eta = \xi$. Z is the propagation direction. The fringe width depends on the interference plane from the beam-splitter and shear between the beams.

4.2 Topological charge inversion

4.2.1 Topological charge inversion by mirror

After passing through mirror Gaussian vortex of the structure $(\eta + i\xi)e^{-(\eta^2+\xi^2)/\sigma_0^2}e^{ik(z-\eta)}$ becomes $(\eta - i\xi)e^{-(\eta^2+\xi^2)/\sigma_0^2}e^{ik(z-\eta)}$. Hence the topological

charge +1 becomes -1 as observed by the set-up and shown in Fig. 4.8 and The results is given in Fig. 4.9. and corresponding theoretical Fig. 4.10. The exact physical reason is yet to be obtained. Though, from experimental figure, it is clear that the front side of wavefront becomes back side due to mirror reflection. This is against the ray optics.

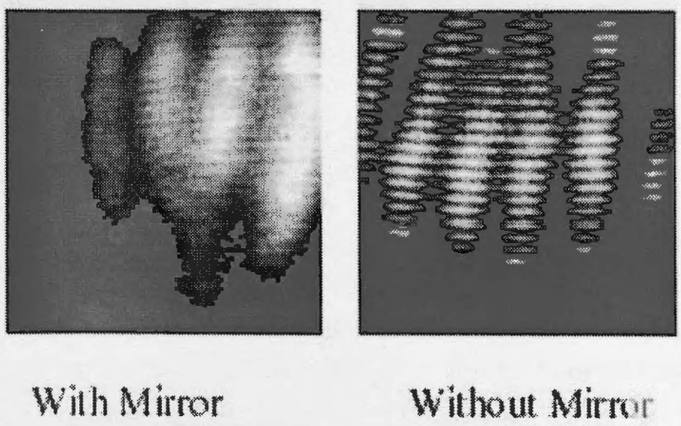

Figure 4.8: Experimental set-up for Topological charge inversion through a mirror

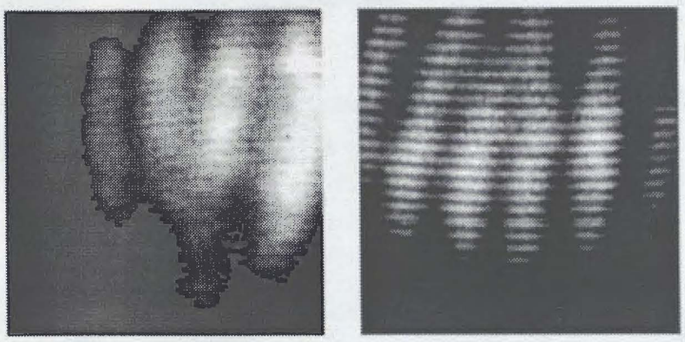

Figure 4.9: Experimental topological charge inversion through a mirror

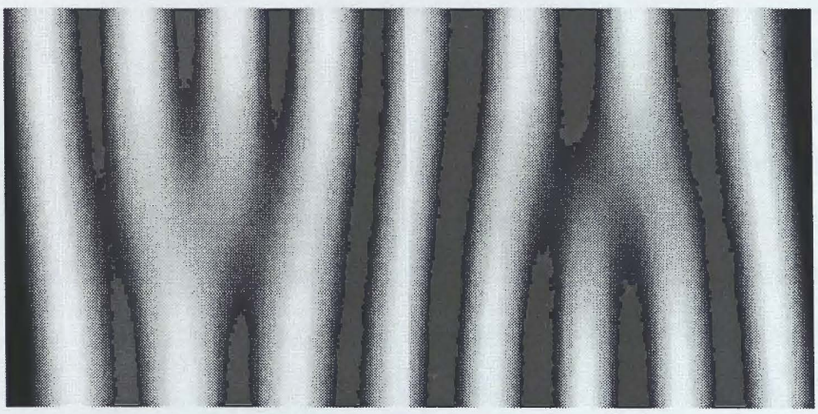

Figure 4.10: Theoretical topological charge inversion through a mirror

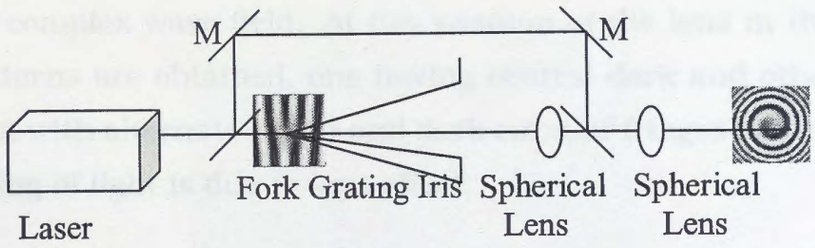

Figure 4.11: Experimental Set-up for interference of plane wave with a vortex of topological charge +1 passing through a lens.

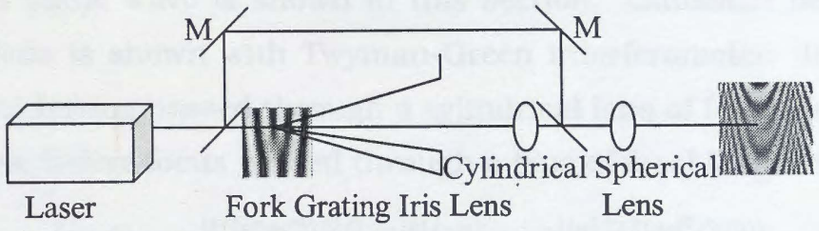

Figure 4.12: Experimental set-up for interference of plane wave with a vortex of topological charge +1 passing through a cylindrical lens and a spherical lens.

Similarly due to uneven focal length in η and ξ directions for a cylindrical lens, an elliptical phase as well as an elliptical intensity is generated at a plane. The phase of elliptical beam changes in angle of scan in η and ξ projection directions of other beam. Accordingly the curly fringe changes in orientation. When a Gaussian passing through a lens interferes with a plane wave or plane wave passing through a lens interferes with a Gaussian, a circular fringe rotating several cycle will appear in the interference pattern at zero shear. Very interestingly this pattern is having a dark or bright core depending upon the position of the lens from laser. Depending on the orientation of cylindrical lens or spherical lens of a particular focal length, from the other lens the horizontal and vertical focus will interchange their position in the propagation. Beam can be rotated by the same amount as the rotation of the lens. For example, if the cylindrical lens is rotated by 360^0 the fringe inverts twice and regains its original structure. The extra white patch of brightness in the interference fringe is due to use of a polarizer in front of a laser in the Twyman-Green interferometer. With a lens in front of polarizer, the Michelson interferometer is equivalent to Twyman-Green interferometer. Polarizer is a crystal and in a particular direction it can transmit more. It gives the

real part of a complex wave field. At two position of the lens in the propagation plane two patterns are obtained, one having central dark and other having central bright spot with alternate bright and dark circular fringes respectively. Hence circular bending of light is due to lens effect.

4.2.2 Topological charge inversion by spherical lens and cylindrical lens

Radial phase singularity inversion of Gaussian beam wavefront formed by interference with a plane wave is shown in this section. Gaussian beam can have inversion by lens is shown with Twyman-Green interferometer. Interference of Gaussian beam having passed through a cylindrical lens of focal length f1 and f2 with plane wave before focus passed through a lens of focal length f is given by,

$$I(\eta,\xi) = |e^{ik((\eta^2+\xi^2)/2f)}e^{-ik(z-\eta)} + e^{-((\eta^2/2f1+\xi^2/2f2))} e^{-ik(z-(\cos(\alpha)\eta^2/2f_1)+(\sin(\alpha)\xi^2)/2f_2)}|^2. \tag{4.7}$$

Interference of Gaussian beam having passed through a cylindrical lens of focal length f1 and f2 with a plane wave after focus, passed through a lens of focal length f is given by

$$I(\eta,\xi) = |e^{ik((\eta^2+\xi^2)/2f)}e^{-ik(z+\eta)} + e^{-((\eta^2/2f1+\xi^2/2f2))} e^{-ik(z-(\cos(\alpha)\eta^2/2f_1)+(\sin(\alpha)\xi^2)/2f_2)}|^2. \tag{4.8}$$

Equation for this interference for topological charge +1 is given by

$$I = ((\eta - d_\eta) + i(\xi - d_\xi))e^{-((\eta-d_{\eta/2})^2+(\xi-d_{\xi/2})^2/(\sigma_0)^2)} e^{ik(\eta^2+\xi^2)/(f-p)}e^{ikz} + ((\eta + d_\eta) + i(\xi + d_\xi))e^{-((\eta+d_{\eta/2})^2+(\xi+d_{\xi/2})^2/(\sigma_0)^2)} e^{ik(\eta^2+\xi^2)/(f+p)}e^{ik(z-\eta)} \tag{4.9}$$

, where p is the movement towards mirror of the spherical lens of focal length f.

The term associated with elliptical beam is elliptical phase and intensity. The difference in before focus and after focus is due to phase change of π or side of linear scan being opposite. where α is the angle in which one beam scans the other beam, z is the propagation distance. Gaussian beam gives two possible structures of interference. One is having the central fringe dark and other is having

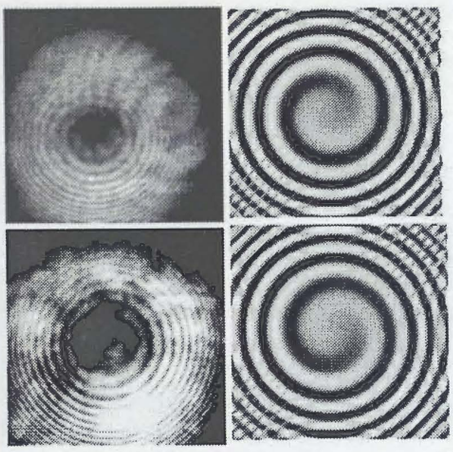

Figure 4.13: Interference of plane wave with a vortex of topological charge +1 passing through a lens before (top) and after focus (bottom) without shear

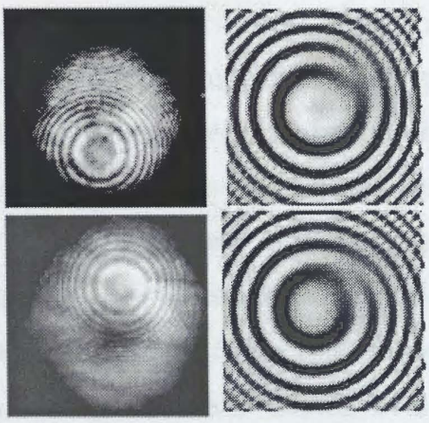

Figure 4.14: Interference of plane wave with a vortex of topological charge +1 passing through a lens before (top)and after focus (bottom) with shear.

the central fringe bright depending on the shear and propagation distance from laser to beam-splitter. Similarly a Gaussian beam passed through a lens and interfering with a plane wave gives two possible structures. One is having a central dark core with circular alternating bright and dark fringes and other is having central bright core with circular alternating dark and bright fringes depending upon the propagation distance of the lens from the laser. Experimental Set-up for interference of plane wave with a vortex of topological charge +1 passing through a lens is shown in Fig. 4.11. As light propagates in particular direction, it can be considered as a vector. Interference depends on the how one beam scans the

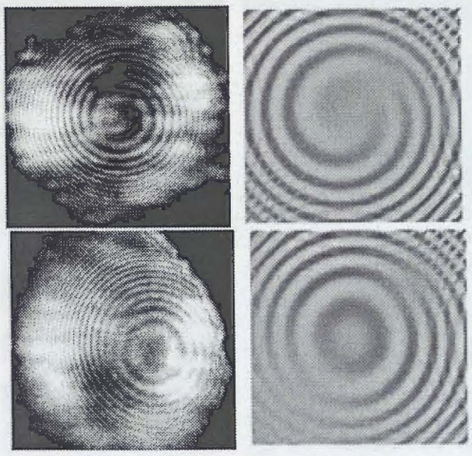

Figure 4.15: Interference of plane wave with a vortex of topological charge +2 passing through a lens with less and more shear.

other beam. A beam can scan the other beam horizontally or vertically or at any angle. In a shearing Sagnac interferometer though path difference is zero two beams can interfere even if there is no lens to image it. Only if there propagation directions are different such that one beam scans the other beam, interference will take place. Otherwise if the propagation direction is same two beams do not scan one another. As a result only intensities are added up and hence there is no interference to take place. In case of Mach-Zehnder interferometer two arms are having of different path lengths, as a result one beam diverges more compared to the other due to a spherical phase. Hence two beams interfere and give curly fringes, within the limit that beam in the longer arm diverges as much as the other beam, one can show at zero shear and same propagation direction two beams intensities are just added up. With increasing shear given by glass block firstly alternate bright and dark fringe will appear in the center. Experimental set-up for interference of plane wave with a vortex of topological charge +1 passing through a cylindrical lens and a spherical lens as shown in Fig. 4.12. A HG beam is equivalent to a plane wave having a constant z dependence or a scaling in intensity. Pattern does not change at a plane but only plane wave will be bigger in size at large propagation distance. One of the applications of studying such elliptical Gaussian interference, spherical Gaussian interference or hyperbolic Gaussian interference is to trap and rotate two dimensional spheri-

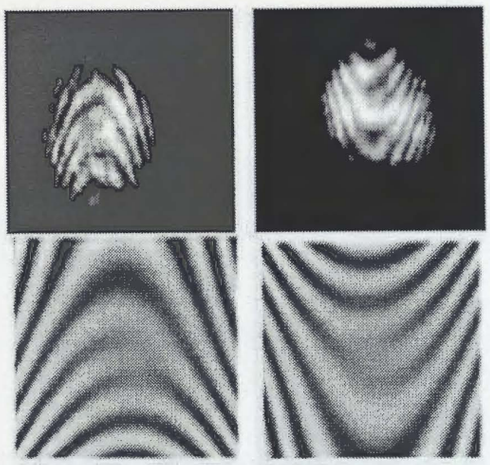

Figure 4.16: Interference of a vortex of topological charge -1 passing through a cylindrical lens and a plane wave passing through a spherical lens with before (top) and after focus (bottom).

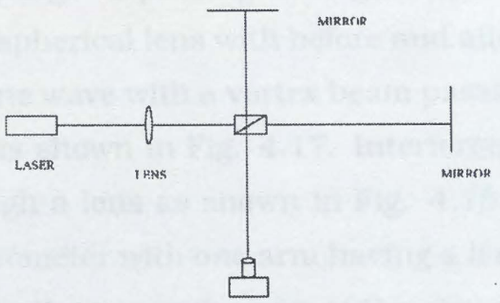

Figure 4.17: Experimental set-up interference of plane wave with a Gaussian passing through a lens in Twyman Green interferometer.

cal, elliptical or hyperbolic micro organism without heating inside the dark core. The elliptical beam changes its orientation by 360^0 after placing the spherical lens at a suitable distance from the cylindrical lens. Interference of plane wave with a vortex of topological charge +1 passing through a lens before and after focus without shear as shown in Fig. 4.13. Otherwise the rotation is π only. Interference of plane wave with a vortex of topological charge +1 passing through a lens before and after focus with shear as shown in Fig. 4.14. Interference of plane wave with a vortex of topological charge +2 passing through a lens with less and more shear is shown in Fig. 4.15. A spherical lens introduces a spherical phase in the Gaussian beam. When spherically diverging Gaussian beam interfere with a plane wave, the plane wave scans the space of Gaussian beam. Interference of

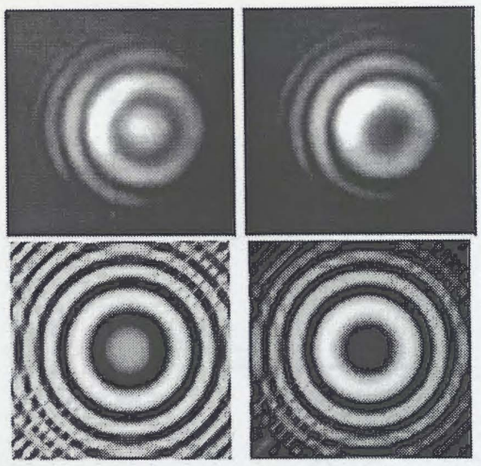

Figure 4.18: Interference of plane wave with a Gaussian passing through a lens.

a vortex of topological charge -1 passing through a cylindrical lens and a plane wave passing through a spherical lens with before and after focus is shown in Fig. 4.16. Interference of plane wave with a vortex beam passing through a cylindrical lens and spherical lens is shown in Fig. 4.17. Interference of plane wave with a Gaussian passing through a lens as shown in Fig. 4.18. Experimental setup of shearing Sagnac interferometer with one arm having a lens is shown in Fig. 4.19.

The lens introduced in the triangular arm of the shearing Sagnac interferometer produces radial shear between two beams according to its movement towards two opposite directions of the mirror. One of the experimental interference pattern of the above mentioned setup when lens is towards one side of the mirror is shown in Fig. 4.20. Hence divergence of the two beams in magnitude gets reversed. As a result curvature of the one beam compared to the other increases on movement in one direction compared to the other direction. When the lens is placed in the middle, the curvature of two beams is in the same ratio and fringes becomes less curved. One of the theoretical interference pattern of the above mentioned setup with vortex of topological charge +1 when lens is towards one side of the mirror is shown in Fig. 4.21. One of the experimental interference pattern of the above mentioned setup with topological charge +2 with shear when lens is nearly middle of the two mirrors is shown in Fig. 4.22. One of the theoretical interference pattern of the above mentioned setup with topological charge +2 with shear when lens is nearly middle of the two mirrors is shown in Fig. 4.23. The more the

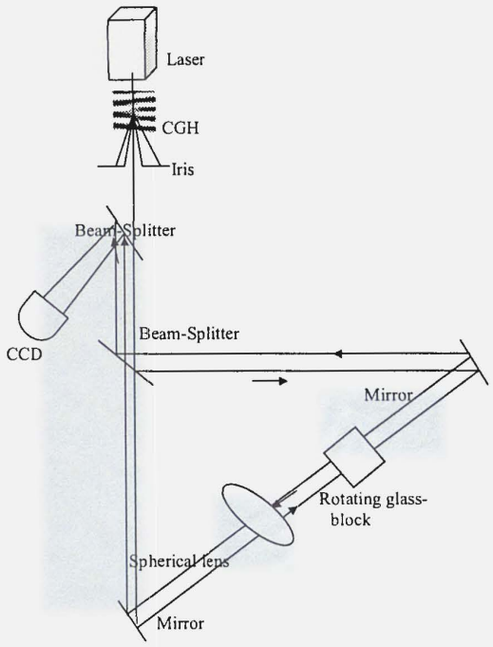

Figure 4.19: Experimental setup of shearing Sagnac interferometer with one arm having a lens.

movement of the lens towards the mirror the fringe looks more curve or circular. Even two same topological charges in the same beam get reversed in sign due to lens effect. While spherical lens move from one mirror to other mirror topological charge of the combined beam (interference pattern) gets inverted. Point of inversion is the center of the arm.

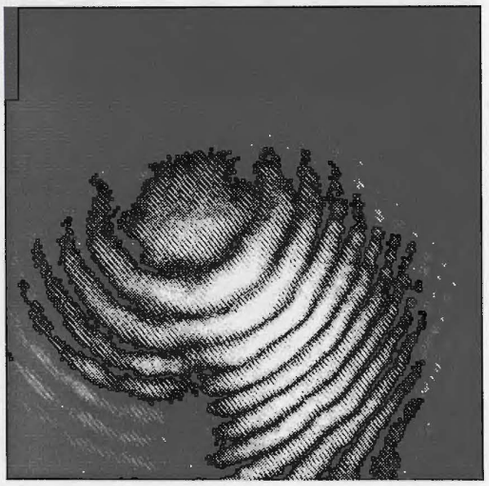

Figure 4.20: Experimental interference pattern of the above mentioned setup when lens is towards one side of the mirror for Gaussian vortex beam.

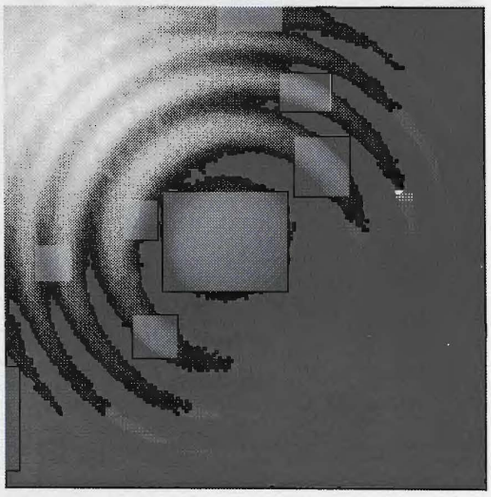

Figure 4.21: Theoretical interference pattern of the above mentioned setup with vortex of topological charge +1 when lens is towards one side of the mirror.

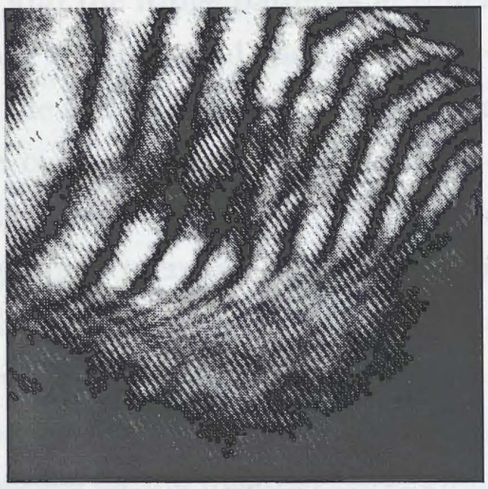

Figure 4.22: Experimental interference pattern of vortex beam introduced in the above mentioned setup with topological charge +2 with shear when lens is nearly middle of the two mirrors.

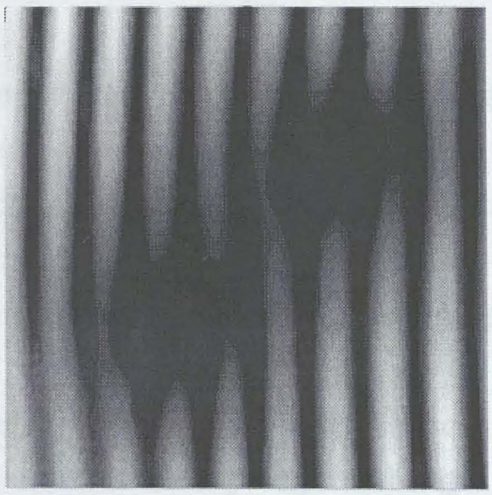

Figure 4.23: Theoretical interference pattern of the vortex beam introduced in the above mentioned setup with topological charge +2 with shear when lens is nearly middle of the two mirrors.

4.3 Interaction of optical vortices

The experimental set up and the fringe patterns at different shears for Gaussian and Gaussian vortex beam of topological charge +1 and +2 are given in Fig. 4.27. Shear is calculated from the formula of shift of ray passing through a glass block. At zero shear two same charge vortex beam annihilate (middle portion of the middle fringe gets erased). It is different from annihilation of charge of each-other. With higher shear, fringe lines increase between two opposite forks and fringe width decreases. In the two opposite charge vortex-vortex interaction charges are added. Shear is given by 20 mm glass block both horizontally and as well as vertically at the same time. Higher topological charge in a vortex acts like individual topological charges sitting together. Breaking of higher order vortex in the individual orders is due to shear in the vortex core and this shear can also be given by lens in the plane of propagation. For example, topological charge +2(-2) interacting with -1(+1) give topological charge +3(-3) interference pattern at zero shear are shown and +1 and -1 interaction give topological charge two fringe. With increasing shear in the vortex core degeneracy gets uplifted and higher order charges get resolved into individual charge fringe. The annihilation of topological charges occurs at zero shear. The above experimental observations can be summarized as

sum rule: Opposite topological charge of different sign vortices of different or same orders are additive;

subtraction rule: topological charge of similar sign vortices of orders(different or same) are subtractive;

annihilation rule:At zero shear same topological charge of same sign vortices of same order annihilate;

splitting rule: The higher topological charge vortices are single charge sitting together as many as the order of the topological charge;

shear rule: The more the shear is the more the separation among beams and vortices simultaneously at shearing Sagnac interferometer and given by expression to calculate shear.

If the fork is upward then it is positive topological charge. If it is downward

then it is negative topological charge. If the scanning is on the negative side of other beam topological charge +1 interfering with plane wave gives upward fork. If the scanning is from positive side of other beam in the give downward fork in the interference pattern. Interferograms were recorded through a CCD by rotating the glass block in Shearing Sagnac interferometer in both the transverse directions and rotating the screws of Beam-splitter for Mach-Zehnder interferometer. The observed interferograms are shown in Fig. 4.24. For illustration, given below the

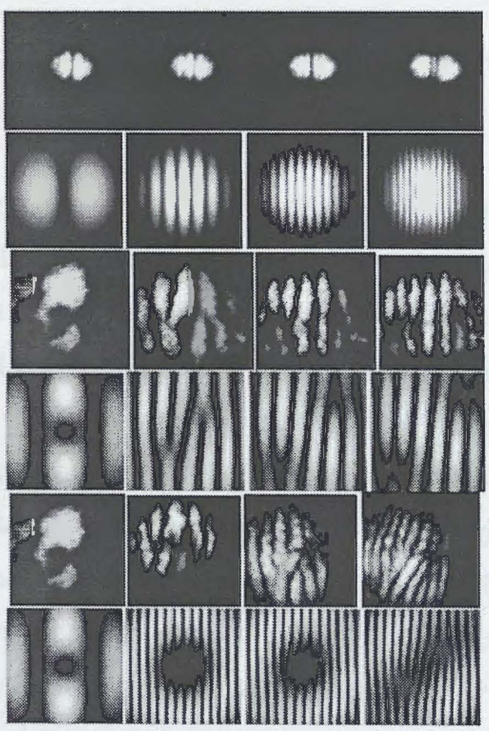

Figure 4.24: Interference fringes with increasing shear for Gaussian, 1st order and second order Gaussian vortex beams with experiment and theory(bottom row) for each respectively

equation used to simulate the fringe pattern produced when a beam with charge +1 vortex interacts with another beam having charge +1 vortex.

$$I = |E_1^*((\eta, d_\eta, \xi, d_\xi, z)E_1((\eta, d_\eta, \xi, d_\xi, z)| +$$
$$|E_2^*((\eta, d_\eta, \xi, d_\xi, z - \eta\cos(\alpha) - \xi\sin(\alpha)))E_2((\eta, d_\eta, \xi, d_\xi, z - \eta\cos(\alpha) - \xi sin(\alpha)))| +$$
$$E_1^*((\eta, d_\eta, \xi, d_\xi, z))E_2((\eta, d_\eta, \xi, d_\xi, z - \eta\cos(\alpha) - \xi sin(\alpha))) +$$
$$E_2^*((\eta, d_\eta, \xi, d_\xi, z - \eta\cos(\alpha) - \xi\sin(\alpha)))E_1((\eta, d_\eta, \xi, d_\xi, z)), \quad (4.10)$$

where I is the intensity of the interference fringe pattern. E_1 and E_2 are fields

for beams with vortex of charge +1 having lateral shifts in η and ξ coordinates. The shear $d_{\eta,\xi}$ in E_1 is in the negative direction in η and ξ while in E_2 it is in the positive direction.

$$E_1 = ((\eta - d_\eta/2) + i(\xi - d_\xi/2))e^{(-((\eta-d_\eta/2)^2+(\xi-d_\xi/2)^2)/\sigma_z^2)} e^{(ik((\eta-d_\eta/2)^2+(\xi-d_\xi/2)^2)/2R)} e^{-ikz} \tag{4.11}$$

and

$$E_2 = ((\eta + d_\eta/2) + i(\xi + d_\xi/2))e^{(-((\eta+d_\eta/2)^2+(\xi+d_\xi/2)^2)/\sigma_z^2)} e^{(ik((\eta+d_\eta/2)^2+(\xi+d_\xi/2)^2)/2R)} e^{-ik(z-\eta\cos(\alpha)-\xi\sin(\alpha))}, \tag{4.12}$$

where α is scanning angle and σ_z beam is diameter at a distance z from the focus. R is the equivalent focal length of the grating. In Fig. 4.25 row 1 shows the interference pattern obtained when a charge +1 vortex interacts with a charge -1 vortex without shear and after introducing the shear. The interaction changes as the shear is introduced. Similarly row 3 shows the interference patterns corresponding to charge +2 interacting with charge -2. The rows 2 and 4 are corresponding theoretical plots. Bessel vortex beam of charge +(1/2) and -(1/2) give topological charge +1 topological charge interference pattern within Bessel beam and Bessel beam interference structure. This phenomena is similar for Gaussian vortex beam of +(1/2) interfering with Gaussian vortex beam of fractional topological charge -(1/2) giving a topological charge 1 interference pattern.

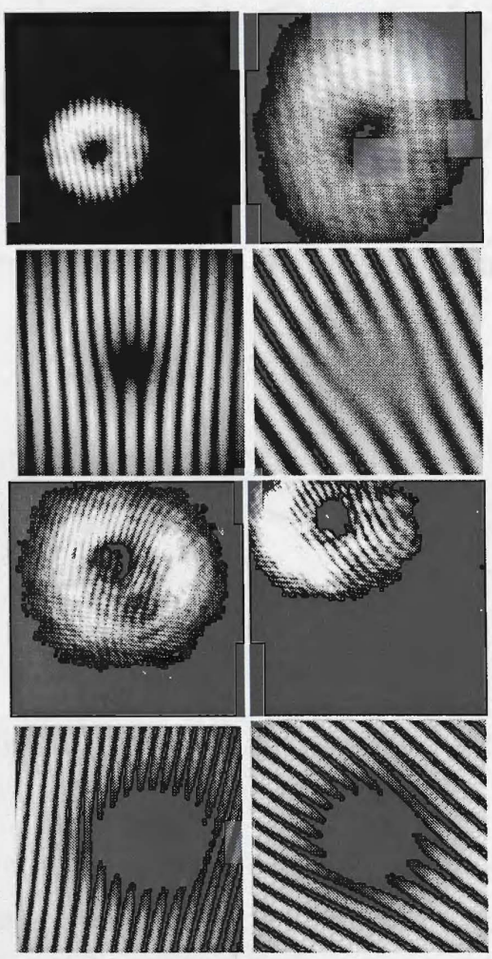

Figure 4.25: Interferograms for vortex-vortex interaction - charge +1 with charge -1 (Rows 1 (experiment) and 2 (theory), left: without shear, right: with shear), charge +2 with charge -2 (Rows 3 (experiment) and 4 (theory), left: without shear, right: with shear)

4.4 White Light Interferometry

White light interference is done by using the full complex function for vortex and plane wave. First write how do you produce white light vortex. We

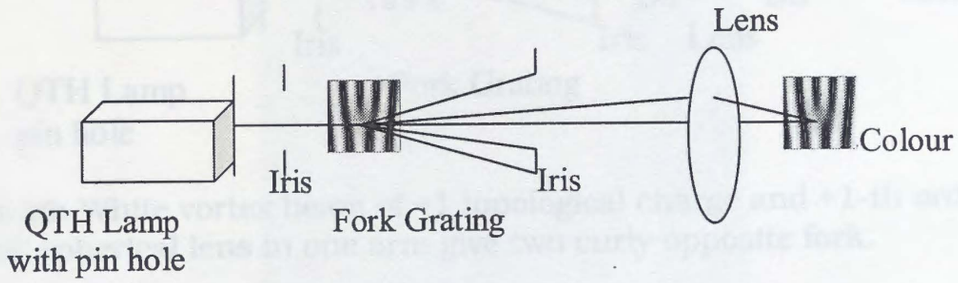

Figure 4.26: White vortex beam of +1 charge and plane wave interference.

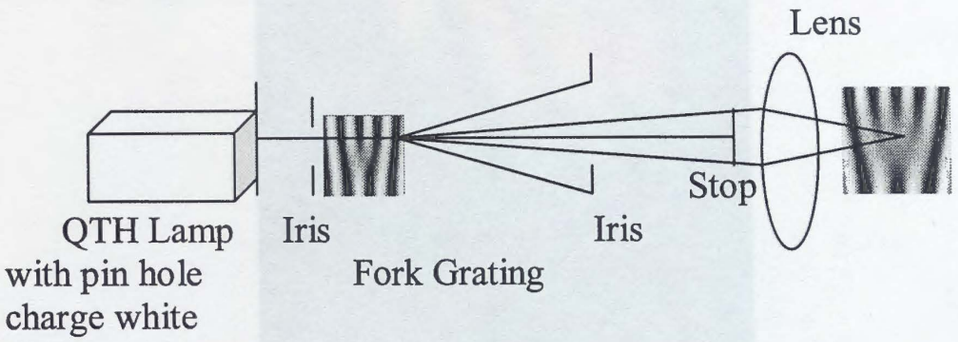

Figure 4.27: White vortex beam of +1 charge and -1 charge interference give charge two.

have used complex contour or complex density plot to simulate the vortex, the colour distribution consisting red, green, yellow and blue. We have seen that with the change of wavelength colour distribution changes. All the existing theory for monochromatic light vortex is valid for colour vortex. Visibility of fringes in the interference is almost 1. White vortex beam of +1 charge and plane wave interference is shown in Fig. 4.26. White vortex beam of +1 charge and -1 charge interference give charge two is shown in Fig. 4.27. White vortex beam of +1 topological charge and 0-th order interference with lens in one arm give curly fork, is shown in Fig. 4.28. Experimental colour interference pattern of Gaussian vortex beam with a plane wave, giving a fork like pattern, is shown in Fig. 4.29. Theoretical colour interference pattern of Gaussian vortex beam with a plane wave,giving

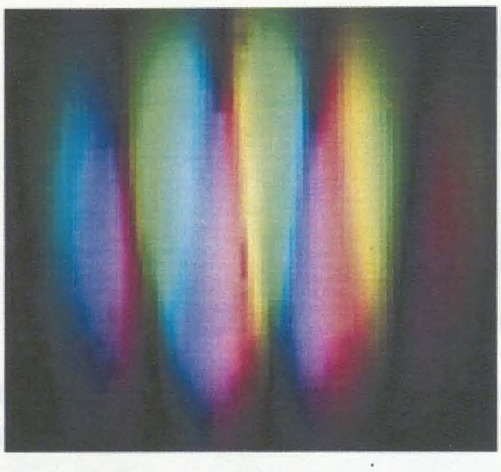

Figure 4.30: Theoretical colour interference pattern of Gaussian vortex beam with a plane wave, giving a fork like pattern.

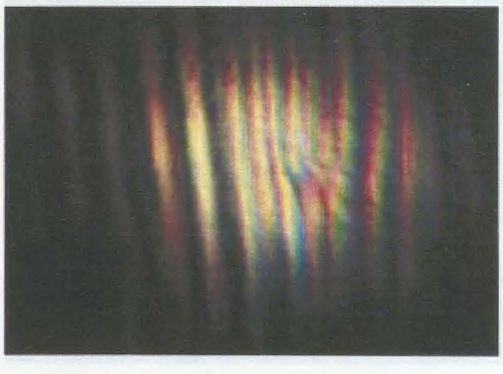

Figure 4.31: Splitting of topological charge two.

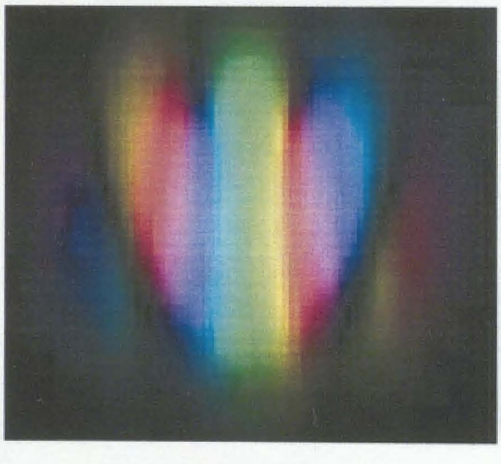

Figure 4.32: Theoretical interference pattern of topological charge two with a plane wave.

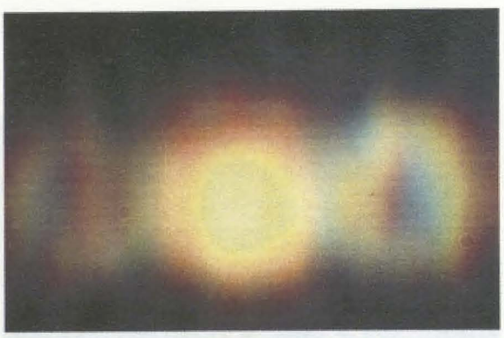

Figure 4.33: Experimental diffraction pattern of spatial coherent white light from a forked holographic grating.

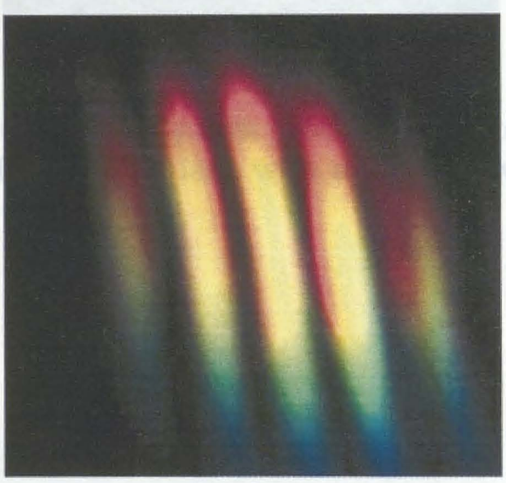

Figure 4.34: Experimental fringe pattern for a plane wave interfering with another plane wave.

Figure 4.35: Experimental Interference pattern of topological charge +2 with a plane wave.

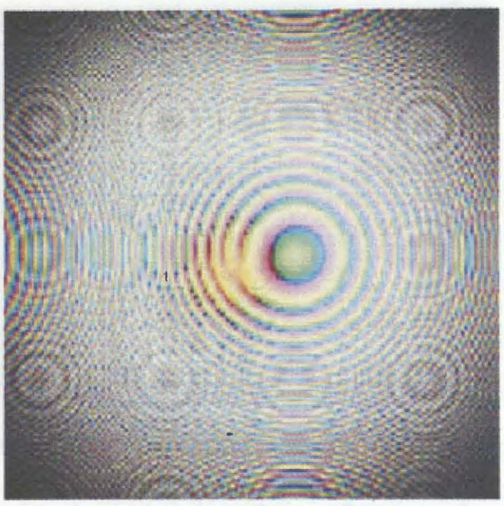

Figure 4.36: Theoretical colour curly fork produced due to interference of a Gaussian vortex beam passed through a lens with a plane wave.

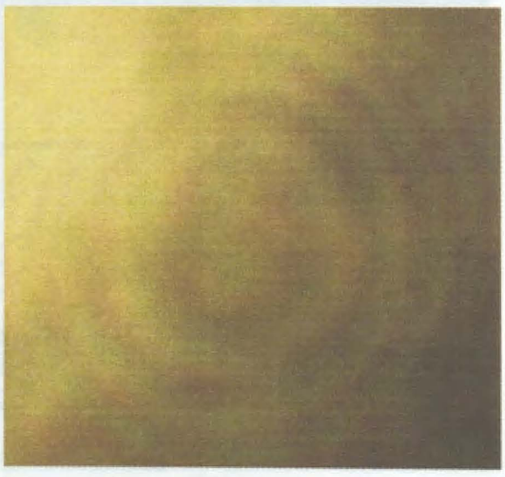

Figure 4.37: Experimental colour curly fork produced due to interference of a Gaussian vortex beam passed through a lens with a plane wave.

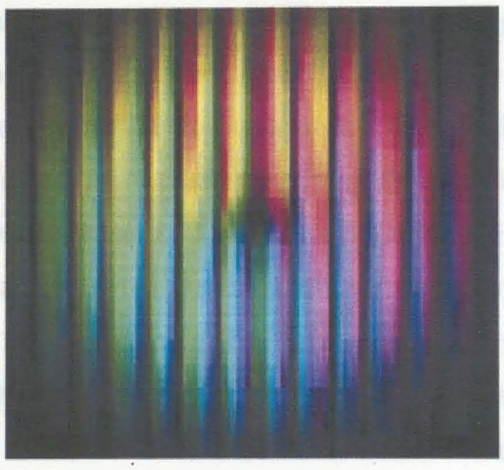

Figure 4.38: Annihilation at due to zero shear for topological charge +1 and topological charge +1 interaction (theoretical).

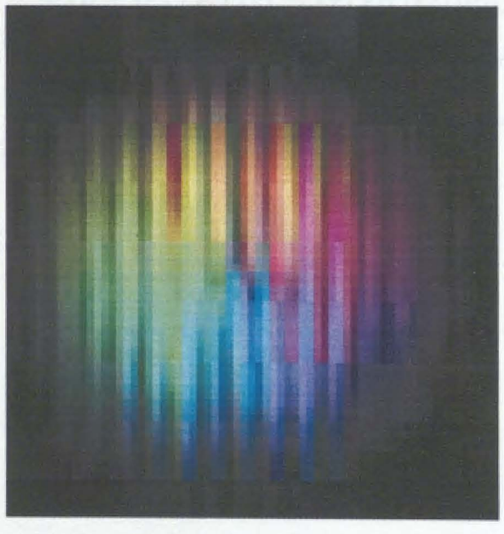

Figure 4.39: Topological charge +1 and topological charge +1 interaction at shear(theoretical).

4.5 Bessel beam, Bessel vortex beam and associated interferences

Bessel vortex beam is the association of vortices with integer and fractional topological charges with Bessel beam. As we know vortices are closely associated with Laguerre beams. One can form Bessel-Laguerre beam of various superposition of Bessel and Laguerre function. Similarly, Bessel-Laguerre vortex beam can be formed with various superposition of Bessel and Laguerre function with vortices. Their interference are studied with itself, with various topological charges, with plane wave and passing through spherical lens of particular focal length. Vortex is nothing but phase singularity or phase indeterminacy when real and imaginary part is zero and it is the tear in the wavefront. True wave front can be obtained or phase singularities can be eliminated by nonzero intensity at the center of the vortex and practically this is the situation. Interference of two Bessel vortex beams with each other is given below

$$
\begin{aligned}
I = |&(\eta + i\xi)^l (Ef/(1 + iz/zR)) J(|m|, u2) \\
&e^{(-(((\eta+d_\eta)^2+(\xi+d_\xi)^2)/\sigma_0^2)/(1+iz/zR))} \\
&e^{(ikz(1-((Sin(\alpha))^2/(2(1+iz/zR)))))} e^{(im\phi)} \\
e^{(-ik(z))} &+ (\eta + i\xi)^l (Ef/(1 - iz/zR)) J(|m|, u1) \\
&e^{(-(((\eta-d_\eta)^2+(\xi-d_\xi)^2)/\sigma_0^2)/(1+iz/zR))} \\
&e^{(-ik(z)(1-((Sin(\alpha))^2/(2(1+iz/zR)))))} e^{-im\phi} \\
&e^{-ik(z-\eta)}|^2
\end{aligned}
\tag{4.13}
$$

Chapter 5

Wigner function of optical vortex:

In recent years optical vortices have found variety of applications. The study of their coherence properties, therefore becomes very important. Wigner distribution function (WDF)originally discovered in quantum mechanics,can be quite useful for this purpose. Since it can provide coherence information in terms of the joint position and momentum (direction) phase space distribution of the optical field. In fact, the WDF has already been applied to study properties of an electron and magnetic field in various optical systems. Here, we present experimental results for the Wigner distribution function (WDF) of an optical vortex and show that they are in agreement with theoretical results.

5.1 Introduction of Wigner function

Wigner function is given by

$$W(\eta,\xi,p_\eta,p_\xi) = \int\int \Gamma(\eta,\xi,d_\eta,d_\xi)e^{-i(p_\eta d_\eta + p_\xi d_\xi)}dd_\eta dd_\xi$$

where $\Gamma(\eta,\xi,d_\eta,d_\xi)$ is the mutual correlation function of a particular object beam. It satisfies the following properties

$$\int W(\eta,\xi,p_\eta,p_\xi,z)dp_\eta dp_\xi = |E(\eta,\xi,z)|^2 \tag{5.1}$$

$$\int W(\eta,\xi,p_\eta,p_\xi,z)d\eta d\xi = |E(p_\eta,p_\xi,z)|^2 \tag{5.2}$$

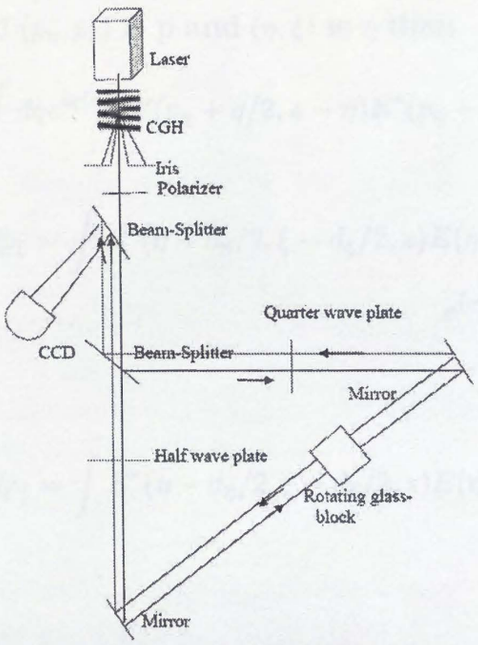

Figure 5.1: Experimental shearing Sagnac set-up to calculate Wigner function used

where,$|E(p_\eta, p_\xi, z)|^2$ is intensity in momentum space. For proof see the Appendix. where q and m are wave vector of the field.

$$E(\eta + d_\eta/2, \xi + d_\xi/2, z - \eta)d\eta d\xi = \int dq e^{iq(\eta+d_\eta/2,\xi+d_\xi/2)} E(q, z - \eta) \tag{5.3}$$

$$E^*(\eta - d_\eta/2, \xi - d_\xi/2, z - \eta)d\eta d\xi = \int dq e^{-im(\eta-d_\eta/2,\xi-d_\xi/2)} E^*(m, z) \tag{5.4}$$

Then

$$W(\eta, \xi, p_\eta, p_\xi, z) = \int\int dq e^{iq(\eta+d_\eta/2,\xi+d_\xi/2)} E(q, z - \eta)$$
$$\int dm e^{-im(\eta-d_\eta/2,\xi-d_\xi/2)} E^*(m, z) e^{-i(p_\eta d_\eta + p_\xi d_\xi)} dd_\eta dd_\xi \tag{5.5}$$

$$W(\eta, \xi, p_\eta, p_\xi, z) = \int dq dm \delta(p_\eta - q/2 - m/2, p_\xi - q/2 - m/2)$$
$$e^{-i(q-m)(\eta,\xi)} E(q, z - \eta) E*(m, z) \tag{5.6}$$

If q is $2(p_\eta, p_\xi) - m$ then

$$W(\eta, \xi, p_\eta, p_\xi, z) = \int dm e^{2i(p_\eta,p_\xi)-m)(\eta,\xi)}$$
$$E(2(p_\eta, p_\xi) - m, z - \eta) E^*(m, z) \tag{5.7}$$

Let $(p_\eta, p_\xi) - m$ is $q/2$ and (p_η, p_ξ) is p and (η, ξ) is η then

$$W(\eta, \xi, p_\eta, p_\xi, z) = \int dq e^{iq(\eta,\xi)} E(p_\eta + q/2, z - \eta) E^*(p_\eta - q/2, z) e^{(-iq(\eta,\xi))} \tag{5.8}$$

$$\int W(\eta, \xi, p_\eta, p_\xi, z) dp_\eta dp_\xi = \int E^*(\eta - d_\eta/2, \xi - d_\xi/2, z) E(\eta + d_\eta/2, \xi + d_\xi/2, z - \eta) e^{(-ip_\eta d_\eta + p_\xi d_\xi)} dd_\eta dd_\xi dp_\eta dp_\xi \tag{5.9}$$

$$\int W(\eta, \xi, p_\eta, p_\xi, z) dp_\eta dp_\xi = \int E^*(\eta - d_\eta/2, \xi - d_\xi/2, z) E(\eta + d_\eta/2, \xi + d_\xi/2, z - \eta) \delta(d_\eta, d_\xi) dd_\eta dd_\xi \tag{5.10}$$

$$\int W(\eta, \xi, p_\eta, p_\xi, z) dp_\eta dp_\xi = E^*(\eta, \xi, z) E(\eta, \xi, z - \eta) \tag{5.11}$$

$$\int W(\eta, \xi, p_\eta, p_\xi, z) d\eta d\xi = \int dq E^*(p - q/2, z) E(p - q/2, z - x) e^{-iq(\eta,\xi)} d\eta d\xi \tag{5.12}$$

$$\int W(\eta, \xi, p_\eta, p_\xi, z) d\eta d\xi = \int dq E^*(p - q/2, z) E(p - q/2, z - \eta) \delta(q) \tag{5.13}$$

q is zero then

$$\int W(\eta, \xi, p_\eta, p_\xi, z) d\eta d\xi = E^*(p, z - \eta) E(p, z) \tag{5.14}$$

$$\int W(\eta, y, p_\eta, p_\xi, z) d\eta d\xi = E^*(p, z - \eta) E(p, z) \tag{5.15}$$

If the field propagate in the same direction then

$$\int W(\eta, \xi, p_\eta, p_\xi, z) d\eta d\xi = |E(p_\eta, p_\xi)|^2 \tag{5.16}$$

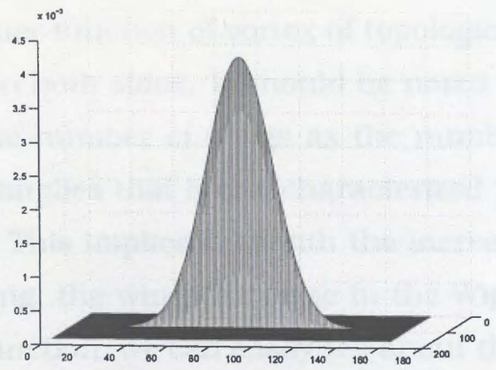

Figure 5.2: Theoretical Wigner function for Gaussian

5.2 Experimental determination of Wigner function

Experimental set-up of shearing Sagnac interferometer used to calculate Wigner function is given in Fig. 5.1. Electromagnetic wave equation for a plane wave passing through a scattering vortex potential, which is for example $\eta^2 + \xi^2$, gives solution that is product of two hermite polynomials in two dimension of order m+n-u and u and where u runs from 0 to m+n and in case of diffraction m runs from 0 to an integer and n runs from any integer to 0. With suitable combination of phases in front of Hermite polynomials, gives a solution of positive ($m < n$) and negative ($m > n$) orders of vortices with central Gaussian at $m = n$. This is because in associated Laguerre polynomial $L_p^l = 1$ for $l = 1$ and $p = 0$. When plane wave is diffracted from holographic grating, phase and amplitude of the electromagnetic wave are modulated. First time, I have calculated interferometrically Wigner function for vortex beam of topological charge +1 and +2 and compared these structures with that of Gaussian beam. Wigner function is calculated from complex mutual coherence function by taking a fourier transform of it. A procedure to find Wigner function for different beams is given in this chapter. How an apparent 4D Wigner function becomes a 2D is explained. We have various order and sign of vortex i.e. +1,+2,+3 and -1,-2,-3 in the diffraction pattern. We have selected through iris a vortex of particular order and interfere it with itself in shearing Sagnac interferometer. These interference fringes are used to find complex mutual correlation function. It is seen that Wigner function of Gaussian is a Gaussian. Wigner function of vortex of topological charge +1 is an Airy pattern

with one side lobe. Wigner function of vortex of topological charge +2 is Airy pattern with 2 side lobes on both sides. It should be noted that Gaussian is having no side wing. The same number of wings as the number of topological charge in the Wigner function implies that it can characterized the topological charge of Gaussian vortex beam. This implies that with the increase of scattering angle or photon path in scattering, the wings increase in the Wigner function. Therefore looking at the Wigner function, we can easily tell about the scattering depth. This information is useful in medical imaging to find the the depth of scatterer. Wigner function also give the information about naturally existing pattern recognition. Hence, Wigner function can give full information related to scattering depth and pattern recognition. It has an application in optical interconnect as guiding light beam and images in the vortex core. The images can be extracted simply by interfering it with a plane wave. Its phase wavefront (image of the scatterer) can be obtained if the beam scans with itself. When propagation directions are same there is no beating but only the two beam intensities will be added. At zero shear topological charges of two beams will annihilate with each other. With increasing shear given by glass block first two opposite forks will appear. With more shear intermediate fringe lines will appear between two opposite forks. The phase of mutual coherence function gives a pattern of a mutual coherence function of one step higher order vortex. Since Gaussian vortex beam divergence is 0.844^o, we have taken a term in the solution $e^{ik((\eta^2+\xi^2)/2R)}$ where k is $2\pi/\lambda$, λ is the wavelength and R is the equivalent focal length of the grating like a diverging lens. The concept behind this is that the diffracted beams are like rays coming from infinity, forming image near focal point and the image is grating. If the grating width is more the equivalent focal length will be less and divergence will be more. Hence the effective focal length is nearly zero. But we have taken it like 0.0002 cm. Calculation remains same and all possible structures remains same at the cost of intensity when the beam diverges.

Expression of a vortex is

$$E = ((\eta - \eta_0) + i(\xi - \xi_0))e^{-(\eta^2+\xi^2)/\sigma_z^2} e^{ik((\eta^2+\xi^2)/2R)} e^{-ik_1 z - iw_1 t} \tag{5.17}$$

As two Gaussian vortex beams of same frequency are interfered, frequencies of

two beams i.e. w_1 and w_2 are same and t is the time. Hence k_1 and k_2 are same and is equal to k. But for Mach-Zehnder interferometer vortex and HG beams pass through different optical elements, hence the patterns are not stable with time compared to shearing Sagnac interferometer. Considering same frequency (homodyne) vortex interference it is correct to omit the frequency part in the expression. Hence the expression for simplicity can be written as

$$E = ((\eta - \eta_0) + i(\xi - \xi_0))e^{-(\eta^2+\xi^2)/\sigma_z^2} e^{ik((\eta^2+\xi^2)/2R)} e^{-ikz} \tag{5.18}$$

where C is a scaling factor of intensity and σ_0 is the beam width at the initial propagation plane. σ_z is the beam width at propagation plane z. Where σ_z is σ_0* tan(γ)and σ_0 is the width at a initial propagation plane, γ is divergence angle, R is the equivalent focal length. For simplicity we have taken C to be 1. Expression of beam with shifted vortex is

$$E = ((\eta - \eta_0) + i(\xi - \xi_0))e^{-(\eta^2+\xi^2)/\sigma_z^2} e^{ik((\eta^2+\xi^2)/2R)} e^{-ikz} \tag{5.19}$$

Expression of left shifted vortex with shifted beam is

$$E_1 = ((\eta - d_\eta) + i(\xi - d_\xi))e^{-((\eta-d_\eta)^2+(\xi-d_\xi)^2)/\sigma_z^2} e^{ik(((\eta-d_\eta)^2+(\xi-d_\xi)^2)/2R)} e^{-ikz} \tag{5.20}$$

Expression of right shifted vortex with shifted beam is

$$E_2 = ((\eta + d_\eta) + i(\xi + d_\xi))e^{-((\eta+d_\eta)^2+(\xi+d_\xi)^2)/\sigma_z^2} e^{ik(((\eta+d_\eta)^2+(\xi+d_\xi)^2)/2R)} e^{-ik(z-\cos(\alpha)\eta-\sin(\alpha)\xi)} \tag{5.21}$$

$$\begin{aligned} I = |E_1(\eta - d_\eta, \xi - d_\xi, z)|^2 + |E_2(\eta + d_\eta, \xi + d_\xi, z - (\cos(\alpha)\eta + \sin(\alpha)\xi))|^2 + \\ E_1^*((\eta, d_\eta, \xi, d_\xi, z))E_2((\eta, d_\eta, \xi, d_\xi, z - \eta\cos(\alpha) - \xi\sin(\alpha))) + \\ E_2^*((\eta, d_\eta, \xi, d_\xi, z - \eta\cos(\alpha) - \xi\sin(\alpha)))E_1((\eta, d_\eta, \xi, d_\xi, z)) \end{aligned} \tag{5.22}$$

$$I = |E_1(\eta - d_\eta, \xi - d_\xi, z)|^2 + |E_2(\eta + d_\xi, \xi + d_\xi, z - \eta\cos(\alpha) - \xi\sin(\alpha))|^2$$
$$+E_1^*(\eta - d_\eta, \xi - d_\xi, z)E_2(\eta + d_\eta, \xi + d_\xi, z - \eta\cos(\alpha) - \xi\sin(\alpha))$$
$$+E_2^*(\eta + d_\eta, \xi + d_\xi, z - \eta\cos(\alpha) - \xi\sin(\alpha))E_1(\eta - d_\eta, \xi - d_\xi, z) \quad (5.23)$$

At zero shear two beams intensities are added up,

$$I_0 = |E_1(\eta, \xi, z)|^2 + |E_2(\eta, \xi, z)|^2. \quad (5.24)$$

This is equal to sum of intensities at different shear. This is due to energy conservation.

$$I_0 = |E_1(\eta - d_\eta, \xi - d_\xi, z)|^2 + |E_2(\eta + d_\eta, \xi + d_\xi, z - \eta\cos(\alpha) - \xi\sin(\alpha))|^2 \quad (5.25)$$

Hence the mutual coherence function from interference is described by

$$(I - I_0) = E_1^*(\eta - d_\eta, \xi - d_\xi, z)E_2(\eta + d_\eta, \xi + d_\xi, z - \eta\cos(\alpha) - \xi\sin(\alpha))$$
$$+E_2^*(\eta + d_\eta, \xi + d_\xi, z - \eta\cos(\alpha) - \xi\sin(\alpha))E_1(\eta - d_\eta, \xi - d_\xi, z) \quad (5.26)$$

In our experiment d_η and d_ξ are given together for a single image frame and by applying both the shear, η and ξ move in same amount due to symmetry. Individual shear is the average of the total shear. Let us find out mutual coherence function Γ_1 from the the interference pattern discussed above. We assume a function M whose real part is M_1 and imaginary part is M_2 i.e. $M = M_1 + iM_2$.

$$M_1 = (I - I_0)/2 \quad (5.27)$$

when phase is changed by 90^0 $\cos(k\eta\cos(\alpha) + k\xi\sin(\alpha))$ becomes $\sin(k\eta\cos(\alpha) + k\xi\sin(\alpha))$ and $\sin(k\eta\cos(\alpha) + k\xi\sin(\alpha))$ becomes $\cos(k\eta\cos(\alpha) + k\xi\sin(\alpha))$. Substituting this we get imaginary part M_2. $M_1 + iM_2$ is equal to Γ provided $(\xi d_\eta - \eta d_\xi)$ is zero. As net shear in individual beam is shift in η or ξ.

$$\eta = \sum d_\eta \quad (5.28)$$

$$\xi = \sum d_\xi \quad (5.29)$$

and as we are giving both shear together for a single image frame, the combined shear becomes d_η or d_ξ,

$$d_\eta = d_\xi \quad (5.30)$$

Hence $(\xi d_\eta - \eta d_\xi)$ is zero. Alternatively, experimentally and theoretically, E_1 and E_2 interference pattern is same in changing sides of two equal beams, means positive shear becomes negative shear and then negative scanning becomes positive scanning. Doing that we get,

$$E_2^*(\eta - d_\eta, \xi - d_\xi)E_1(\eta + d_\eta, \xi + d_\xi)e^{i(k\eta\cos(\alpha)+k\xi\sin(\alpha)} = E_2^*(\eta + d_\eta, \xi + d_\xi)E_1(\eta - d_\eta, \xi - d_\xi)e^{-i(k\eta\cos(\alpha)+k\xi\sin(\alpha)} \quad (5.31)$$

$$E_2^*(\eta - d_\eta, \xi - d_\xi)E_1(\eta + d_\eta, \xi + d_\xi)e^{i(k\eta\cos(\alpha)+k\xi\sin(\alpha)} = E_1^*(\eta - d_\eta, \xi - d_\xi)E_2(\eta + d_\eta, \xi + d_\xi)e^{i(k\eta\cos(\alpha)+k\xi\sin(\alpha)} \quad (5.32)$$

Then we can take substitution of this equal term. Initially we used polarizer and retardation plates in our experiment at the same axes, we get real part of it,

$$\Gamma_1 = Re|E_1^*(\eta - d_\eta, \xi - d_\xi)E_2(\eta + d_\eta, \xi + d_\xi)e^{i(k\eta\cos(\alpha)+k\xi\sin(\alpha))}|. \quad (5.33)$$

Later,half-wave plate is rotated by 45^0. Then the phase of the two beams compared to the earlier two beams is changed 90^0. Then separable phase is also changed by 90^0. Then imaginary part of mutual correlation function is obtained. It is seen the intensity change from rotating plates and rotating by 90^0. This is due to polarization explained in 2D.

$$\Gamma_2 = Im|E_1^*(\eta - d_\eta, \xi - d_\xi)E_2(\eta + d_\eta, \xi + d_\xi)e^{i(k\eta\cos(\alpha)+k\xi\sin(\alpha))}| \quad (5.34)$$

$$\Gamma = M_1 + iM_2 \quad (5.35)$$

then

$$M_1 = \Gamma_1 \quad (5.36)$$

$$M_2 = \Gamma_2 \quad (5.37)$$

$$\Gamma_1(\eta, \xi, d_\eta, d_\xi) = Re|E_1^*(\eta - d_\eta, \xi - d_\xi)E_2(\eta + d_\eta, \xi + d_\xi)e^{(ik\eta\cos(\alpha)+ik\xi\sin(\alpha))}| \quad (5.38)$$

Hence imaginary part of complex mutual coherence function Γ_2.

$$\Gamma_2(\eta, \xi, d_\eta, d_\xi) = Im|E_1^*(\eta - d_\eta, \xi - d_\xi)E_2(\eta + d_\eta, \xi + d_\xi)e^{(ik\eta\cos(\alpha)+ik\xi\sin(\alpha))}| \quad (5.39)$$

Complex mutual coherence function is defined by

$$\Gamma = \Gamma_1 + i\Gamma_2 \tag{5.40}$$

Hence as E_1 and E_2 are same and otherwise, due to symmetry of the problem the contribution from the term $(\xi d_\eta - \eta d_\xi)$ is zero. Hence total mutual coherence function is written as

$$\Gamma = E_1^*(\eta - d_\eta, \xi - d_\xi)E_2(\eta + d_\eta, \xi + d_\xi)e^{(ik\eta\cos(\alpha)+ik\xi\sin(\alpha))} \tag{5.41}$$

Wigner function is given by

$$W(\eta, \xi, p_\eta, p_\xi) = \int \Gamma e^{-i(p_\eta d_\eta + p_\xi d_\xi)} dd_\eta dd_\xi \tag{5.42}$$

Mutual correlation function of Gaussian is written as,

$(\sigma_0/\sigma_z)e^{-ikz+iArcTan[z/zR]-((\eta+d_\eta/2)^2+(\xi+d_\xi/2)^2)/(\sigma_z^2)-ik((\eta+d_\eta/2)^2+(\xi+d_\xi/2)^2)/(2R_z)}(\sigma_0/\sigma_z)e^{+ikz+iArcTan|}$

Wigner distribution function of Gaussian beam is written as,

$(e^{((1/2(((-p_\eta^2)\sigma_z^2+2ik\eta+(2kp_\eta\sigma_z^2\eta)/R_z-(4\eta^2)/\sigma_z^2-(k^2\sigma_z^2\eta^2)/R_z^2-(4\xi^2)/\sigma_z^2-(\sigma_z^2((p_\xi R_z-ky))^2)/R_z^2-2ArcTan[(\eta-z)/zR]}$
$e^{+2iArcTan(z/zR)})))))\sigma_0^2)$.

Theoretical Wigner function for Gaussian is shown in Fig. 5.2. Few Experimental and theoretical real and imaginary data for complex mutual coherence function at different shear from complete data set for calculation of Wigner function for Gaussian beam at a propagation plane of 200 cm from grating is shown in Fig. 5.3. Experimental Wigner function for Gaussian is Fig. 5.4. Theoretical expression for Wigner distribution function for topological charge +1 without divergence consideration is given by,

$((1/64)(2\pi)e^{((-(1/8))((p_\eta^2+p_\xi^2))\sigma_0^2+ik\eta-(2\eta^2)/\sigma_0^2-(2\xi^2)/\sigma_0^2)}\sigma_0^2((((p_\eta^2+p_\xi^2))$
$\sigma_0^4 - 8\sigma_0^2((1+p_\xi\eta-p_\eta\xi)) + 16((\eta^2+\xi^2))))).$

Theoretical expression for Wigner distribution function for topological charge +1 with divergence consideration is given by,

$(((1/(64R^2))((e^{((-(1/8))((p_\eta^2\sigma_0^2+p_\xi^2\sigma_0^2-8ik\eta+(4kp_\eta\sigma_0^2\eta)/R+(4kp_\xi\sigma_0^2\xi)/R+(4((4R^2+k^2\sigma_0^4))((\eta^2+\xi^2)))/(R^2\sigma_0^2))))$
$\sigma_0^2((4kR\sigma_0^4((p_\eta\eta+p_\xi\xi)) + 4k^2\sigma_0^4((\eta^2+\xi^2))$
$+ R^2((((p_\eta^2+p_\xi^2))\sigma_0^4 - 8\sigma_0^2((1+p_\xi\eta-p_\eta\xi)) +$
$16((\eta^2+\xi^2))))))Erf(1/(Sign(\sigma_0)))^2)))))$. In that case,in position space the value of

R is 0.0002. But momentum space (Wigner distribution function) the value of R is nearly 100 c.m.

$$d_\eta = d_\xi = 0 \tag{5.43}$$

in mutual coherence function. This is why η, ξ are not variable in the Wigner distribution function and this is responsible for constant complex contribution. With increasing shear two beams are separated. But with the change of d_η and d_ξ, η and ξ changes. As fourier transform is over d_η and d_ξ and $\eta$and ξ is constrained over $d_\eta$and d_ξ. Hence net change of η is sum of d_η and similarly net change of $\xi$is sum of d_ξ. Each and every point in the beam shifted equally with each particular shear value. So at zero shear each point of the two beam is zero position in displacement. Hence dimension reduction is due to the constrained terms d_η and d_ξ with η and ξ in mutual coherence function. Hence we have able to calculate apparent 4D Wigner function by substituting

$$\eta = \sum d_\eta \tag{5.44}$$

$$\xi = \sum d_\xi \tag{5.45}$$

in the theoretical plot of Wigner function. Hence the plot becomes a 3D plot in 2D. Hence their is a complex part of mutual coherence function depending on the how d_η and d_ξ move. But due to symmetry Wigner distribution function remain same in interchanging two beams. Theoretical phase of mutual coherence function of order +1 is shown in Fig. 5.5. Experimental phase of mutual coherence function of order +1 is shown in Fig. 5.6. Few Experimental and theoretical real and imaginary data from complete data set for calculation of Wigner function for vortex of topological charge +1 at a propagation plane of 190 c.m. from grating is shown in Fig. 5.7. Few experimental and theoretical real and imaginary data from complete data set for calculation of Wigner function for vortex of topological charge +1 at a propagation plane of 215 cm. from grating is shown in Fig. 5.8. Theoretical fourier transform of Wigner function for vortex of topological charge +1 in 2D for constant η and ξ and the more η and ξ the separation between vortices increases is shown in Fig. 5.9. Experimental fourier transform of Wigner function for vortex of topological charge +1 in 2D is shown in Fig. 5.10. Experimental fourier transform of Wigner function for vortex of topological charge

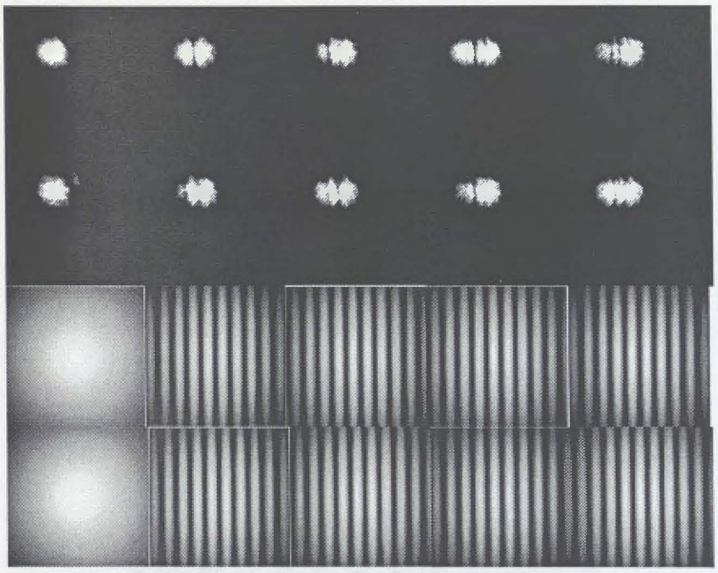

Figure 5.3: Few Experimental and theoretical real and imaginary data for complex mutual coherence function at different shear from complete data set for calculation of Wigner function for Gaussian beam at a propagation plane of 200 cm. from grating.

+1 in 2D in contour plot and it shows charge +1 vortex beam gets charge +2 is shown in Fig. 5.11. Theoretical Wigner function of Gaussian beam at 200 cm is shown in Fig.5.12. Theoretical Wigner function of vortex of topological charge +1 at 190 cm is shown in Fig. 5.13. The Wiggles in the Wigner distribution function can be reduced by taking smaller steps in shear values and making the discrete data nearly continuous. In our experimental calculation α is taken as zero. Means scanning is horizontal. If the experimental fringe tilt is there that fringe is

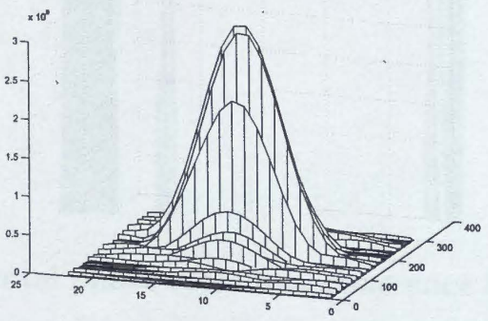

Figure 5.4: Experimental Wigner function for Gaussian

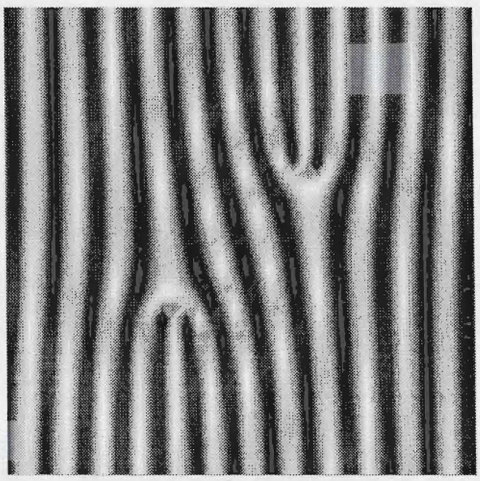

Figure 5.5: Theoretical phase of mutual coherence function of order +1

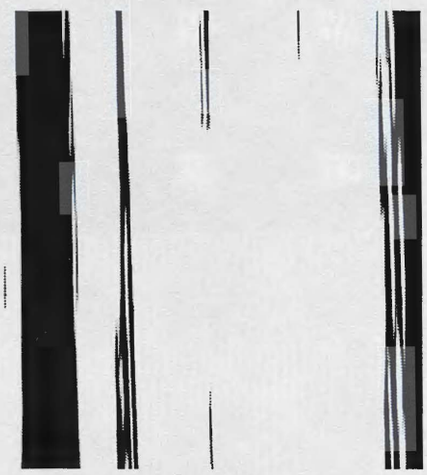

Figure 5.6: Experimental phase of mutual coherence function of order +1

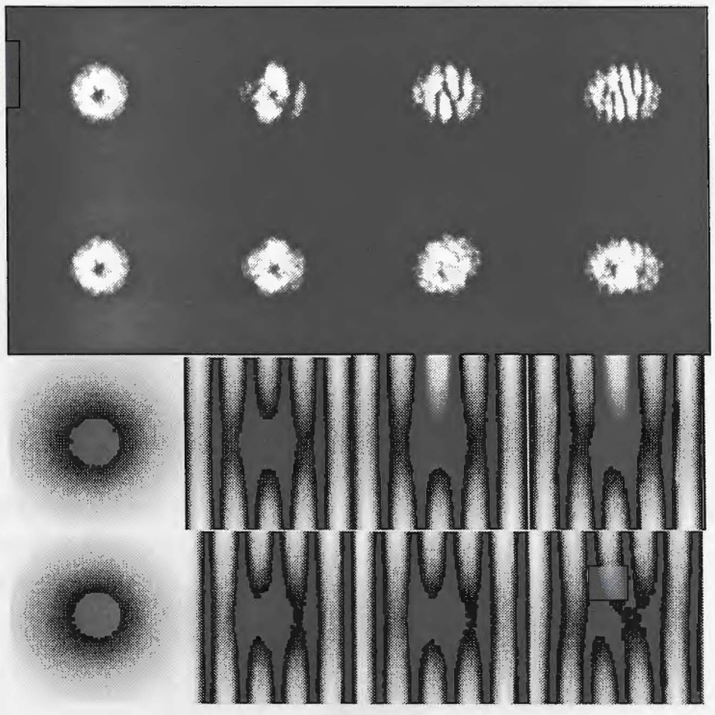

Figure 5.7: Few Experimental and theoretical real and imaginary data from complete data set for calculation of Wigner function for vortex of topological charge +1 at a propagation plane of 190 c.m. from grating.

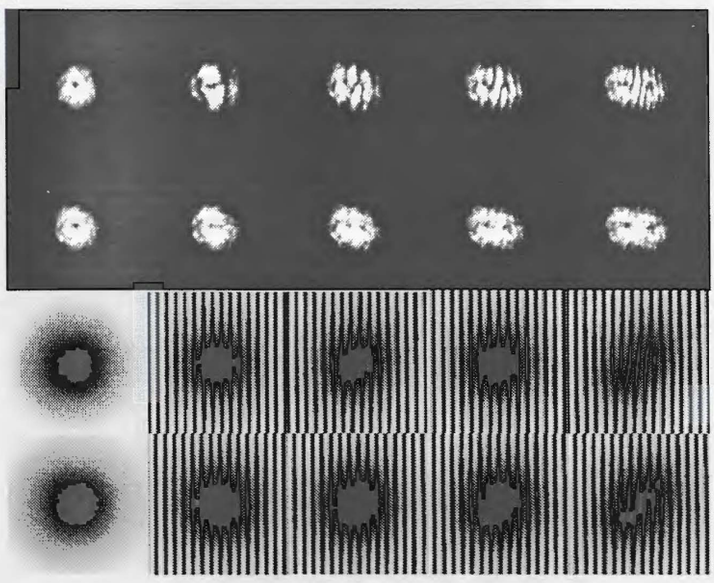

Figure 5.8: Few Experimental and theoretical real and imaginary data from complete data set for calculation of Wigner function for vortex of topological charge +1 at a propagation plane of 215 cm. from grating.

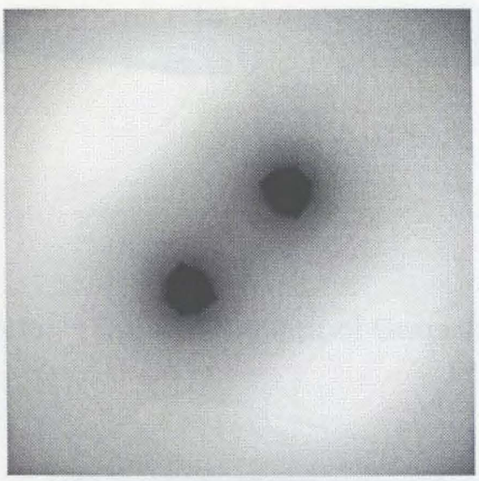

Figure 5.9: Theoretical fourier transform of Wigner function for vortex of topological charge +1 in 2D for constant η and ξ and the more η and ξ the separation between vortices increases

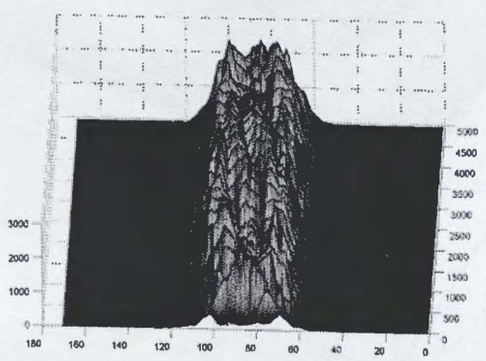

Figure 5.10: Experimental fourier transform of Wigner function for vortex of topological charge +1 in 2D

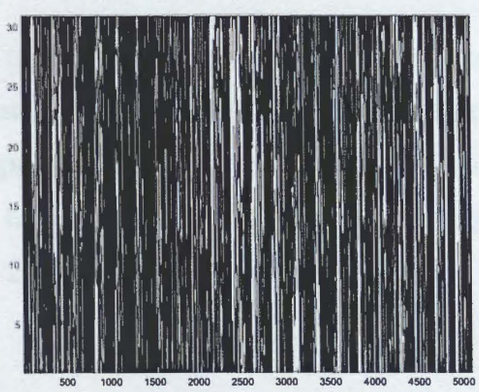

Figure 5.11: Experimental fourier transform of Wigner function for vortex of topological charge +1 in 2D in contour plot and it shows charge +1 vortex beam gets charge +2

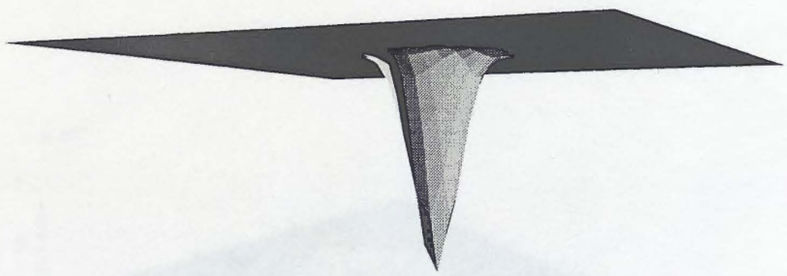

Figure 5.12: Theoretical Wigner function of Gaussian beam at 200 cm.

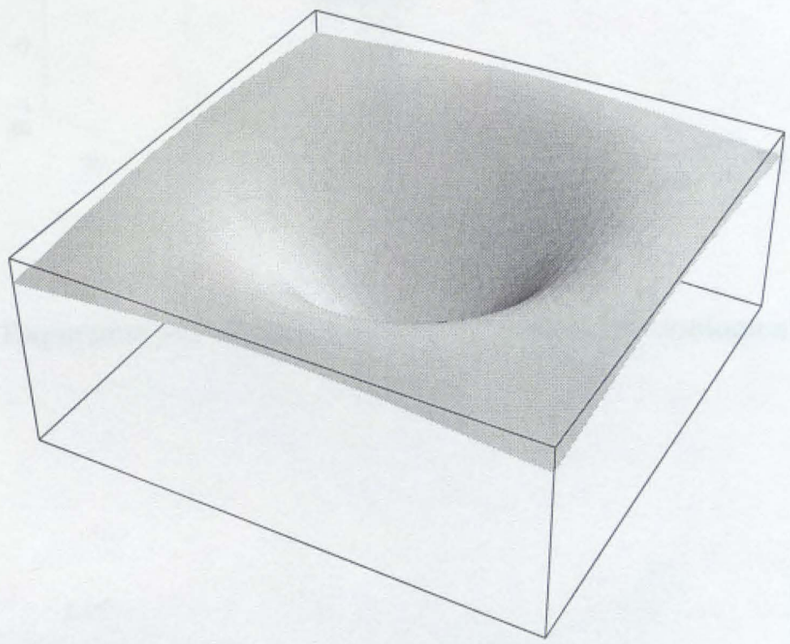

Figure 5.13: Theoretical Wigner function of vortex of topological charge +1 at 190 cm.

made horizontal. In the equation dx and dy is substituted with d_η and d_ξ. Hence kirkwood definition of phase space and Wigner function merge in the same footing with our calculation. Experimental Wigner function of vortex of topological charge +1 at 190 cm is shown in Fig. 5.14. Experimental Wigner function of vortex of topological charge +1 at 215 cm is shown in Fig. 5.15.

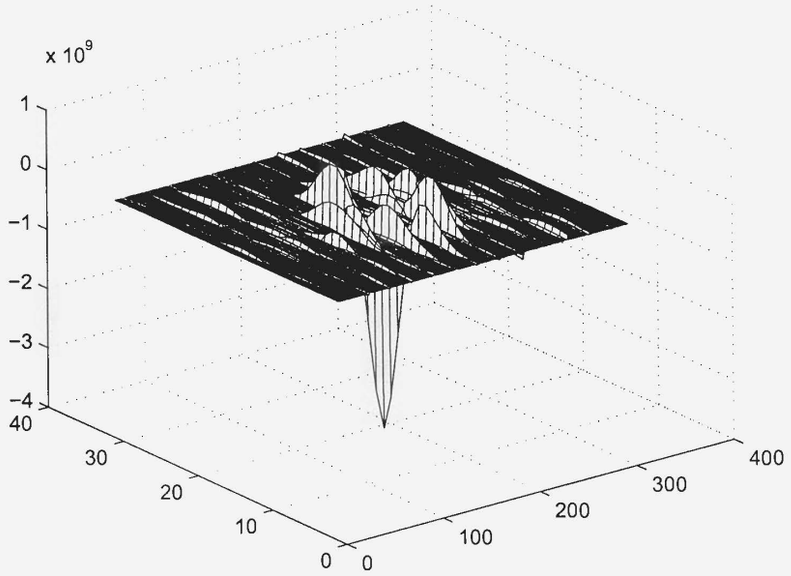

Figure 5.14: Experimental Wigner function of vortex of topological charge +1 at 190 cm.

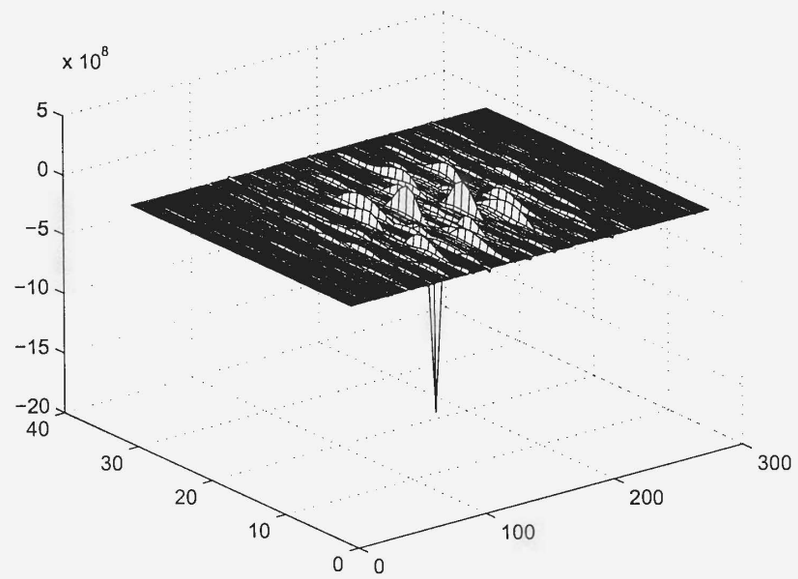

Figure 5.15: Experimental Wigner function of vortex of topological charge +1 at 215 cm.

5.3 Intensity and momentum distribution retrieval from Wigner function

Intensity in position space from Wigner function in position space is defined by

$$I(\eta,\xi) = \int W(p_\eta, p_\xi) dp_\eta dp_\xi \tag{5.46}$$

Experimentally, dp_η and dp_ξ can be calculated from fourier transform of d_η and d_ξ, as d_η and d_ξ are changes in η and ξ. Then the function is calculated by performing the integration by multiplying Wigner function with dp_η and dp_ξ. Similarly intensity in momentum space(phase) is defined by

$$\phi(p_\eta, p_\xi) = \int W(p_\eta, p_\xi) d\eta d\xi \tag{5.47}$$

Discrete fourier transform is done with the condition of changing shear in very a small steps such that image of vortex-vortex interaction is not changed effectively. Hence the data points in fourier transformed space are very close and smoothen the data grid. Then we have joined this grid data that gives result very close to the continuous fourier transform. It is observed that the position space area of Gaussian, vortex of topological charge +1 and vortex of charge +2 increases respectively, intensity gets decreased. The difference between theory and experimental scaling (C) is due to CCD gain and due to use of different software for theoretical and experimental plot. Now, since position space and momentum space are conjugate variables, intensity in the position space can be used to find intensity in momentum space. Although it is not possible to calculate it experimentally from the WDF in our experimental set-up since for finding the WDF, η and ξ are taken constants. It is seen that intensity cannot be fully retrieve experimentally with beam dimension limit. As it is taken in CCD, hence Wigner distribution is 2D. As it is momentum distribution, not a phase space, hence phase cannot be retrieved from Wigner distribution function. In 4D Wigner distribution function is phase space distribution.

5.4 Coherence properties through Wigner function

The coherence is studied through shearing Sagnac Interferometer. Wigner distribution function is calculated at two propagation distances. It is seen that distribution remains same for the two cases, except that at 190 cm. the peak and side airy wings are shorter compared to at 215 cm., indicating less intensity at the center as the beam propagates. Wigner function of topological charge +1 at two propagation planes, 190 cm. and 215 cm. from grating is calculated. At a small distances of propagation two beams are more coherent than at large distances. If the beams are more coherent Wigner function gives a better resolution in structure. This is because in momentum space and position space distribution are vice-versa. As beams become more coherent with smaller distances and separation, the Wigner distribution becomes narrower in momentum distribution. With propagation distance coherence of the beam becomes poorer. Fourier transform of Wigner function of topological charge +1 gives vortex beam of topological charge +2. Similarly fourier transform of Wigner function of topological charge +2 vortex is a topological charge +4 vortex. It depends upon the total shear in the mutual coherence function and constant η and ξ. Theoretical fourier transform of Wigner function for vortex of topological charge +1 for constant η and ξ. Experimental fourier transform of Wigner function for vortex of topological charge +1 in 2D. Experimental fourier transform of Wigner function for vortex of topological charge +1 in contour plot and it shows charge +1 vortex beam gets charge +2.

Chapter 6

Application

It has been discussed earlier that the wave equation with a scattering potential can give solutions in the form of vortex or Bessel beam. For light beam this potential is provided by computer generated holograms or other diffractive optical elements. Taking the analogy, for atomic beam similar potential can be created by interfering light beams to get atomic vortex or atomic Bessel beams. However, in this chapter we will be discussing about application of vortices and their study to implementation of logic gates, optical imaging and in developing an understanding of some of the natural phenomena.

6.1 Implementation of logic gates

In chapter 4, we have seen that charge inversion of an optical vortex with various optical elements. This charge inversion can be translated into NOT gate immediately. Here, we show that using a beam splitter (that transmits as well as reflects a beam), lenses and mirrors, one can implement an optical controlled NOT (CNOT) gate based on the charge inversion of an optical vortex.

6.2 Optical imaging

Imaging of scatterer in the diffraction regime is the interference of diffracted patterns with right proportion of intensities that can be made by our proposed set up of using a lens to combine the reflected or transmitted diffracted orders. A

forked holographic grating is imaged using this method. To image an object immersed in a turbid medium or tumar tissue, optical coherence tomography and non-invasive speckle ensemble addition, are two of the processes among existing methods of biological tissue imaging. It is seen theoretically that if first order is more intense for a particular scatterer, image of the scatterer will look better. A computer simulation of interference of diffracted orders is studied to get back the image of the scatterer. Diffraction is a special case of scattering when beam size is comparable with the scatterer size. Diffraction occurs when beam size is little bigger than the deformed scatterer size. This situation arises in many cases when the passing laser beam width is little greater than the tissue phantom or biological tissue to image it. Diffraction patterns are regularize speckles. Regularize speckles are vortices or Bessel beams or solitons. The central order consists of ballistic photons and both side orders snake photons. First order is the image bearing beam. Hence obviously first order diffraction efficiency needs to be more. With the increasing order,the topological charge increases and on both sides of the diffraction pattern charges are of opposite sign. Gaussian vortex beam is generated in the diffraction patterns with central ballistic being Gaussian. A computer generated hologram which looks like a tuning fork is used as a grating. To get back the image of the fork different orders by a lens are interfered for the case of transmitted diffracted orders as well as for reflected diffracted orders. A low focal length lens in front of the beam-splitter is used such that diffracted orders which are same as of transmitted orders for small propagation distance, interfere properly and if not interfere properly one has to use more lenses or a single lens having high power. To get back the fork grating with the same orientation all diffracted orders are combined with the orientation angle or scanning angle α is given by

$$D = |\sum_{l=-4}^{4} (a)^{|l|}((\eta) + iSign(l)(\xi))^{|l|} e^{(((\eta)^2+(\xi)^2)/\sigma_0^2)} e^{-ik_l(z-Sign(l)(x\cos(\alpha)-y\sin(\alpha)))}|^2 \quad (6.1)$$

Where k_l is $2 * \pi/\lambda_l$ and λ_l is the wavelength of l-th order. Expression of a vortex of topological charge +3 which is scanning other beam by supposing in negative direction horizontally is

$$E_3 = C(\eta + i\xi)^3 e^{-(\eta^2+\xi^2)/\sigma_0^2} e^{-ik_3(z-\eta)}$$

where C is a scaling factor of intensity and σ_0 is the beam width. For simplicity we have taken C to be 1. Where k_3 is the $(2 * \pi/\lambda_3)$and λ_3 is the wavelength of the third order. Similarly wave number and wavelength are defined for other orders. Expression of a vortex of topological charge +2 which is scanning other beam by supposing in negative direction horizontally is

$$E_2 = C(\eta + i\xi)^2 e^{-(\eta^2+\xi^2)/\sigma_0^2} e^{-ik_2(z-\eta)}$$

Expression of a vortex of topological charge +1 which is scanning other beam by supposing in negative direction horizontally is

$$E_1 = C(\eta + i\xi)^1 e^{-(\eta^2+\xi^2)/\sigma_0^2} e^{-ik_1(z-\eta)}$$

Expression of a Gaussian propagating in the middle

$$E_0 = e^{-(\eta^2+\xi^2)/\sigma_0^2} e^{-ik_0(z)}$$

Expression of a vortex of topological charge -1 which is scanning other beam by supposing in positive direction horizontally is

$$E_{-1} = C(\eta - i\xi)^1 e^{-(\eta^2+\xi^2)/\sigma_0^2} e^{-ik_{-1}(z+\eta)}$$

Expression of a vortex of topological charge -2 which is scanning other beam by supposing in positive side horizontally is

$$E_{-2} = C(\eta - i\xi)^2 e^{-(\eta^2+\xi^2)/\sigma_0^2} e^{-ik_{-2}(z+\eta)}$$

Expression of a vortex of topological charge -3 which is scanning other beam supposing in positive side horizontally is

$$E_{-3} = C(\eta - i\xi)^3 e^{-(\eta^2+\xi^2)/\sigma_0^2} e^{-ik_{-3}(z+\eta)}$$

Expression of beam with shifted vortex is

$$E = ((\eta - \eta_0) + i(\xi - \xi_0)) e^{-(\eta^2+\xi^2)/\sigma_0^2} e^{-ikz} \tag{6.2}$$

Interference between two beams having amplitude A and B is given by

$$I = |Ae^{-ikz} + Be^{-ik(z-\eta cos(\alpha)-\xi sin(\alpha))}|^2 \tag{6.3}$$

Figure 6.1: Experimental set up for Imaging of scatterer by interfering transmitted diffracted orders

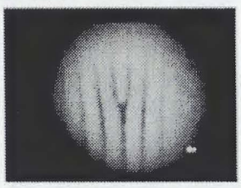

Figure 6.2: Actual grating taken from microscope.

where α is the angle in which one beam scans the other beam. z is the propagation distance. The fringe width depends on the interference plane from the beam-splitter and shear between the beams. Interference of the diffracted patterns is given by the equation

$$I = |aE_3 + bE_2 + cE_1 + E_0 + dE_{-1} + eE_{-2} + fE_{-3}|^2 \tag{6.4}$$

As a result we get back the image of the scatterer. Experimental set up for Imaging of scatterer by interfering transmitted diffracted orders is shown in Fig. 6.1. It is seen that if the intensity scaling factor c and d is more compared to a,b,e,f ,we get better resolution in image but we get better image for the case a,b,e,f are non zero. That is, if higher orders are absent we get a poor image resolution. If first order diffraction efficiency is less, we get poor image resolution. The experiment as well as theory shows that with the increase of first order diffraction efficiency and number of diffraction order the image clarity as well as resolution

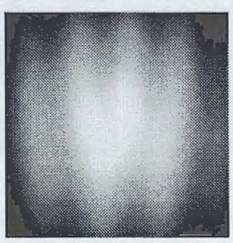

Figure 6.3: Tomography of scatterer when first order diffraction efficiency is less.

Figure 6.4: Tomography of scatterer with first orders diffraction combine with central order

Figure 6.5: Tomography of scatterer with all orders combine and when first order diffraction efficiency is more

will be more. Suppose the central order is blocked, we get two first order diffraction patterns to superpose and we get two opposite fork of topological charge 1 side by side. Similarly if we block central order as well as first orders except second orders, we get two opposite topological charge two fork side by side. With increasing shear the intermediate fringe lines increase. These are represented by equations for first orders to interfere

$$I = |E_1 + E_{-1}|^2, \tag{6.5}$$

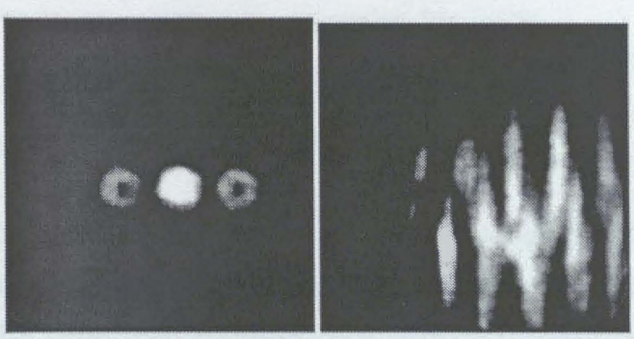

Figure 6.6: Experimental tomography of diffraction grating with less order and less diffraction efficiency

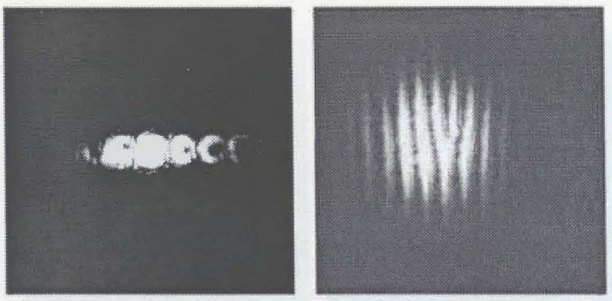

Figure 6.7: Experimental figure of tomography of scatterer with all orders combine

and for second orders

$$I = |E_2 + E_{-2}|^2 \tag{6.6}$$

The method is tested by imaging of single human hair and crossed hair with all orders combined by lens. This imaging methodology is applicable for imaging various size objects depending on the coherent or incoherent beam width. Actual grating taken from microscope is shown in Fig. 6.2. Tomography of scatterer when first order diffraction efficiency is less is shown in Fig. 6.3. Tomography of scatterer with first orders diffraction combine with central order is shown in Fig. 6.4. Tomography of scatterer with all orders combine and when first order diffraction efficiency is more is shown in Fig. 6.5. Experimental tomography of diffraction grating with less order and less diffraction efficiency is shown in Fig. 6.6. Experimental figure of tomography of scatterer with all orders combine is shown in Fig. 6.7. Experimental figure of tomography of hair and a cross hair with all orders combine by lens is shown in Fig. 6.8. Interference of all orders giving white colour optical imaging is shown in Fig. 6.9.

6.3 Explaining natural phenomena

I have already discussed that vortices can be found starting from macroscopic scale to microscopic scale in variety of physical systems. Solution of almost the all natural waves can be produced in laboratory with advancement of diffractive optics. In fact, they are generic to all waves. These are beams with analytic function like Bessel, Laguerre their combination or any related complex function. Study-

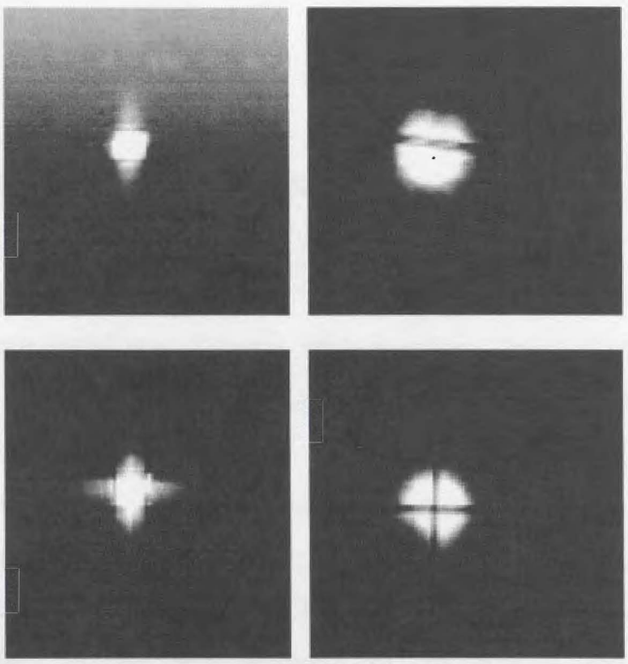

Figure 6.8: Experimental figure of tomography (optical imaging) of hair and a cross hair with all orders combine by lens

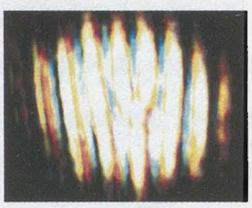

Figure 6.9: Interference of all orders giving white light colour optical imaging.

ing these beams can be useful for interpreting natural structures and how they are formed. A Study of these beams explains various physical phenomena like vortices in BEC and Milky Way galaxy formation. The study is related to the understanding of scattering depth, biological tissue imaging and pattern recognition like finger print diagnosis. Even the prediction of phenomena like diffraction and interference can be extended for matter wave (atom laser). The more the power in the laser,there will be more number of diffraction order. This phenomenon is noticed when high intense laser beam is passed through plasma.

Conclusions and Future Outlook

In conclusion, we have produced beams with vortices (optical) through computer generated hologram and spatial light modulator. Propagation and properties of these beams with vortices have been studied in the laboratory. Topological charge inversion is studied. CNOT gate has been implemented in the laboratory. Monochromatic and polychromatic beams with optical vortices have been studied in the laboratory. Wigner distribution function of optical vortex is experimentally obtained. White light experiment should be done again because sometimes Gaussian vortex beam may be completely white in colour. In future, we plan to study photon correlation of Gaussian vortex beam and their scattering by micro-spheres through digital photo correlator. We plan to study fluorescence of dye doped micro-spheres through optical microscope. We have plans for optical tweezing and spanning. I shall study optical trapping of light, that arises due to nonlinearity in phase in light, introduced by matter. This is observed through multiple similar structures in light. This arises due to scattering and diffraction of light from matter. I shall study intensity effect of vortex beam or Bessel beam when light is at resonance with atoms in Rb cell. I can plan to study fluorescence properties of light through optical microscope and Rb cell. In future, I will work on other functional beams,including special functional beams other than Gaussian and Bessel. It is very challenging to find Wigner distribution function for fractional topological charge Gaussian vortex and Bessel beam, both experimentally and theoretically. This phenomena is though quantum explain classically. My desire is to achieve the Wigner distribution function of multi beams experimentally and many more. Wigner distribution of shifted vortex in Gaussian vortex beam can also be made.

Appendix

$$\Gamma(\eta,\xi,d_\eta,d_\xi) =< E_1^*(\eta,\xi,d_\eta,d_\xi,z)E_2(\eta,\xi,d_\eta,d_\xi,z) > \tag{6.2}$$

$$E_1^*(\eta,\xi,d_\eta,d_\xi,z) = ((\eta-d_\eta)-i(\xi-d_\xi))e^{-((\eta-d_\eta)^2+(\xi-d_\xi)^2)/\sigma_0^2}e^{ikz} \tag{6.3}$$

$$E_2(\eta,\xi,d_\eta,d_\xi,z) = ((\eta+d_\eta)+i(\xi+d_\xi))e^{-((\eta+d_\eta)^2+(\xi+d_\xi)^2)/\sigma_0^2}e^{-ik(z-\eta)} \tag{6.4}$$

$$W(p_\eta,p_\xi) = \int_{-\infty}^{\infty}\int_{-\infty}^{\infty}\Gamma e^{-i(p_\eta d_\eta+p_\xi d_\xi)}dd_\eta dd_\xi \tag{6.5}$$

As η and ξ are constant contribution to Wigner distribution function, we can omit this two terms from variable list. This constant term contributing constant complex contribution. Γ for topological charge +1 gaussian vortex beam is given by,

$$\Gamma = \int_{-\infty}^{\infty}\int_{-\infty}^{\infty}((\eta-d_\eta)-i(\xi-d_\xi))e^{-((\eta-d_\eta)^2+(\xi-d_\xi)^2)/\sigma_0^2} ((\eta+d_\eta)+i(\xi+d_\xi))e^{-((\eta+d_\eta)^2+(\xi+d_\xi)^2)/\sigma_0^2}e^{ik\eta} \tag{6.6}$$

After expanding mutual correlation function, the expression for Wigner distribution function is given by,

$W(p_\eta,p_\xi) = \int\int((\eta-d_\eta)-i(\xi-d_\xi))e^{-((\eta-d_\eta)^2+(\xi-d_\xi)^2)/\sigma_0^2}((\eta+d_\eta)+i(\xi+d_\xi))e^{-((\eta+d_\eta)^2+(\xi+d_\xi)^2)/\sigma_0^2}e^{ik\eta}e^{-i(p_\eta d_\eta+p_\xi d_\xi)}dd_\eta dd_\xi$

$$\int_{-\infty}^{\infty}\int_{-\infty}^{\infty}((\eta-d_\eta)-i(\xi-d_\xi))e^{((\eta-d_\eta)^2+(\xi-d_\xi)^2)/\sigma_0^2}$$
$$((\eta+d_\eta)+i(\xi+d_\xi))e^{-((\eta+d_\eta)^2+(\xi+d_\xi)^2)/\sigma_0^2}e^{ik\eta}e^{-i(p_\eta d_\eta+p_\xi d_\xi)}dd_\eta dd_\xi$$
$$=\int_{-\infty}^{\infty}\int_{-\infty}^{\infty}((\eta^2+\xi^2-d_\eta^2-d_\xi^2)+i(\xi\eta+\eta d_\xi-\xi d_\eta-d_\eta d_\xi)e^{ik\eta}e^{-i(p_\eta d_\eta+p_\xi d_\xi)}dd_\eta dd_\xi$$
$$-\int_{-\infty}^{\infty}\int_{-\infty}^{\infty}i(\eta\xi+\xi d_\eta-\eta d_\xi-d_\eta d_\xi)e^{-(2/\sigma_0^2)(\eta^2+\xi^2)}e^{-(2/\sigma_0^2)(d_\eta^2+d_\xi^2)}e^{ik\eta}e^{-i(p_\eta d_\eta+p_\xi d_\xi)}dd_\eta dd_\xi \tag{6.7}$$

$$\int_{-\infty}^{\infty}\int_{-\infty}^{\infty}((\eta^2+\xi^2-d_\eta^2-d_\xi^2)+i(\xi\eta+\eta d_\xi-\xi d_\eta-d_\eta d_\xi))$$
$$e^{ik\eta}e^{-i(p_\eta d_\eta+p_\xi d_\xi)}dd_\eta dd_\xi$$
$$-\int_{-\infty}^{\infty}\int_{-\infty}^{\infty}i(\eta\xi+\xi d_\eta-\eta d_\xi-d_\eta d_\xi)e^{-(2/\sigma_0^2)(\eta^2+\xi^2)}e^{-(2/\sigma_0^2)(d_\eta^2+d_\xi^2)}e^{ik\eta}e^{-i(p_\eta d_\eta+p_\xi d_\xi)}dd_\eta dd_\xi$$
$$=\int_{-\infty}^{\infty}\int_{-\infty}^{\infty}(\eta^2+\xi^2)e^{-2/\sigma_0^2(\eta^2+\xi^2)}e^{-2/\sigma_0^2(d_\eta^2+d_\xi^2)}e^{ik\eta}e^{-i(p_\eta d_\eta+p_\xi d_\xi)}dd_\eta dd_\xi$$
$$-\int\int e^{-2/\sigma_0^2(\eta^2+\xi^2)}(d_\eta^2+d_\xi^2)e^{-2/\sigma_0^2(d_\eta^2+d_\xi^2)}e^{ik\eta}e^{-i(p_\eta d_\eta+p_\xi d_\xi)}dd_\eta dd_\xi+$$
$$\int_{-\infty}^{\infty}\int_{-\infty}^{\infty}2i(\eta d_\xi-\xi d_\eta)e^{-2/\sigma_0^2(\eta^2+\xi^2)}e^{-2/\sigma_0^2(d_\eta^2+d_\xi^2)}e^{ik\eta}e^{-i(p_\eta d_\eta+p_\xi d_\xi)}dd_\eta dd_\xi \tag{6.8}$$

$$\int_{-\infty}^{\infty}\int_{-\infty}^{\infty}(\eta^2+\xi^2)e^{-2/\sigma_0^2(\eta^2+\xi^2)}e^{-2/\sigma_0^2(d_\eta^2+d_\xi^2)}e^{ik\eta}e^{-i(p_\eta d_\eta+p_\xi d_\xi)}dd_\eta dd_\xi-$$
$$\int_{-\infty}^{\infty}\int_{-\infty}^{\infty}e^{-2/\sigma_0^2(\eta^2+\xi^2)}(d_\eta^2+d_\xi^2)e^{-2/\sigma_0^2(d_\eta^2+d_\xi^2)}e^{ik\eta}e^{-i(p_\eta d_\eta+p_\xi d_\xi)}dd_\eta dd_\xi$$
$$+\int_{-\infty}^{\infty}\int_{-\infty}^{\infty}2i(\eta d_\xi-\xi d_\eta)e^{-2/\sigma_0^2(\eta^2+\xi^2)}e^{-2/\sigma_0^2(d_\eta^2+d_\xi^2)}e^{ik\eta}e^{-i(p_\eta d_\eta+p_\xi d_\xi)}dd_\eta dd_\xi$$
$$=(\eta^2+\xi^2)e^{-2/\sigma_0^2(\eta^2+\xi^2)}e^{ik\eta}\int_{-\infty}^{\infty}e^{-2/\sigma_0^2(d_\eta^2)}e^{-i(p_\eta d_\eta)}dd_\eta\int_{-\infty}^{\infty}e^{-2/\sigma_0^2(d_\xi^2)}e^{-i(p_\xi d_\xi)}dd_\xi$$
$$+e^{-2/\sigma_0^2(\eta^2+\xi^2)}e^{ik\eta}\int_{-\infty}^{\infty}(id_\eta)^2e^{-2/\sigma_0^2(d_\eta^2)}e^{-i(p_\eta d_\eta)}dd_\eta\int_{-\infty}^{\infty}(id_\xi)^2e^{-2/\sigma_0^2(d_\xi^2)}e^{-i(p_\xi d_\xi)}dd_\xi$$
$$+2e^{-2/\sigma_0^2(\eta^2+\xi^2)}e^{ik\eta}\int_{-\infty}^{\infty}(\eta(id_\xi))e^{-2/\sigma_0^2(d_\xi^2)}e^{-i(p_\xi d_\xi)}dd_\xi$$
$$-2e^{-2/\sigma_0^2(\eta^2+\xi^2)}e^{ik\eta}\int_{-\infty}^{\infty}(\xi(id_\eta))e^{-2/\sigma_0^2(d_\eta^2)}e^{-i(p_\eta d_\eta)}dd_\eta \tag{6.9}$$

Using, $D_p(z)\sim e^{-(z^2)/4}z^p(1-(p(p-1))/(2z^2))+p(p-1)(p-2)/(2.4z^4)+....)(|argz|<$

$(3/4)\pi and$

$$\int_{-\infty}^{\infty}\int_{-\infty}^{\infty}(ix)^{\nu}e^{-\beta^2x^2-iqx}dx$$
$$= 2^{-\nu/2}\sqrt{\pi}\beta^{-\nu-1}e^{-q^2/8(\beta^2)}D_{\nu}(q/(\beta\sqrt{2})),$$

(6.10)

$Re\beta > 0, Re\nu > -1, \arg\,(\mathrm{ix}) = \pi/2, sign(x).we$
$get,$

$$\int_{-\infty}^{\infty}e^{-(2/\sigma_0^2)(d_\eta^2)}e^{-i(p_\eta d_\eta)}dd_\eta$$
$$= \sqrt{\pi}(2/\sigma_0^2)^{-1}e^{-p_\eta^2(\sigma_0^2)/8*2}e^{-p_\eta^2(\sigma_0^2/(2*2*4))}$$

(6.11)

using, $\nu = 0$, $\beta^2 = 2/\sigma_0^2$

$$\int_{-\infty}^{\infty}e^{-(2/\sigma_0^2)(d_\eta^2)}e^{-i(p_\eta d_\eta)}dd_\eta$$
$$= \sqrt{\pi}(2/\sigma_0^2)^{-1}e^{-p_\eta^2(\sigma_0^2)/4*2}$$

(6.12)

Similarly,

$$\int_{-\infty}^{\infty}e^{-(2/\sigma_0^2)(d_\xi^2)}e^{-i(p_\xi d_\xi)}dd_\xi$$
$$= \sqrt{\pi}(2/\sigma_0^2)^{-1}e^{-p_\xi^2(\sigma_0^2)/4*2}$$

(6.13)

Combining previous expressions,

$$(\eta^2+\xi^2)e^{-(2/\sigma_0^2)(\eta^2+\xi^2)}e^{ik\eta}\int_{-\infty}^{\infty}e^{-(2/\sigma_0^2)(d_\eta^2)}e^{-i(p_\eta d_\eta)}dd_\eta$$
$$\int_{-\infty}^{\infty}e^{-(2/\sigma_0^2)(d_\xi^2)}e^{-i(p_\xi d_\xi)}dd_\xi$$
$$= (\eta^2+\xi^2)e^{-(2/\sigma_0^2)(\eta^2+\xi^2)}e^{ik\eta}(\pi(\sigma_0^4)/4)$$
$$e^{-(p_\eta^2+p_\xi^2)(\sigma_0^2)/4*2}$$

(6.14)

$$\int_{-\infty}^{\infty}(id_\eta)^2 e^{-(2/\sigma_0^2)(d_\eta^2)}e^{-i(p_\eta d_\eta)}dd_\eta$$
$$= (2)^{-1}\sqrt{\pi}(2/\sigma_0^2)^{-3/2}$$
$$e^{-p_\eta^2(\sigma_0^2)/4*2*2}e^{-p_\eta^2(\sigma_0^2)/4*2*2}$$
$$((p_\eta^2(\sigma_0^2)/2*2)(1-(2/(2(p_\eta^2(\sigma_0^2)/2*2)))))$$

(6.15)

$\nu = 2, \beta^2 = 2/\sigma_0^2$

$$\int_{-\infty}^{\infty}(id_\xi)^2 e^{-(2/\sigma_0^2)(d_\xi^2)}e^{-i(p_\xi d_\xi)}dd_\xi$$
$$= (2)^{-1}\sqrt{\pi}(2/\sigma_0^2)^{-3/2}e^{-p_\xi^2(\sigma_0^2)/4*2*2}e^{-p_\xi^2(\sigma_0^2)/4*2*2}$$
$$((p_\xi^2(\sigma_0^2)/2*2)(1-(2/(2(p_\xi^2(\sigma_0^2)/2*2)))))$$

(6.16)

$$e^{-(2/\sigma_0^2)(\eta^2+\xi^2)}e^{ik\eta}\int_{-\infty}^{\infty}(id_\eta)^2 e^{-(2/\sigma_0^2)(d_\eta^2)}e^{-i(p_\eta d_\eta)}dd_\eta\int_{-\infty}^{\infty}(id_\xi)^2 e^{-(2/\sigma_0^2)(d_\xi^2)}e^{-i(p_\xi d_\xi)}dd_\xi$$
$$= e^{-(2/\sigma_0^2)(\eta^2+\xi^2)}e^{ik\eta}(1/4)\pi(\sigma_0^2)^3(1/4(\sqrt{2}))e^{(-p_\xi^2+p_\eta^2)(\sigma_0^2)/4*2}$$
$$(((\sigma_0^2)/2*2)p_\eta^2-1)(((\sigma_0^2)/2*2)p_\xi^2-1)$$

(6.17)

$$\int_{-\infty}^{\infty}(\eta(id_\xi))e^{-(2/\sigma_0^2)(d_\xi^2)}e^{-i(p_\xi d_\xi)}dd_\xi$$
$$= (2)^{-1/2}\sqrt{\pi}(2/\sigma_0^2)^{-2}e^{-p_\xi^2(\sigma_0^2)/4*2*2}(p_\xi(\sigma_0)/2*\sqrt{2})$$

(6.18)

$$\int_{-\infty}^{\infty}(\xi(id_\eta))e^{-(2/\sigma_0^2)(d_\eta^2)}e^{-i(p_\eta d_\eta)}dd_\eta$$
$$= (2)^{-1/2}\sqrt{\pi}(2/\sigma_0^2)^{-2}e^{-p_\eta^2(\sigma_0^2)/4*2*2}(p_\eta(\sigma_0)/2*\sqrt{2})$$

(6.19)

$$2e^{-(2/\sigma_0^2)(\eta^2+\xi^2)}e^{ik\eta}\int_{-\infty}^{\infty}(\eta(id_\xi))e^{-(2/\sigma_0^2)(d_\xi^2)}e^{-i(p_\xi d_\xi)}dd_\xi$$
$$-e^{-(2/\sigma_0^2)(\eta^2+\xi^2)}e^{ik\eta}2e^{-(2/\sigma_0^2)(\eta^2+\xi^2)}e^{ik\eta}\int_{-\infty}^{\infty}(\xi(id_\eta))e^{-(2/\sigma_0^2)(d_\eta^2)}e^{-i(p_\eta d_\eta)}dd_\eta$$
$$=2e^{-(2/\sigma_0^2)(\eta^2+\xi^2)}e^{ik\eta}(2)^{-1}(2)^{-4}(\sigma_0^2)^4e^{-(p_\eta^2+p_\xi^2)(\sigma_0^2)/4*2*2}$$
$$(-\xi(p_\eta)(\sigma_0)/2*\sqrt{2}+\eta(p_\xi)$$
$$(\sigma_0)/2*\sqrt{2})$$

(6.20)

$\nu=1,\beta^2=2/\sigma_0^2$

$$(\eta^2+\xi^2)e^{-2/\sigma_0^2(\eta^2+\xi^2)}e^{ik\eta}\int_{-\infty}^{\infty}e^{-2/\sigma_0^2(d_\eta^2)}e^{-i(p_\eta d_\eta)}dd_\eta$$
$$\int_{-\infty}^{\infty}e^{-2/\sigma_0^2(d_\xi^2)}e^{-i(p_\xi d_\xi)}dd_\xi$$
$$+e^{-2/\sigma_0^2(\eta^2+\xi^2)}e^{ik\eta}\int_{-\infty}^{\infty}(id_\eta)^2e^{-2/\sigma_0^2(d_\eta^2)}e^{-i(p_\eta d_\eta)}dd_\eta$$
$$\int_{-\infty}^{\infty}(id_\xi)^2e^{-2/\sigma_0^2(d_\xi^2)}e^{-i(p_\xi d_\xi)}dd_\xi$$
$$+2e^{-2/\sigma_0^2)(\eta^2+\xi^2)}e^{ik\eta}\int_{-\infty}^{\infty}(\eta(id_\xi))e^{-(2/\sigma_0^2)(d_\xi^2)}e^{-i(p_\xi d_\xi)}dd_\xi$$
$$-2e^{-(2/\sigma_0^2(\eta^2+\xi^2)}e^{ik\eta}\int_{-\infty}^{\infty}(\xi(id_\eta))e^{-(2/\sigma_0^2)(d_\eta^2)}e^{-i(p_\eta d_\eta)}dd_\eta$$
$$=(\eta^2+\xi^2)e^{-(2/\sigma_0^2)(\eta^2+\xi^2)}e^{ik\eta}(\pi(\sigma_0^2)^2/4)e^{-(\eta^2+\xi^2)(\sigma_0^2)/4*2}$$
$$+e^{-(2/\sigma_0^2)(\eta^2+\xi^2)}e^{ik\eta}(1/4)\pi(\sigma_0^6)(1/4\sqrt{2})e^{-(p_\xi^2+p_\eta^2)(\sigma_0^2)/4*2}((((\sigma_0^2)/2*2)p_\eta^2-1)+(((\sigma_0^2)/2*2)p_\xi^2-1))$$
$$+2e^{-(2/\sigma_0^2)(\eta^2+\xi^2)}e^{ik\eta}(2)^{-1}(2)^{-4}(\sigma_0^2)^4$$
$$e^{-(p_\eta^2+p_\xi^2)(\sigma_0^2)/4*2*2}(-\xi(p_\eta)(\sigma_0)/2*\sqrt{2}+\eta(p_\xi)$$
$$(\sigma_0)/2*\sqrt{2})$$

(6.21)

Therefore,the Wigner distribution function is given by,

$$((1/64)(2\pi)(e^{(-1/8)((p_\eta^2+p_\xi^2)\sigma_0^2))+ik\eta-2\eta^2/\sigma_0^2-2\xi^2/\sigma_0^2)}$$
$$(((p_\eta^2+p_\xi^2))\sigma_0^4-8\sigma_0^2$$
$$((1+(\eta(p_\xi)-\xi(p_\eta))))$$
$$+16((\eta^2+\xi^2))).$$

(6.22)

Matlab Program to calculate Wigner distribution function

As a procedure, at first co-aligned images are subtracted with sheared images with real and imaginary parts and then they are combined and then fourier transform is done. Real part is plotted.

```
A=imread('C:\sanjoy\sv\00r.tif','tif');
 a0=double (A);
a1=a0(1:1024,1:920); save r.dat a1 -ASCII load C:\sanjoy\sv\r.dat;
sr=r(:,:); B=imread ('C:\sanjoy\sv\00Im.tif','tif'); b0=double
(B); b1=b0(1:1024,1:920); save im.dat b1 -ASCII  load
C:\sanjoy\sv\im.dat; sim=im(:,:); san2r=imread
('C:\sanjoy\sv\11r.tif','tif'); s2ar=double (san2r);
s2r=s2ar(1:1024,1:920); save a1r.dat s2r -ASCII; load
C:\sanjoy\sv\a1r.dat; p2r=a1r(:,:); san2im=imread
('C:\sanjoy\sv\11Im.tif','tif'); s2aim=double(san2im);
s2im=s2aim(1:1024,1:920); save a1im.dat s2im -ASCII load
C:\sanjoy\sv\a1im.dat; p2im=a1im(:,:); m2r=minus(p2r,sr)/2.;
m2im=minus(p2im,sim)/2.; save m35qr.txt m2r -ASCII save m35qim.txt
m2im -ASCII; similarly, other "*.tif" files are loaded and
similarly processed and I obtain upto m145qr.txt and m145qim.txt.
load C:\sanjoy\sv\m35qr.txt; load C:\sanjoy\sv\m40qr.txt; load
C:\sanjoy\sv\m45qr.txt; load C:\sanjoy\sv\m50qr.txt; load
C:\sanjoy\sv\m55qr.txt; load C:\sanjoy\sv\m60qr.txt; load
C:\sanjoy\sv\m65qr.txt; load C:\sanjoy\sv\m70qr.txt; load
C:\sanjoy\sv\m75qr.txt; load C:\sanjoy\sv\m80qr.txt; load
C:\sanjoy\sv\m85qr.txt; load C:\sanjoy\sv\m90qr.txt; load
C:\sanjoy\sv\m95qr.txt; load C:\sanjoy\sv\m100qr.txt; load
C:\sanjoy\sv\m105qr.txt; load C:\sanjoy\sv\m110qr.txt; load
C:\sanjoy\sv\m115qr.txt; load C:\sanjoy\sv\m120qr.txt; load
C:\sanjoy\sv\m125qr.txt; load C:\sanjoy\sv\m130qr.txt; load
C:\sanjoy\sv\m135qr.txt; load C:\sanjoy\sv\m140qr.txt; load
C:\sanjoy\sv\m145qr.txt; load C:\sanjoy\sv\m35qim.txt; load
```

```
C:\sanjoy\sv\m40qim.txt; load C:\sanjoy\sv\m45qim.txt; load
C:\sanjoy\sv\m50qim.txt; load C:\sanjoy\sv\m55qim.txt; load
C:\sanjoy\sv\m60qim.txt; load C:\sanjoy\sv\m65qim.txt; load
C:\sanjoy\sv\m70qim.txt; load C:\sanjoy\sv\m75qim.txt; load
C:\sanjoy\sv\m80qim.txt; load C:\sanjoy\sv\m85qim.txt; load
C:\sanjoy\sv\m90qim.txt; load C:\sanjoy\sv\m95qim.txt; load
C:\sanjoy\sv\m100qim.txt; load C:\sanjoy\sv\m105qim.txt; load
C:\sanjoy\sv\m110qim.txt; load C:\sanjoy\sv\m115qim.txt; load
C:\sanjoy\sv\m120qim.txt; load C:\sanjoy\sv\m125qim.txt; load
C:\sanjoy\sv\m130qim.txt; load C:\sanjoy\sv\m135qim.txt; load
C:\sanjoy\sv\m140qim.txt; load C:\sanjoy\sv\m145qim.txt;
x65(1:1024,1:920)=m35qr(1:1024,1:920);
x65(1:1024,(1+920):(920+920))=m40qr(1:1024,1:920);
x65(1:1024,(1+920+920):(920+920+920))=m45qr(1:1024,1:920);
x65(1:1024,(1+3*920):(4*920)=m50qr(1:1024,1:920);
x65(1:1024,(1+4*920):(5*920))=m55qr(1:1024,1:920);
x65(1:1024,(1+5*920):(6*920))=m60qr(1:1024,1:920);
x65(1:1024,(1+6*920):(7*920))=m65qr(1:1024,1:920);
x65(1:1024,(1+7*920):(8*920))=m70qr(1:1024,1:920);
x65(1:1024,(1+8*920):(9*920))=m75qr(1:1024,1:920);
x65(1:1024,(1+9*920):(10*920))=m80qr(1:1024,1:920);
x65(1:1024,(1+10*920):(11*920))=m85qr(1:1024,1:920);
x65(1:1024,(1+11*920):(12*920))=m90qr(1:1024,1:920);
x65(1:1024,(1+12*920):(13*920))=m95qr(1:1024,1:920);
x65(1:1024,(1+13*920):(14*920))=m100qr(1:1024,1:920);
x65(1:1024,(1+14*920):(15*920))=m105qr(1:1024,1:920);
x65(1:1024,(1+15*920):(16*920))=m110qr(1:1024,1:920);
x65(1:1024,(1+16*920):(17*920))=m115qr(1:1024,1:920);
x65(1:1024,(1+17*920):(18*920))=m120qr(1:1024,1:920);
x65(1:1024,(1+18*920):(19*920))=m125qr(1:1024,1:920);
x65(1:1024,(1+19*920):(20*920))=m130qr(1:1024,1:920);
x65(1:1024,(1+20*920):(21*920))=m135qr(1:1024,1:920);
```

```
x65(1:1024,(1+21*920):(22*920))=m140qr(1:1024,1:920);
x65(1:1024,(1+22*920):(23*920))=m145qr(1:1024,1:920);
y65(1:1024,(1):(920))=m35qim(1:1024,1:920);
y65(1:1024,(1+920):(2*920))=m40qim(1:1024,1:920);
y65(1:1024,(1+2*920):(3*920))=m45qim(1:1024,1:920);
y65(1:1024,(1+3*920):(4*920))=m50qim(1:1024,1:920);
y65(1:1024,(1+4*920):(5*920))=m55qim(1:1024,1:920);
y65(1:1024,(1+5*920):(6*920))=m60qim(1:1024,1:920);
y65(1:1024,(1+6*920):(7*920))=m65qim(1:1024,1:920);
y65(1:1024,(1+7*920):(8*920))=m70qim(1:1024,1:920);
y65(1:1024,(1+8*920):(9*920))=m75qim(1:1024,1:920);
y65(1:1024,(1+9*920):(10*920))=m80qim(1:1024,1:920);
y65(1:1024,(1+10*920):(11*920))=m85qim(1:1024,1:920);
y65(1:1024,(1+11*920):(12*920))=m90qim(1:1024,1:920);
y65(1:1024,(1+12*920):(13*920))=m95qim(1:1024,1:920);
y65(1:1024,(1+13*920):(14*920))=m100qim(1:1024,1:920);
y65(1:1024,(1+14*920):(15*920))=m105qim(1:1024,1:920);
y65(1:1024,(1+15*920):(16*920))=m110qim(1:1024,1:920);
y65(1:1024,(1+16*920):(17*920))=m115qim(1:1024,1:920);
y65(1:1024,(1+17*920):(18*920))=m120qim(1:1024,1:920);
y65(1:1024,(1+18*920):(19*920))=m125qim(1:1024,1:920);
y65(1:1024,(1+19*920):(20*920))=m130qim(1:1024,1:920);
x65(1:1024,(1+20*920):(21*920))=m135qim(1:1024,1:920);
y65(1:1024,(1+21*920):(22*920))=m140qim(1:1024,1:920);
y65(1:1024,(1+22*920):(23*920))=m145qim(1:1024,1:920);
m=complex(x65,y65); save wignerq.txt m -ASCII load
C:\sanjoy\sv\wignerq.txt; x=wignerq(:,:); u=fftshift(x);
w=fft2(u);
v=fftshift(real(w));w=fftshift(imag(w));o=fftshift(abs(w));save
wignerreal.txt v -ASCII;save wignerimag.txt v -ASCII;save
wignerabs.txt o -ASCII; load C:\sanjoy\sv\wignerreal.txt;
r=wignerreal(500:530,2500:2800); surf(r); colormap(white); axis
```

```
off;This gives real part of Wigner function. load
C:\sanjoy\sv\wignerimag.txt; s=wignerimag(500:530,2500:2800);
surf(s); colormap(white); axis off; This gives imaginary part of
Wigner function. load C:\sanjoy\sv\wignerabs.txt;
p=wigabs(500:530,2500:2800); surf(p); This will give absolute part
of Wigner distribution function.
```

References

[1] M. S. Soskin and M. V. Vasnetsov,"progress in optics", North-holland, Elsevier, Edited by Emil Wolf, **42**, 219 (2001).

[2] M. Padgett and L. Allen,"Light with a twist in its tail",Contemp. Phys. **41**, 275 (2000).

[3] J. F. Nye and M. V. Berry,"Dislocations in wave trains," Proc. R. Soc. London Ser.A **336**,165(1974).

[4] E.P.Wigner," On the Quantum Correction For Thermodynamic Euilibrium", Phys. Rev. **40**, 749 (1932).

[5] R. Gase,"Representation of Laguerre-Gaussian Modes by the Wigner Distribution Function",IEEE, J. Quantum Electron.,**31**, 1811(1995).

[6] G. S. Agarwal and J. Banerji,"Spatial coherence and information entropy in optical vortex field", Opt. Lett. **27**, 800 (2002).

[7] R. Simon and G. S. Agarwal,"Wigner representation of Laguerre-Gaussian beam", Opt. Lett.**25**, 1313 (2000).

[8] Ravindra Pratap Singh, Sanjoy Roychowdhury, Virendra Kumar Jaiswal, "Wigner distribution of an optical vortex", J. Mod. Opt. **53**, 1803 (2006).

[9] Masud Mansuripur and Ewan M. Wright,"Linear optical vortices,"Opt. Phot. News **40**, Feb (1999).

[10] C. Iaconis and I. A. Walmsley,"Direct measurement of the two-point field correlation function,"Opt. Lett. **21**, 1783 (1996).

[11] Chung-Chieh Cheng and M. G. Raymer,"Propagation of Transverse Optical Coherence in Random Multiple-Scattering Media,"Phys. Rev. A. **62**,023811-1 (2000).

[12] A. Wax and J. E. Thomas,"Measurement of smoothed Wigner phase-spacedistributions for small-angle scattering in a turbid medium," J. Opt. Soc. Am. A **15**,1896 (1998).

[13] Jose A. Ferrari, Erna M. Frins, Wolfgang Dultz,"Complex self-coherence function determination using geometric phase techniques," Opt. Commun. **152** 252 (1998).

[14] Adam P. Wax. ,"Optical phase space distributions for coherence tomography"Ph. D. Thesis, Duke university,1999.

[15] Bilha Segev,"Causality and propagation in the Wigner, Husimi, Glauber, and Kirkwood phase space representations," Phys. Rev. A **63**, 052114 (2001).

[16] Jose A. Ferrari, Eugenio Garbusi, and Erna M. Frins, "Generation of non-diffracting beams by spiral fields," PRE **67**, 036619-1 (2003).

[17] M. Vaupel,and C. O. Weiss,"Circling optical vortices,"Phys. Rev. A. **51**,4078 (1994).

[18] Gabriel Martinez-Niconoff,"Interference between caustics of diffraction fields,"Opt. Lett. **23**,750 (1998).

[19] Bernd Thaller,"Visual Quantum Mechanics Selected Topics with Computer-Generated Animations of Quantum-Mechanical Phenomena"Springer-Verlag,2000.

[20] I V Basisty, V A Pas'ko, V V Slyusar, MS Soskin and M V Vasnetsov,"Synthesis and analysis of optical vortices with fractional topological charges"J. Opt. A:Pure Appl. Opt. **6**,S166 (2004).

[21] Ajoy Ghatak, S Loknathan,"Quantum Mechanics Theory and Applications"Fourth Edition, Macmilan, 1999.

[22] E. Abramochkin and V. Volostnikov,"Beam transformat and nontransformed beams"Opt. Commun. **83**,123 (1991).

[23] L. Allen, M. W. Beijersbergen,R. J. C. Spreeuw and J. P. Woerdman,"Orbital angular momentum of light and the transformation ofLaguerre-Gaussian Laser modes," Phys. Rev. A **45**,8185 (1992).

[24] Guy Indebetouw, "Optical Vortices and their propagation," J. Mod. Opt. **40**, 73 (1993).

[25] Gabriel Molina-Terriza, Ewan M. Wright, Lluis torner,"Propagation and control of noncanonical optical vortices,"Opt. Lett. **26**,163 (2001).

[26] D.F.Walls, "Evidence for the quantum nature of light" review article, Nature 280, 451 (1979).

[27] D. Voloschenko and O. D. Lavrentovich and O.D. Lavrentovich, "Optical vortices generated by dislocations in a cholesteric liquid crystal," Opt. Lett.**25**, 317 (2000).

[28] B Parys, J-F Allard, F Desmullier, D Houde and A Cornet,"Coherence analysis of diffused femtosecond laser pulses," J. Opt. A: Pure App. Opt. **6**, L23 (2004).

[29] Xiang Zhu and Daniel T. Cassidy,"Electronic subtracter for trace-gas detection with InGaAsP diode lasers",App. Opt. **34**, 8303 (1995).

[30] K. Razdan,D. A. Van Baak,"Demonstrating optical beat notes through heterodyne experiments", Am. J. Phys. **70**, 1061 (2002).

[31] H. He. N. R. Heckenberg and H. Rubinsztein-Dunlop,"Optical particle trapping with higher-order dougnut beams produced using high efficiency computer generated holograms,"J. Mod. Opt.**42**,217-223(1995).

[32] C. F. R. Caron, R. M. Potvliage, "Bessel-modulated Gaussian beams with quardratic radial dependence", Opt. Commun., **164**, 83 (1999).

[33] Cheng-Shan Guo, Xuan Liu and Xiu-Yun Ren, Hui-Tian Wang,"Optimal annular computer-generated holograms for the generation of optical vortices," J. Opt. Soc. Am. A **22**,385 (2005).

[34] Shao Hua Tao, Woei Ming Lee, and Xiaocong Yuan,"Experimental study of holographic generation of fractional Bessel beams" App. Opt. **43**,122 (2004).

[35] Ganzalo Paez, Marija Strojnik, and Gaillermo Garcia Torales,"Vectorial Shearing interferometer", App. Opt. **39**, 5172(2000).

[36] M. H. Jakubowski, K. Steiglitz, and R. Squier,"State transformations of colliding optical solitons and possible application to computation in bulk media" Phys. Rev. E **58**, 6752 (1998).

[37] Jianke Yang and Dmitry E. Pelinovsky, "Stable vortex and dipole vector solitons in a saturable nonlinear medium," Phy. Rev. E 67, 016608 (2003).

[38] Gerd Leuchs and Natalia Korolkova, "Entangling Fiber Solitons Quantum Noise Engineering for Interferometry and Communication," Opt. Phot. news, Feb. **64** (2002).

[39] V. Pyragaite, A. Stabinis,"Interference of intersecting singular beams," Opt. Comm. **220**,247 (2003).

[40] G. Andrelczyk, L. Dobrek, M. Gajda, M. Lewenstein, "Optical generation of vortices in trapped Bose-Einstein condensates, " Phy.Rev. A **64**, 043601 (2001).

[41] L. Dobrek, M. Gajda, M. Lewenstein , K. Sengstock,G.Birkl, and W. Ertmer, "Optical generation of vortices in trapped Bose-Einstein condensates," Phys. Rev. A,**60** R3381 (1999).

[42] M. A. Bolshtyansky,A. Yu.Savchenko, and B.Ya.Zeldovich,"Use of skew rays in multimode fibers to generate speckle field with non zero vorticity,"Opt. Lett. **24**, 433 (1999).

[43] S. Barreiro and J. W. R. Tabosa,"Generation of Light Carrying Orbital angular momentum via Induced Coherence Grating in cold atoms,"Phys. Rev. Lett. **90**, 133001 (2003).

[44] Martin Hegner,"The light fantastic,"Nature **419**, September (2002).

[45] Joseph Rosen and David Abookasis,"Noninvasive optical imaging by speckle ensemble,"Opt. Lett. **29**, 253 (2004).

[46] Raphael Kh. Drampyan,"Observation of speckle pattern and interference fringe "fork" in simulated Raman scattering beam profile,"Second International Conference on Singular Optics (Optical Vortices):Fundamentals and Applications **4403**, 241 (2000).

[47] Daniela Dragoman, Mircea Dragoman, and Karl-Heinz Brenner," Amplitude and phase recovery of rotationally symmetric beams," App. Opt. **41**, 5512(2002).

[48] Anton Z.capri," Problems and Solutions in Nonrelativistic Quantum Mechanics" World Scientific, (2002).

[49] Mathieu Fortin, Michel Piche and Ermanno F.Borra,"Optical tests with Bessel beam interferometry", Opt. Exp. **12**, 5887 (2004).

[50] I. S. Gradshteyn and I. M. Ryzhik,"Table of Integrals,Series, and Products," Academic press,fifth edition, 1994,p 382,1093.

[51] E.ORAN BRIGHAM,E-Systems.Inc,"The Fast Fourier Transform," Prentice-Hall,Inc., 1974,p 45,91,135.

List of Publications

1. *Noncanonical vortex transformation and propagation in a two-dimensional optical system*, R. P. Singh and Sanjoy R. chowdhury, J. Opt. Soc. Am. A **20**, 573 (2003).

2. *Trajectory of an optical vortex:Canonical vs. noncanonical*, R. P. Singh and Sanjoy R. chowdhury, Opt. Commun. **215**, 231 (2003).

3. *Non-conservation of topological charge:experiment with optical vortex*, Ravindra P. Singh and Sanjoy Roychowdhury, J. Mod. Opt. **51**, 177 (2004).

4. *Implementing controlled NOT gate with optical vortex*, Sanjoy Roychowdhury, Virendra K. Jaiswal,R. P. Singh, Opt. Commun. **236**, 419 (2004).

5. *Wigner distribution of an optical vortex*, Ravindra Pratap Singh, Sanjoy Roychowdhury, Virendra Kumar Jaiswal, J. Mod. Opt. **53**, 1803 (2006).

6. *Vortex-vortex interaction in shearing Sagnac interferometer* , Sanjoy Roychowdhury, V. K. Jaiswal, and R. P. Singh, Frontiers in Optics 2003 / Laser Science XIX (87th OSA annual meeting), Tucson, Arizona, October 5-9, 2003, PDP8.

7. *Axial nature of an optical vortex*, R. P. Singh, Sanjoy Roychowdhury, and V. K. Jaiswal, Frontiers in Optics 2005/ Laser Science XVI (89th OSA annual meeting), Tucson, Arizona, October 16-20, 2005, FThG4.